BIOMEDICAL APPLICATIONS OF EMULSION TEMPLATED SCAFFOLDS

A Dissertation

by

ROBERT SCOTT MOGLIA

Submitted to the Office of Graduate and Professional Studies of
Texas A&M University
in partial fulfillment of the requirements for the degree of

DOCTOR OF PHILOSOPHY

Chair of Committee,	Elizabeth Cosgriff-Hernandez
Committee Members,	Duncan Maitland
	Melissa Grunlan
	Brian Saunders
Head of Department,	Gerard Coté

May 2014

Major Subject: Biomedical Engineering

ABSTRACT

Each year, millions of patients undergo reconstructive surgery to treat injuries caused by trauma, deformities, or tumor resection. Repair of these defects often requires the use of tissue grafts to promote healing. Current treatment options rely on a limited supply of donor tissue or synthetic materials that lack bioactivity and have a high rate of revision treatments. Tissue engineered grafts provide a temporary matrix that supports tissue regeneration and circumvents complications associated with traditional treatment options. In addition to biodegradable and biocompatible requirements, an injectable scaffold would offer the advantage of space-filling irregular defects without the need for expensive fabrication to shape or custom-build devices. To this end, we have utilized emulsion templating to create injectable polyHIPE scaffolds that are biodegradable, highly porous, polymerize at body temperature, and possess appropriate and tunable mechanical properties for tissue regeneration.

PolyHIPE grafts developed for this purpose exhibited tunable pore sizes (5 μm to 1 mm) and a wide range of mechanical properties (modulus = 50 kPa-50 MPa). The biodegradable macromers used in these polyHIPEs were designed to polymerize at body temperature and have a low viscosity prior to cure, eliminating the use of toxic solvents common in fabricating biodegradable polyHIPEs. New methodology was developed to permit the rational selection of macromers based on prediction of molecular hydrophobicity and structural analysis of surfactant chemical structure in contrast to the traditional trial-and-error approach. Redox initiation was also studied as a means to

decrease polyHIPE cure times from hours to minutes, comparable to current bone cements used currently in the clinic. This new initiation method also improved mechanical properties and had minimal effects on pore structure. The use of a double-barrel syringe also allowed emulsions to be stored for up to 6 months prior to cure with no negative effects on pore structure.

Finally, these polyHIPEs were used to make porous microspheres, via a double-emulsion technique, to improve scaffold bioactivity. These microspheres successfully incorporated rhBMP-2 growth factor, a potent osteoinductive agent used in many bone graft procedures. Current rhBMP-2 delivery methods are expensive and pose safety risks due to the excessive amounts of growth factor used. These microspheres offer a means to gradually deliver site-specific dosages of rhBMP-2 directly in the polyHIPE scaffolds, potentially improving tissue regeneration.

In summary, we have developed a library of injectable porous materials that can be used to improve tissue regeneration. Furthermore, the emulsion structure-property relationships explored here can be used in designing future polyHIPEs for tissue engineering or other applications.

DEDICATION

I would like to thank my family and friends for shaping me into the person I am today, and my wife, Stephanie, for believing in me even when I did not.

ACKNOWLEDGEMENTS

My time here in “Aggieland” has been a formative part of my education, career, and life, in part because of all those who helped and guided me along the way. I would like to thank my advisor, Dr. Elizabeth Cosgriff-Hernandez, for taking me on to work with these polyHIPE scaffolds and for developing my scientific and professional skills. I would also like to thank my committee for their guidance and resources towards completing my studies. Specifically Dr. Melissa Grunlan for use of her FTIR, Dr. Duncan Maitland for his flow perfusion apparatus, and Dr. Brian Saunders for running cell studies and testing some of these devices in mock surgeries.

I learned that research can be both incredibly rewarding and incredibly frustrating at the same time. On the bad days, it helped to be surrounded by an entire laboratory of friends like Mary Beth Browning, Dave Dempsey, Jenny Robinson, Tyler Touchet, Nick Sears, Alysha Kishan, Mike Whitely, and Roya Nezarati. They have always been there to help troubleshoot problems, be an extra pair of hands, or act as a sounding board for new ideas. I need to specifically thank Jenny for being the “cell whisperer” and successfully culturing cells on these scaffolds in addition to helping me talk through improvements to our emulsions, Tyler for helping me develop the PUU prepolymers synthesis, and Nick for keeping all of our lab equipment running (even if it took an entire roll of duct-tape).

Graduate school also let me experience the joys of mentorship. I was fortunate enough to work alongside fantastic undergraduate researchers who have all gone on to

bigger and better things. My first mentee, Caity Wilson, probably taught me more than I did her. She, Dawn Harrison, Andrew Moorman, Nicole Cordner, Megan Brooks, Prachi Dhavalikar, and Hannah Pearce were incredibly helpful and the only reason I ever finished studies in a reasonable time.

Finally, I would again like to thank my family for encouraging me throughout my entire life, and pushing me to always do my best. Special thanks go to my wife, Stephanie, for supporting me through both the best and worst times.

TABLE OF CONTENTS

Page

LIST OF FIGURES

Page

LIST OF TABLES

Page

CHAPTER I

INTRODUCTION AND LITERATURE REVIEW

1.1 Critical Sized Bone Defects

Bone is a nanocomposite of a stiff mineralized hydroxyapatite matrix and elastic collagen fibrils. The matrix gives it great strength in compression, while the collagen resists tensile loads. The combination of the two further improves mechanical properties, especially resisting bending forces and fracture. These characteristics, plus bone's microstructure make it the most robust tissue in the body, capable of supporting several times a patient's body weight.[1-4] Bone can be divided into two types: cortical and cancellous. Cortical bone is dense with porosities from 5-30%, and makes up the diaphysis of long bones (**Figure 1.1)**.[5] While cortical bone is primarily used for load bearing, cancellous bone is much more porous (30-90%) and houses bone marrow which produces blood cells.

The compressive modulus of cortical bone is 17 GPa and strength of 220 MPa, with tensile properties about 20% weaker.[1, 6-8] Cancellous bone is much weaker, with a modulus equal to 50-100 MPa, and strength 5-10 MPa.[2, 9-17] Taylor et al. stated that the highest stresses occurred at the femur midshaft with an average strain between 1200-1500 μstrain for walking and 2000-3000 for running.[8, 18, 19] Assuming an elastic modulus of 17 GPa, this equates to physiological stresses only between 20.4 and 51 MPa which is very similar to *in vivo* loads in other large mammals (40-80 MPa).[6] One method to assess bone quality is fracture toughness, which can be determined with tensile testing or

nanoindentation. An accepted toughness for cortical bone is 5 MPa$\sqrt{m}$.[1] Fatigue strength is also important, and Taylor et al. estimated that human long bones are loaded approximately 2 million times per year.[8] The study found bone fatigue strengths as low as 23 MPa, indicating failure after 10^5 cycles and concluding that most bone tissue would fail every 6 months in the absence of natural repair processes.

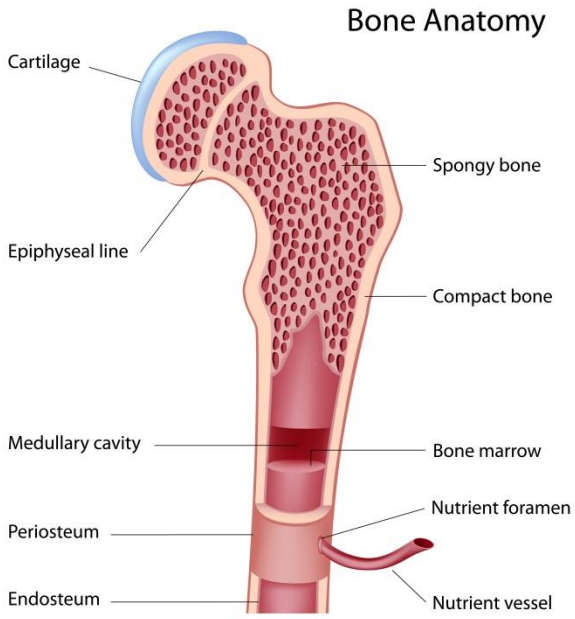

Figure 1.1. Physiology of compact bone. Adapted from reference 5.

This constant state of repair is a result of a balance between osteoclasts and osteoblasts. Osteoclasts, once activated, break down bone that is either damaged or unnecessary. Osteoblasts follow the osteoclasts and begin replacing the osseous tissue with stronger new material. Once repaired, some osteoblasts change their role to become osteocytes (bone cells) and continue to lay down mineralized bone matrix. However,

larger injuries, termed critical size bone defects, fail to heal naturally and often require reconstructive surgery.[20, 21] These defects are typically a result of traumatic injury, tumor resection, or congenital deformities. Tissue grafts promote healing at the defect site by providing a template to guide regeneration. In 2004 alone, there were approximately 1.1 million grafting procedures at an estimated cost of $5 billion.[22]

1.2 Soft Tissue Regeneration

The majority of bodily tissues can be classified as "soft" tissue, and each tissue in the human body has properties specific to its function, e.g. epithelial, adipose, connective, and musculoskeletal tissue. These functions include maintaining body contours, body locomotion, and providing mechanical cushioning.[23] Tissue mechanical properties vary between phenotypes, for example muscle has elastic properties to facilitate movement[24] whereas cartilage is designed to lubricate joints and resist wear. A common property of these tissues is their elasticity and their ability to withstand cyclic loading while maintaining their function. Examples of tissues and their properties can been seen in **Table 1.1**.

Table 1.1. Tensile properties of selected soft tissues.

Tissue	Young's Modulus, MPa	Ultimate Strain, %	Ref.
Anterior Cruciate Ligament	113 ± 45	28 ± 7	25
Smooth Muscle: Relaxed	0.006	300	24
Smooth Muscle: Contracted	0.010	300	24
Articular Cartilage	0.9-20		26

Loss of soft tissue can result from trauma, burns, tumor resection, congenital deformities, or disease. While some tissues can be replaced with autologous grafts (e.g. skin, ligaments) others are commonly replaced with prosthetics (cartilage).

1.3 Treatment Options

1.3.1 Current Treatments Current treatment options for replacing damaged or missing tissue have their respective strengths and weaknesses but none are perfect solutions for restoring function. These treatments can be classified into three categories: autografts, allografts, and alloplasts. Tissue engineering has the potential to create new treatments with the best strengths and no shortcomings of the current options.

1.3.2 Autografts and Allografts Autologous grafts are tissues harvested from elsewhere on the patient's body, examples of bone autografts are the iliac crest or ribs. These grafts are considered the gold standard of current treatments because they contain the patient's native cells, mature microstructures, vascularized tissue, and no risk of rejection. This allows the graft to quickly replace the function of the damaged bone, tendon, or muscle. Typical success rates are high, between 70-100% in vertebral fusions one of the most common uses for autografts.[27] Although autografts have the highest potential for growth, remodeling, and their ability to osseointegrate, they have limitations. First, the amount of donor tissue per patient is relatively low. Second, retrieval of donor tissue usually results in donor site pain and morbidity.[27, 28]

Allografts are more available than autografts, with similar success rates.[27] Bone allografts are typically harvested from cadavers and ground up into a powder or paste,

allowing them to be used in a variety of applications. Ligament allografts can be used successfully, but have similar limitations to bone. These grafts have high regenerative capabilities, but carry an inherent risk of disease transmission, which can be mitigated by decellularizing the material. However, this process decreases the mechanical properties of allografts.

A common problem of both auto and allografts is reliability. The quality of the procedure is highly dependent on graft quality which varies greatly from patient to patient. This causes a problem for surgeons because a procedure that works for one person may not work for another, and it is difficult to predict this beforehand resulting in costly revision surgeries and a decreased quality of life.

1.3.3 Alloplastic Grafts A wide variety of alloplastic materials have also been utilized including stainless steel, titanium, methylmethacrylate resins, polyethylene, silicone elastomers, and hydroxyapatite ceramics.[2, 9, 15, 29-33] Some advantages of alloplasts are the tunable mechanical properties, repeatable results, and their high availability. Drawbacks and complications inherent in the use of current alloplastic materials include inadequate tissue integration, limited biodegradability, and stress shielding.

The first materials used for bone replacement were high strength metals such as steel and titanium. However, these materials are orders of magnitude stiffer than bone which shields the bone from carrying loads. This causes the bone remodeling process to favor resorption instead of rebuilding. Most recipients of metal implants have been elderly patients that are less active, but people are living longer now than ever before.

This results in more active seniors which puts increased stresses on metal implants with weaker bone, thus more failures and revisions.

Polymeric biomaterials were developed because of their tunable properties that are similar to different body tissues. Poly(methylmethacrylate) was the first polymer used as bone cement for metal implants. This polymer is mixed in the operating suite and poured into the bone before the implant is inserted. The polymerization is extremely exothermic, requiring large amounts of ice to keep the surrounding tissue from burning up.[34-38] Another problem with PMMA is that it is not biodegradable *in vivo*. Poly(lactic-co-glycolic acid) (PLGA) polymers have been used to fabricate biodegradable tissue grafts for bone. The biodegradability and mechanical properties of this polymer is highly controllable by varying the components. Other biodegradable polyesters that can be formed *in situ* such as polycaprolactone (PCL) and poly(propylene fumarate) (PPF) have been developed and used for soft and hard tissue grafts.[17, 38-48] Although biodegradable and injectable, these materials lack the porosity necessary to repair critical size defects. *In situ* curing hydrogels have improved mass transport properties for soft tissue repair but lack the mechanical strength necessary for orthopaedic applications.[49] A scaffold fabrication method that is injectable and porous, with tunable mechanical properties would provide a significant improvement over current methods.

1.4 Tissue Engineered Grafts

1.4.1 Tissue Engineering Strategies In contrast to current treatments, tissue engineering strategies promote tissue regeneration by seeding living cells on or attracting

endogenous cells to a biomaterial scaffold and delivering appropriate bioactive cues to aid in cell differentiation and tissue growth.[50] As such, tissue engineered grafts combine the remodeling of autografts with the availability and tunable properties of synthetic grafts, thus limiting the complications associated with each of these traditional implants.[15, 51] These grafts could temporarily replace the function of the damaged tissue while regenerating and transferring loads to the developing tissue gradually.

1.4.2 Tissue Engineering Scaffold Requirements Tissue engineering scaffolds typically consist of biodegradable materials that slowly erode at a rate complementary to tissue growth and facilitate full integration of the de novo tissue with the host tissue.[50] In addition to the choice of a suitable biomaterial, the success of tissue engineered constructs depends on the three-dimensional scaffold architecture. An interconnected porous structure enables cellular ingrowth and proliferation, vascularization, and nutrient and metabolic waste transport.[2, 9, 10, 16, 30] Orthopaedic applications also require scaffolds with adequate mechanical properties to withstand physiological loading and restore tissue function without causing deleterious stress-shielding effects.[2, 15, 16, 29, 52-66] As noted earlier, maximum *in vivo* loads are estimated between 20-51 MPa.[8] While neat polymers can surpass this mark[17, 66, 67], only a few polymeric scaffolds have approached the lower limit.[68] It should be noted that this is the maximum physiological stress, and researchers have speculated that scaffold's minimum properties should approximate cancellous bone with a modulus equal to 50-100 MPa, and strength 5-10 MPa.[2, 9-17]

TE grafts can also utilize the patient's own cells or use suitable donor cells to minimize rejection, avoiding lifetime use of anti-rejection drugs and the decreased

immune response they cause. Finally, the ability to match the irregular geometries of these types of bone defects is necessary to promote osseointegration and full healing. Injectable grafts that cure *in situ* are preferable in this aspect to more costly and time-consuming computer-aided design molds.[38, 45, 69, 70] In summary, the advancement of bone tissue engineering strategies is strongly dependent on the development of high-porosity scaffolds that meet these key requirements.

1.4.3 Scaffold Pore Size and Porosity Tissue engineered scaffolds must be porous to allow for cells to proliferate and develop into tissue. A large number of porous scaffolds' ability to support cells/tissues have been evaluated both *in vitro* and *in vivo*. Several studies have tried to determine the ideal pore size for tissue engineered scaffolds by measuring *in vivo* and *in vitro* results. The majority of studies showed that porosities between 57 and 75% with 80-500 μm pores regenerated tissue similarly but there were some differences, discussed briefly here.[71-83]

Akay et al.(2004) found that although pore size didn't effect cell depth, 40 μm pores had an increased number of osteoblasts whereas larger pores had faster migration of cells through the scaffold.[54] Other researchers failed to find any correlation between these properties and cell response. In carbonate apatite scaffolds, Itoh et al. found no difference in fibroblast proliferation with 49-79% porosity.[82] Similarly, Takahashi et al. found cell proliferation had no clear dependence on pore size in their woven scaffolds.[72] However, they found that proliferation increased with porosity due to the increased amount of space and improved nutrient transport[72] and Lewandrowski et al. observed the same results with increased porosity.[71] However, Chu et al. did not find a correlation

between porosity and bone ingrowth in hydroxyapatite scaffolds with 400 µm channels and instead they insist that channel orientation can influence bone formation.[83] Clearly, there are many complex phenomena in effect which has led to this confusion and disagreement. Kruyt et al. compared two scaffolds and found that scaffolds with 60% porosity and 400µm (60/400) pores had greater goat MSC DNA than the 70/800 scaffolds, but the 70/800 grafts grew more bone *in vivo*.[81] This study highlights why no single test is indicative of graft success, and that caution must be taken before comparing *in vivo* and *in vitro* results. Similar results were also seen in studies by Kujala et al. and Fisher et al.[79, 80]

Hulbert et al. has stated that the minimum pore size is 100 µm for bone regeneration (**Table 1.2)**.[78, 84] However, a study by the Ratner group showed that 30-40 µm pores with 15 µm interconnects best regenerated bone and induced angiogenesis, a critical aspect of large tissue repair.[85] Liu et al. observed that increasing pore size from 34 to 45.7 µm also increased bone formation, which agrees with Ratner's findings.[75, 85] Furthermore, no maximum or optimal pore size has been discovered, as evidenced by the following studies. Roy et al. fabricated β-tricalcium phosphate scaffolds with 125-150 µm pores and 80-88%, and their results supported Takahashi et al.'s findings.[86] They observed that tissue ingrowth and bone formation increased with porosity, in rabbit cranial defects.[86] Two studies of porous HA scaffolds with various pore sizes (106-600 µm) observed increased alkaline phosphatase, osteocalcin, and bone formation with 300-400 µm pores.[76, 77] They also observed capillary formation at pore sizes above this mark.[76, 77] Kujala et al. found that 505 µm pores elicited more fibrosis than scaffolds

with 209 μm pores.[80] And other studies found seemingly contradictory results with smaller pores (90 μm) causing earlier chondrogenesis and larger pores (120 μm) skipping right to osteogenesis.[73, 74, 77] While Fisher et al. found no difference in bone formation for PPF scaffolds with different porosities or pore sizes.[79]

Due to the complex nature of tissue regeneration, no single best option has been found. Further studies are needed to truly guide graft design but until then graft materials must be tunable to meet the changing demands and theories about tissue regeneration.

Table 1.2. Type of tissue formed *in vivo* vs interconnect size.

Tissue	Interconnect Size, μm	Ref
Fibrous	5-15	[84]
Osteoid	40-100	[84]
Mineralized Bone	100	[84]

1.4.4 Scaffold Fabrication Strategies Tissue engineers have developed numerous fabrication strategies to create 3D bone grafts to meet the various requirements outlined above.[12, 14, 16, 17] The selected fabrication process dictates scaffold architecture which is a critical design feature given the effect of architecture on construct mechanical properties, degradation rate, and cellular response. In particular, generation of a scaffold with high porosity that retains sufficient mechanical strength for orthopaedic applications remains challenging. The most common techniques to produce porous scaffolds include particulate leaching, gas foaming, thermal induced phase separation, and fiber bonding.[38, 45] Several of these strategies provide exceptional architectural control; however, matching construct geometry to the contours of the defect

is generally limited to the mold used in fabrication or post-fabrication shaping. *In situ* forming scaffolds can fill irregular shaped defects, improve contact between the scaffold and surrounding tissue, and eliminate the need for costly molding techniques.[87]

Electrospinning allows for the generation of highly porous fibrous meshes.[14, 88] these meshes are typically in the form of tubes or sheets, ideal for regenerating skin or vascular tissue. While they have tunable tensile properties, electrospun meshes cannot be loaded in compression. Also, the flat meshes are not ideal for the complex geometries needed to regenerate bone. Finally, electrospun meshes will never be injectable since they require the use of solvents and a grounded collector.

Gas foaming is the process whereby pores are generated in a polymer melt by the production of gas from either chemical or physical means.[12] These foams can be controlled to possess a wide range of pore sizes 190-400 μm and interconnected porosities.[12, 13] Scaffolds produced in this manner could be formed in a mold to generate complex shapes. However, these foams usually have a non-porous skin which needs to be removed prior to implantation.[12] Also, the high temperatures and pressures typically required to generate the pores prevent them from being formed *in situ*.

Thermal induced phase separation (TIPS) creates porous polymer scaffolds by quickly quenching a polymer melt. This changes the solubility of the solvent causing it to separate out of the polymer phase, and form droplets. Freeze-drying the foams removes the solvent, leaving a porous polymeric scaffold. The process can be controlled in such a way to create long aligned pores or spherical pores.[44, 89] These scaffolds can be

shaped to fit any defect, but the solvent and low temperatures prevent them from being injectable.

Porogen leaching is a very simple method to produce scaffolds. The porogen, typically a salt, is mixed with a liquid polymer melt, cured, and then the salt is dissolved out[16, 17] and sintering the porogen can create open porous structures. These scaffolds can be injectable and biodegradable if the proper salt and polymer are chosen.[85, 90, 91] However, the pores left by salt crystals have sharp corners which act as stress concentrators and lower the mechanical properties of salt leached scaffolds limiting their use in load-bearing applications.[17, 45, 46, 92]

Hydrogels have become very popular with soft tissue engineering because of their ease of fabrication and resultant physical properties.[38, 47, 85, 91, 93-98] Their mechanical properties can be tuned to match most soft tissues in the human body. PEG hydrogels are useful because cells do not naturally bind to them, but this can be controlled by incorporating motifs such as RGD peptides. Recent studies have utilized injectable hydrogels for bone regeneration;[38] however, their low mechanical strength does not permit defect stabilization and requires additional fixation.

Shape memory polymers have the ability retain a temporary geometry and later return to their original dimensions upon exposure to external stimuli such as heat.[99] These materials have garnered interest in the biomedical field for use in minimally invasive surgeries because they can be compressed to a small size and then actuate to their functional shape *in situ*. Recently, shape memory polymers have also been investigated as space-filling scaffolds to match irregular defects and overcome

shortcomings of current treatments.[100-103] Their mechanical properties typically approximate soft-tissues[102], making them a viable alternative to injectable scaffolds.[101] However, it is not clear if cells could be encapsulated into the foams and survive the shear forces and temperatures associated with shape programming, and non-uniform expansion in irregular defects may change material characteristics such as pore size and mechanical properties.

1.5 Polymerized High Internal Phase Emulsions (PolyHIPEs)

Polymerization of high internal phase emulsions (polyHIPEs) is a relatively new method to produce high porosity scaffolds.[53, 104] High internal phase emulsions (HIPEs) are characterized by an internal droplet phase volume fraction greater than 74%. Polymerizing the HIPE's continuous phase locks in the emulsion geometry at the gel point to generate a high porosity monolith or polyHIPE, **Figure 1.2**.[53-66, 105] A wide range of porosities (75-99%), pore sizes (1-100 μm), compressive moduli (2 kPa-60 MPa) and morphologies (open- vs. closed-pore) can be produced by varying the HIPE composition and processing variables.[11, 49, 54, 55, 106, 107] The spherical pores also eliminate stress concentrators, like those seen in salt leached scaffolds, increasing mechanical properties. A unique feature of the polyHIPE system is that the HIPE retains a viscosity that is suitable for injection prior to cure. An injectable polyHIPE system requires 1) biodegradable macromers with low viscosities for emulsion formation and 2) reaction thermodynamics that allow for HIPE polymerization at physiological conditions.

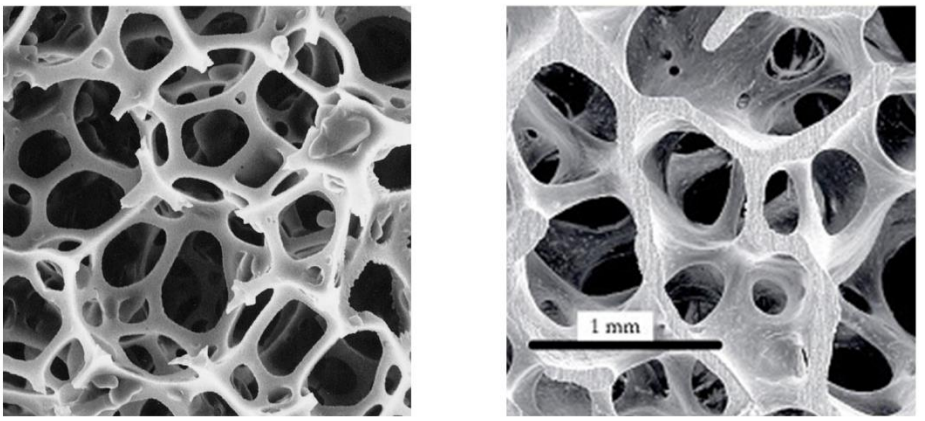

Figure 1.2. Comparison of polyHIPE structure to cancellous bone. PolyHIPE scaffold on the left and bone tissue on the right, from reference 56.

Previous research on the development of polyHIPE bone grafts has focused on styrene-based or unsaturated polyester-based macromers.[56, 65, 108, 109] Several research groups have developed methods to control PS/DVB polyHIPE pore architecture such as surfactant concentration, and aqueous addition rate.[53, 54, 56, 63, 67, 110-112] These scaffolds were fabricated with 5-100 µm and interconnects from 0.6-30 µm, see **Table 1.3**.[54, 67, 113] Although these styrene-based systems had controllable pore morphology, they were non-biodegradable which limited their use as tissue engineered scaffolds. Biodegradability was achieved by substituting in unsaturated polyesters such as PCL and polyfumarates; however, the macromers studied were often too viscous to form HIPEs without the use of toxic diluents, such as toluene. [17, 35, 36, 45, 71] These biodegradable polyHIPEs had much larger pore sizes (5-3000 µm) but smaller interconnects than their vinyl counterparts.[56, 109, 114-116] This increase in pore size is hypothesized to result from decreased emulsion stability with the addition of PCL macromer.[11, 56, 109, 115, 116] An exception to this is the polyHIPE fabricated by David et al., where the macrospores were formed by CO_2 gas, a

product of urea formation between isocyanate functional groups in the presence of water.[109]

Table 1.3. Selected polyHIPE compositions and pore sizes.

Materials	Surfactant	Pore Diameter (μm)	Interconnect Size (μm)	Ref
PS, DVB	Span 80	73-90 40-100 35-104 20-45 5-100	16-26 15-30 11-26 1-16 NR	110 54 117 65 67
PS, DVB, THF	Span 80	5-100	1-5	55
PS, DVB, Toluene	Span 80	10	NR	118
DVB, EVB	Span 80	20-30	0.65-2.55	113
PS, PMMA, PLA	Span 80 Span 85 Tween 85 Synperonic PE L121	5-20	NR	11
PCL-vinyl	Span 80 Span 85 Tween 80 Synperonic PE L121	5-100	NR	56
PCL, tBA, DVB	Span 80	5-3000	0.2-2	115
PCL-triol, HDI, THF	PGPR 4125	5-100, CO_2=1000	0.1-10	109
HA polyHIPE	NR	NR	NR	106
PPF, PFDA, Toluene	Span 80	10-400, >500	2-5	114
Semi-IPN PCL-diols and vinyls	Span 80	60-285	0.1-1	116
IPN, Semi-IPN PS,DVB, dodecanediol	Span 80 PGPR 90	0.61-2.83	~0.2	108
Hydrogel—polyHIPE Hydroxyapatite	Span 80	100	NR	94

Despite the different researchers and properties, the surfactant choice is very consistent. Span 80 was chosen for all but a handful of previous polyHIPE studies, and

every PS-DVB composition.[54, 55, 67, 108, 110, 113, 117, 118] Utilizing new surfactants like Tween 80, Synperonics, and PGPR, allowed for PCL-based polyHIPEs to be fabricated successfully.[11, 56, 109] Further use of new surfactants could facilitate the use of new biodegradable polymers and pore structures.

1.6 Tailoring Polymer Mechanical Properties

This large range in pore sizes with positive *in vivo* results allows researchers to focus on other properties (e.g. compressive strength) with confidence that resultant pore sizes will be sufficient for tissue regeneration.[40, 90, 119-124] Tissue graft mechanical properties are influenced by many factors, including: bulk material properties, pore size, and porosity. Increasing the porosity and pore size of a scaffold may increase tissue regeneration but usually decreases mechanical properties as well. Understanding how one affects the other is important for scaffold design. As described below, sometimes the easiest way to improve the construct's strength is to change the material's properties.

1.6.1 Effect of Porosity on Mechanical Properties Mechanical properties of scaffolds are inversely related to porosity, but the connection is less clear with pore size. Barralet et al., Lin et al., Burdick et al., Fisher et al., and Porter et al. all observed a drop in mechanical properties with an increase in porosity, for a variety of scaffold materials.[40, 90, 119, 122, 123] Burdick and Fisher's studies state that 80% porosity is the critical point, above which properties deteriorate.[40, 122] Porter et al. report that only elastic bending modulus was unchanged by increased porosity.[119] Barralet further states that increased pore size decreased mechanical strength and modulus[90], but this was not

seen in other studies. A study by Borden et al. increased pore size from 72-164 μm, without changing porosity, and found a decrease in modulus from 297 to 232 MPa.[124] Burdick et al. increased pore size from 45 to 300 μm and found an increase in modulus with no change in yield strength[122], contradicting Borden et al.[124]

1.6.2 Tuning Polymer Chemistry Polymer physical properties are strongly influenced by their chain/network structure. Higher molecular weight polymers have increased modulus and toughness over low molecular weight materials.[120] This is due to chain entanglements resisting deformation of the polymer. However, networked polymers behave differently. In this case, crosslink density is a key determinant in mechanical properties. The lower the molecular weight between crosslinks, the higher the crosslink density and the higher the modulus. Materials may also become brittle if crosslink density gets too high. Although counterintuitive, the network may be so tightly-woven that it stearically hinders interchain crosslinking resulting in many highly crosslinked but separate networks instead of one giant network throughout the whole material. This behavior is seen most frequently in low molecular weight multi-functional monomers, such as EGDMA.

1.6.3 Composite Materials with Improved Mechanical Properties Composites are a combination of multiple components to yield materials with new and unique properties not seen in either individual component. These materials may have increased strength or reduced weight, some examples are reinforced concrete or cortical bone. Because cortical bone is made up of rigid hydroxyapatite matrix and elastic collagen, researchers have attempted to make similar materials. Porter et al. created composites of

β-tricalcium phosphate and PPF and found that increasing the ratio of rigid β-TCP enhanced all mechanical properties.[119]

Another way to tailor the scaffold mechanical properties is by creating polyHIPEs with interpenetrating polymer networks (IPNs) or semi-IPNs. IPNs are defined by multiple crosslinked networks that are not covalently bonded together but cannot be separated without breaking chemical bonds, whereas semi-IPNs contain only one crosslinked network intertwined by separate polymer chains. IPNs are useful because they combine the properties of their component networks to yield a material with new and unique attributes, e.g., raising the Tg[125, 126], or increasing elasticity[48, 116, 127]. Polyurethane-polystyrene (PU-PS) IPNs have been made numerous times to toughen the brittle PS.[108, 125, 126]

1.7 Permeability in Porous Scaffolds

Pore interconnectivity is necessary to facilitate mass transport through the graft, and can be quantified via Darcy's permeability constant, *K*.[91, 128] At low flow rates, such as those seen in permeability tests, *K* can be solved using Darcy's law (Equation 1). In this form, v_0 is the superficial velocity and is defined as the number of cubic meters of fluid passing through a square meter of the porous medium every second.[128] Fluid viscosity, μ, length of the scaffold, ∂x, and the pressure differential, ∂P, are the other variables. Permeability has been mathematically linked to pore size, porosity, and tortuosity, τ. Tortuosity is a unit-less measure of the fluid path length through the porous medium, which is also determined experimentally.

$$(1.1) \quad K = -v_0 \mu \frac{\partial x}{\partial P}$$

Several researchers have studied permeability in tissue engineered scaffolds to find relationships between pore structures and cell/tissue viability.[129] Botchwey et al. developed a 1-dimensional model to compare glucose diffusion in scaffolds resulting from different types of bioreactors.[129] Their study found that internal flow rates increased with increased pore size or a decreased tortuosity.[129] For the scaffolds tested, a minimum flow of 7.4 x 10^{-5} m/s was required for glucose to fully permeate the graft (thickness = 2.5 mm).[129]

Permeability can be related to solute diffusion[129] and cell viability, but no required values have been stated. The goal of researchers has been to increase porosity with the assumption that this will increase permeability and diffusion. The higher the diffusion coefficient, the better the mass transport and the larger the graft can be. Cancellous and cortical bones have *K* values between 4.45x10^{-8} and 1.1x10^{-13} m^2,[130, 131] similar to reported permeabilities of several porous scaffolds.[132, 133]

1.8 Summary and Future Directions

Tissue engineered grafts have the potential to regenerate large tissue defects as well or better than current treatments. Research efforts have focused on how materials, scaffold fabrication, and scaffold properties affect tissue regeneration but there is still more to be understood. Creation of an injectable and biodegradable scaffold for tissue engineered grafts would allow the grafts to fill complex shapes easily and completely, improving tissue integration and regeneration. These grafts must have tunable properties

that match a variety of native tissues and allow use for hard or soft tissue reconstruction. For the grafts to be successful, attention must be paid to scaffold degradation, porosity, pore size, mechanical properties, and permeability.

CHAPTER II

INJECTABLE POLYHIPES AS HIGH POROSITY BONE GRAFTS[*]

2.1 Introduction

Large bone defects resulting from traumatic injury, tumor resection, or congenital deformities fail to heal naturally and often require reconstructive surgery. Bone grafts promote healing at the defect site by providing a template to guide new tissue formation. Tissue engineering strategies promote bone regeneration by seeding living cells on or attracting endogenous cells to a biomaterial scaffold and delivering appropriate bioactive cues to aid in cell differentiation and tissue growth.[50] As such, tissue engineered bone grafts combine the osseointegration and remodeling of autografts with the availability and tunability of synthetic grafts, thus limiting the complications associated with each of these traditional implants.[15, 51]

Tissue engineering scaffolds typically consist of biodegradable materials that slowly erode at a rate complementary to tissue growth and facilitate full integration of the de novo tissue with the host tissue.[50] In addition to the choice of a suitable biomaterial, the success of tissue engineered constructs depends on the three-dimensional architecture of the scaffold. An interconnected porous structure enables cellular ingrowth and proliferation, vascularization, and the transport of nutrients and metabolic waste. [2, 9, 10, 16, 30] Orthopaedic applications also require scaffolds with

[*] Reprinted with permission from "Injectable PolyHIPEs as High-Porosity Bone Grafts," by Robert S. Moglia, Jennifer L. Holm, Nicholas A. Sears, Caitlin J. Wilson, Dawn M. Harrison, and Elizabeth Cosgriff-Hernandez, Biomacromolecules 2011, 12 (10), 3621-3628. Copyright (2011) American Chemical Society.

adequate mechanical properties to withstand physiological loading and restore tissue function without causing deleterious stress-shielding effects.[2, 15, 16, 29, 52] Finally, the ability to match the irregular geometries of these types of bone defects is necessary to promote osseointegration and full healing. Injectable grafts that cure *in situ* are preferable in this aspect to more costly and time-consuming computer-aided design molds. In summary, the advancement of bone tissue engineering strategies is strongly dependent on the development of high-porosity scaffolds that meet these key requirements.

Tissue engineers have developed numerous fabrication strategies to create 3D bone grafts.[2, 9-17] The selected fabrication process dictates scaffold architecture which is a critical design feature given the effect of architecture on construct mechanical properties, degradation rate, and cellular response. In particular, generation of a scaffold with high porosity that retains sufficient mechanical strength for orthopaedic applications remains challenging. The most common techniques to produce porous scaffolds include particulate leaching, gas foaming, thermal induced phase separation, and fiber bonding.[12, 14, 16, 17] Many of these strategies provide exceptional architecture control; however, control of the construct geometry (e.g. to match the contours of the defect) is generally limited to the mold used in fabrication or post-fabrication shaping. *In situ* forming scaffolds can fill irregular shaped defects, improve contact between the scaffold and surrounding tissue, and eliminate the need for costly molding techniques.[38, 45] Poly(methyl methacrylate) (PMMA) bone cements are perhaps the most widely used injectable material in orthopaedics; however, PMMA is non-degradable which may

impede bone healing.[38] Recently, investigators have developed highly crosslinked, degradable networks such as poly(propylene fumarates) and polyanhydrides that can be formed *in situ* using either thermal or photoinitiated crosslinking.[34-37] Although biodegradable and injectable, these materials lack the porosity necessary to repair critical size defects. In contrast, *in situ* curing hydrogels have sufficient mass transport properties but lack the mechanical strength necessary for orthopaedic applications. A scaffold fabrication method that is injectable and porous, yet retains high mechanical strength would provide a significant improvement over current methods.

Polymerization of high internal phase emulsions (polyHIPEs) is a method for the production of high porosity scaffolds.[114] High internal phase emulsions (HIPEs) are characterized by an internal droplet phase volume fraction greater than 74%. Polymerization of the HIPE's continuous phase locks in the emulsion geometry at the gel point to generate a high porosity monolith or polyHIPE.[53, 104] A wide range of porosities (75-99%), pore sizes (1-100 μm), compressive moduli (2 kPa-60 MPa) and morphologies (open- vs. closed-pore) can be produced by varying the HIPE composition and processing variables.[53-66] A unique feature of the polyHIPE system is that the HIPE retains a viscosity that is suitable for injection prior to cure. An injectable polyHIPE system requires 1) biodegradable macromers with suitable viscosities for emulsion formation and 2) reaction thermodynamics that allow for HIPE polymerization at physiological conditions. Previous research on the development of polyHIPE bone grafts has focused on styrene-based or unsaturated polyester-based macromers.[11, 54, 55, 106, 107, 114] Although past styrene-based systems had excellent pore morphology, they were non-

biodegradable which limited their use as tissue engineered scaffolds. Biodegradability was achieved by substituting in unsaturated polyesters; however, the macromers studied were often too viscous to form HIPEs without the use of a toxic diluent, such as toluene.[56, 65, 108, 109]

We have developed a biodegradable and injectable polyHIPE system based on propylene fumarate dimethacrylate (PFDMA) macromers. The viscosity of PFDMA is suitable for HIPE formation and reactive methacrylate end groups enable *in situ* crosslinking into rigid monoliths at 37˚C. Furthermore, fumarate-based polymers have shown great promise as bone grafts with established osteoconductivity *in vivo*.[35, 36, 134] PFDMA polyHIPEs exhibited ~75% porosity, pore sizes ranging from 4 to 29 μm, and an average compressive modulus and strength of 33 and 5 MPa, respectively. The ability to synthesize a fully biodegradable polyHIPE without a toxic diluent that can also cure at physiological temperatures is an important adaptation of emulsion templating. These new polyHIPEs have potential application as an injectable, tissue engineered bone graft.

2.2 Materials and Methods

2.2.1 Materials Polyglycerol polyricinoleate (PGPR 4125) was donated by Paalsgard and PEG 600 dilaurate was donated from Unitex Chemical. All other chemicals were purchased from Sigma Aldrich. All chemicals were used as received.

2.2.2 PFDMA Synthesis PFDMA was synthesized in a two-step process adapted from Timmer *et.al.*[41] First, propylene oxide was added dropwise to a solution of fumaric acid and pyridine in 2-butanone (2.75:1.0:0.033 mol). The reaction was refluxed at 80˚C

until the fumaric acid completely reacted, approximately 19 hours. Residual propylene oxide and 2-butanone were then removed in two distillations steps and the product redissolved in dichloromethane. The solution was then washed in 0.2 M NaOH/brine (6:4 v/v) until basic to remove residual acidic byproducts, washed with brine, and stirred over anhydrous sodium sulfate to remove residual water. Dichloromethane was removed using rotary evaporation to yield the diester bis (1,2 hydroxypropyl) fumarate product as a colorless liquid. The diester was then end-capped with methacrylate groups in an addition process with triethylamine and methacryloyl chloride. Hydroquinone was added to inhibit crosslinking during the synthesis. The molar ratios of the diester, methacryloyl chloride, triethylamine, and hydroquinone were 1:2.1:2.1:0.016, respectively. The reaction was maintained below -10˚C to reduce undesirable side reactions and stirred vigorously overnight under a nitrogen blanket. The macromer was filtered to remove triethylamine salt and neutralized overnight in 2 M potassium carbonate. The solution was washed in 0.1 M NaOH/brine (6:4 v/v) to remove residual byproducts, washed with brine, and stirred over anhydrous sodium sulfate to remove residual water. The dichloromethane was removed by rotary evaporation and the PFDMA structure confirmed using 1H NMR (300 MHz, $CdCl_3$) δ 1.33 (dd, 3H, CH3), 1.92 (s, 3H, CH3), 4.20 (m, 2H, -CH2-), 5.30 (m, 1H, -CH-), 5.58 (s, 1H, -C=CH2), 6.10 (s, 1H, -C=CH2), 6.84 (m, 2H, -CH=CH-). The final product was a low viscosity liquid with a pale yellow to amber appearance.

2.2.3 Surfactant Study Sorbitan monooleate (Span 80), PEG 600 dilaurate, Tween 80, and PGPR 4125 were studied to observe their effect on PFDMA HIPE

formation. Each surfactant had different hydrophilic-lipophilic balance (HLB) values and different hydrogen bond donor sites (**Table 2.1**). PFDMA, surfactant, and DI water (2, 0.4, 8g, respectively) were vortexed for 5 minutes. The mixture qualified as a HIPE if all of the water incorporated and it had a high viscosity similar to mayonnaise. The scouting compositions which resulted in HIPEs were fabricated full-scale to investigate the effect of surfactant structure on pore architecture.

Table 2.1. The effect of hydrogen bond donor site location and HLB value on HIPE formation.

	Hydrogen Bond Donor Site Location			
Surfactant	**Polar Head**	**Hydrophobic Tail**	**HLB value**	**HIPE Formed**
Span 85	1	0	1.8	no
Span 80	3	0	4.3	no
PGPR 4125	0	3	4.7	yes
PEG 600 Dilaurate	0	0	11.7	no
Tween 80	3	0	15	no

2.2.4 HIPE Fabrication HIPEs were prepared using the FlackTek Speedmixer DAC 150 FVZ-K. Briefly, PFDMA was mixed with the surfactant PGPR in the Speedmixer cup prior to emulsification. The PGPR concentrations used in this study were 5, 10, 15, and 20 wt%. Once thoroughly mixed, the aqueous solution of calcium chloride (1% v/v), ammonium persulfate (5 wt %) and deionized water was then added to the organic phase in the speedmixer cup. The calcium chloride was used to prevent Ostwald ripening while the ammonium persulfate initiated radical crosslinking of the macromer chains. HIPEs were then transferred to a 37°C aluminum bead bath for 12

hours to facilitate cross-linking. The resulting polyHIPE foams were placed under vacuum for 24 hrs to remove water prior to characterization.

2.2.5 Gravimetric Analysis PolyHIPE porosity was measured gravimetrically. Briefly, dried HIPE samples were cut into cubic sections (9 x 9 x 3 mm) and weighed. Following equation 1, the HIPE porosity can be calculated by comparing HIPE density (ρ_H) with the bulk polymer's density (ρ_P). Reported values are an average of nine sections per polyHIPE composition.

$$\text{Porosity} = 1 - \frac{\rho_H}{\rho_P} \quad (2.1)$$

2.2.6 SEM Analysis Scanning electron microscopy (SEM) was utilized to characterize the polyHIPEs pore architecture. Circular specimens were sectioned into quarters, fractured at the center of the quarter, sputter-coated with gold, and imaged using FE-SEM (JEOL JSM-7500F). Images at 250x were utilized to determine the average pore size when the pores were 25-100 µm. Higher magnification (500x, 1000x) images were utilized to determine the average pore size when the pores were less than 25µm. Each section was imaged in a rastor pattern yielding five images. Measurements were made on the first 10 pores along the image median to minimize user bias. Averages pore sizes for each polyHIPE composition are reported (n=150). A statistical correction was calculated to account for non-perfect spherical pores, $h^2 = R^2 - r^2$, where R is the void diameter's equatorial value, r is the diameter value measured from the micrograph, and h is the distance from the center. The average diameter values were multiplied by this correction factor resulting in a more accurate description of pore diameter.

2.2.7 In vitro Cell Proliferation Investigation of 3T3 fibroblast viability was done to assess polyHIPE cytocompatibility. Cell viability was determined using the Live/Dead Viability/Cytotoxicity Kit (Molecular Probes). NIH/3T3 Swiss mouse fibroblast were purchased (ATCC-CCL92) and cultured *in vitro* with Dulbecco's Modified Eagle Medium (DMEM), Glutamax, high glucose supplemented with 10% heat-inactivated fetal bovine serum (FBS) and 1% Penicillin-Strepotomycin solution (Gibco). The polyHIPE sample comprised of 5 wt% PGPR, 75/25 volume fraction, and mixed at 500 rpm was chosen for cytocompatibility testing because it possessed the largest pore sizes and contained the least amount of surfactant which could potentially disrupt the cell membrane. PolyHIPE foams were prepared for cell seeding as follows: UV irradiation (1 hour per side), ethanol wetting ladder and progressive solvent extraction, and overnight media incubation supplemented with 40 v/v% FBS in DMEM. Following overnight incubation in 37°C, 5% CO_2, medium was removed, specimens were dried in the hood for 30min, washed 1x with PBS and pre-conditioned with growth medium for 15 min. Cells were seeded into wells at 10,000 cells/cm^2. Live/Dead staining was conducted at 24 hours and images taken using fluorescence microscope (Nikon Eclipse TE2000-S).

2.2.8 Mechanical Testing The foams mechanical properties were all tested with an Instron 3300, equipped with a 1000-N load cell. Three specimens were taken from each sample. The test specimens were cut into flat rectangular shapes (9 x 9 x 3 mm) and compressed at 50 μm/s.[92] The calculations in ASTM method D1621-04a [135] were used to determine the compressive modulus. Briefly, a straight edge and computer software were

used to determine the linear region of the stress-strain curve by extending a line from the steepest slope of the curve to the zero-load axis. The point at which this line crossed the axis was determined to be where strain equaled zero and all data points were shifted accordingly. The elastic modulus was equal to the slope of the line in the linear region, as outlined in the ASTM method. Reported moduli data was an average of the three sections for each sample tested (n=9).

2.2.9 Statistical Analysis The data are displayed as mean ± standard deviation for each composition. A Student's t-test was performed to determine any statistically significant differences between compositions. All tests were carried out at a 95% confidence interval (*P<0.05).*

2.3 Results and Discussion

2.3.1 PFDMA Synthesis and Analysis PFDMA was synthesized by the two-step reaction described previously. The first step produced a diester intermediate, bis-(1,2-hydroxypropyl) fumarate, which was then functionalized with methacrylate endgroups, **Figure 2.1**. Following purification, the structure of the resulting PFDMA product was confirmed with 1H NMR. The integration ratio of methacryloyl protons to fumarate protons in the 1H NMR spectra, **Figure 2.2**, confirmed the structure of PFDMA as a single fumarate unit with two terminal methacrylate groups. The average functionalization was calculated to be ~83%. The methacrylate and fumarate groups provided sites for radical crosslinking of the macromer to permit cure of the HIPE at physiological temperatures. Furthermore, fumarate-based bone grafts have shown

promising osteoconductivity results *in vivo*.[35, 36, 134] The resulting macromer had a sufficiently low viscosity (125 cP) and hydrophobicity to permit HIPE formation.

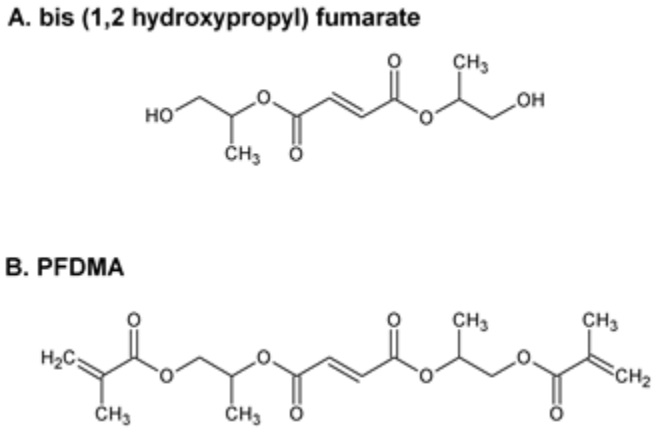

Figure 2.1. Molecular structure of (A) bis (1,2 hydroxypropyl) fumarate and (B) PFDMA.

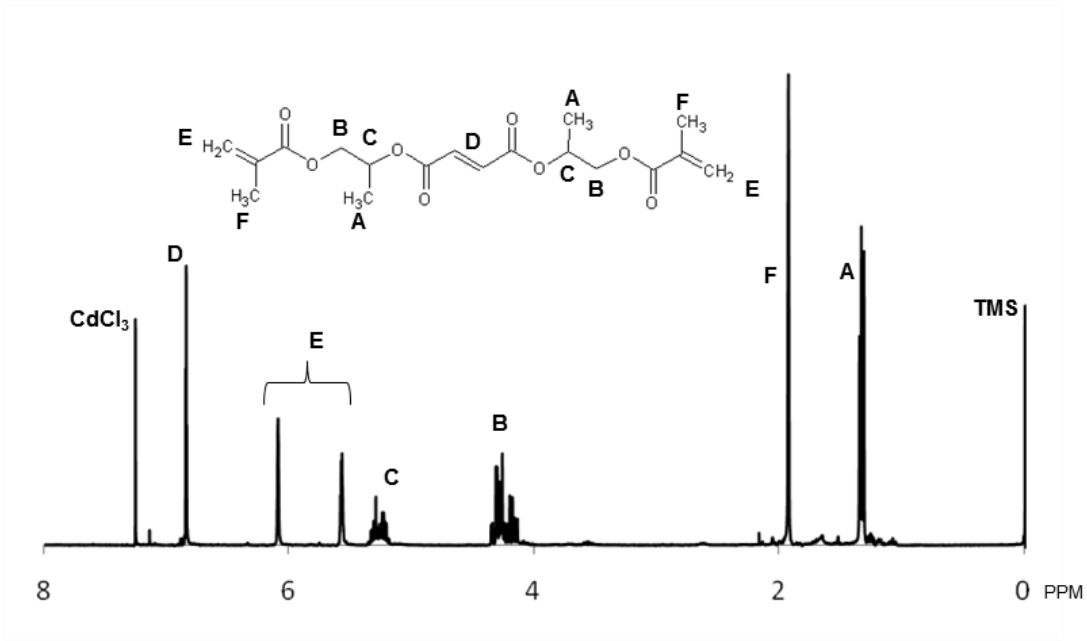

Figure 2.2. Nuclear magnetic resonance spectrum of PFDMA.

Model predictions of the octanol-water partition coefficients (LogP) were used in these studies as a means of comparing molecular hydrophobicity.[136] LogP values are a measure of the differential solubility of a compound between two immiscible solvents, typically water and a hydrophobic solvent such as octanol. Log P values range from negative to positive where a negative value corresponds to a hydrophilic molecule and a positive value a hydrophobic one. The method used in these studies for LogP prediction was developed at Molinspiration (miLogP2.2 – November 2005). The LogP value of each compound was calculated from the sum of its non-overlapping molecular fragments. The group contributions were obtained by fitting calculated LogP with experimental LogP for a training set of more than twelve thousand molecules. The LogP value of PFDMA (3.4) was comparable to macromers that have previously formed stable HIPEs, **Table 2.2**.

Table 2.2. Estimated octanol-water partition coefficients.

Molecule	**LogP** [a]
Styrene	2.8
Divinyl benzene	3.6
PFDA	2.3
PFDMA	3.4
PPF (n = 5)	2.4
PPF (n = 6)	3.1

[a]Octanol-water diffusion coefficient calculated with the Molinspiration miLogP model based on molecular structures.

2.3.2 Selection of HIPE Surfactant Surfactant choice and concentration play a large role in emulsion stability and successful HIPE formation.[53, 56, 63, 67] Selection of HIPE surfactants has largely been based on trial and error and historical precedence. One

method of characterizing surfactants is their hydrophilic-lipophilic balance (HLB) classification. Typically, empirical testing is used to ascertain what HLB values are suitable for each application with an HLB range of 2-6 designated for water-in-oil emulsions.[111] Although several investigators have indicated the limitations of the HLB approach, in this study, we attempt to identify structural features and predictors that may be used to rationally select surfactants for new HIPE macromers. It was hypothesized that a relationship between surfactant HLB and organic phase hydrophobicity may exist which could then be used to select appropriate surfactants for the PFDMA HIPE. Log P values were utilized as a comparison between established HIPE macromers/monomers and PFDMA, **Table 2.2**. The most widely studied polyHIPE system is styrene and divinylbenzene with LogP values ranging from 2.8 - 3.6. The surfactant Span 80 (HLB = 4.3) is typically used to stabilize styrene-based HIPEs. Therefore, it was hypothesized that PFDMA HIPEs with a log P of 3.4 should also form stable emulsions with Span 80. Surprisingly, Span 80 did not stabilize PFDMA emulsions despite the similarity between LogP and HLB values. Additional surfactants and combinations of surfactants with similar structures as Span 80 but a range of HLB values from 1.8-15 were investigated, **Table 2.1,** but these too failed to form stable HIPEs with PFDMA. These studies indicate that HLB alone is insufficient as a selection criteria for stable HIPE formation.

Surfactant structures were compared to determine differences that might affect PFDMA emulsification. It was determined that all of the surfactants tested had hydrogen bond donor sites in the polar head, **Figure 2.3.** PFDMA has multiple hydrogen bond acceptor sites in its backbone that could interact with the polar head of the surfactant. It

was hypothesized that this hydrogen bonding could prevent the polar head of the surfactant from interacting with the aqueous phase of the emulsion, thereby attenuating its ability to stabilize the organic/water interface. Previous fumarate and ester-based systems that were effectively stabilized with Span 80 utilized a non-polar solvent (e.g. toluene) which may have interrupted the hydrogen bonding.[11, 56, 114, 137] To avoid using a toxic diluent, a surfactant without hydrogen bond donor sites in the polar head was needed with the appropriate HLB value. The organic soluble emulsifier, polyglycerol polyricinoleate (PGPR), was selected to test this theory based on its comparable HLB (~4.7) and lack of hydrogen bond donor sites in its polar region. This surfactant has also been used to generate water-in-oil HIPEs with ester-based macromers.[108, 109, 138] Successful formation of PFDMA HIPEs resulted with the addition of PGPR suggests that hydrogen bonding does indeed play a critical role in surfactant stabilization of high internal phase emulsions. Further investigation of surfactants that lack donor sites in their polar head could expand the number of biodegradable polymers utilized in emulsion templating given that many biodegradable polymers (e.g. polyesters) have hydrogen bond acceptor sites in their backbone.

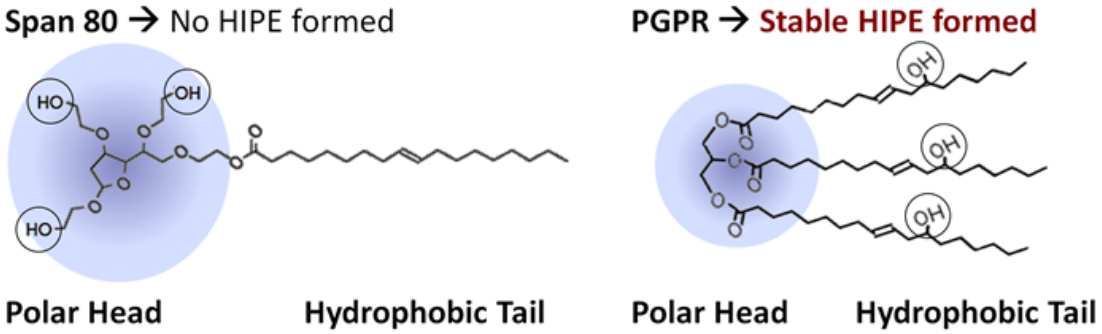

Figure 2.3. Comparison of hydrogen bond donor sites in two common surfactants. (A) Span 80 has 3 in the polar head, whereas (B) PGPR 4125 has 3 in the hydrophobic tail.

2.3.3 Injectable Porous Scaffolds Stable PFDMA HIPEs were incubated at 37°C to initiate radical crosslinking of the unsaturated double bond of the methacrylate groups. The resulting polyHIPE monoliths exhibited ~75% porosity and an average compressive modulus and strength of 33 and 5 MPa, respectively. SEM analysis was utilized to determine pore size and morphology. Polymerization of the continuous phase of the HIPE locked in the emulsion geometry resulting in a high-porosity foam with a closed-pore morphology and average pore size ranging from 4 – 29 µm, **Figure 2.4**. These studies represent an important milestone in the development of an injectable bone graft. Specifically, these polyHIPEs utilize a biodegradable and osteoconductive polymer, have a suitable pre-cure viscosity for injection; and cure at physiological temperatures to a rigid, high-porosity monolith. The potential utility of this new polyHIPE system as an injectable bone graft is illustrated in **Figure 2.4**. Cytocompatibility analysis of 5 wt% PGPR specimens yielded good viability of 3T3 fibroblasts after 24 hours as illustrated in **Figure 2.5**.

Figure 2.4. Injectable PFDMA polyHIPEs can be used *in situ* to space fill complex defects without the need for expensive CAD software.

An open-pore morphology is a common design goal for tissue engineering applications to facilitate tissue ingrowth and nutrient/waste transport. Previous studies have investigated the mechanisms that govern pore opening in the polyHIPE system.[53, 63, 114] Interconnect formation in HIPE systems has been attributed to shrinkage of the thin polymer film separating droplets that occurs as monomer is converted to higher density polymer. If this film between droplets is sufficiently thin, shrinkage results in a window opening and expanding. Therefore, whether a HIPE forms an open- or closed-pore morphology upon polymerization is related to both initial film thickness between droplets and densification during polymerization which initiates pore opening.[53, 56] Film thickness is dictated by the aqueous phase volume and droplet size; whereas, densification is related to structural features of the polymer. Current studies are underway to investigate these two mechanisms with the goal of generating open-pore, fumarate-based polyHIPEs.

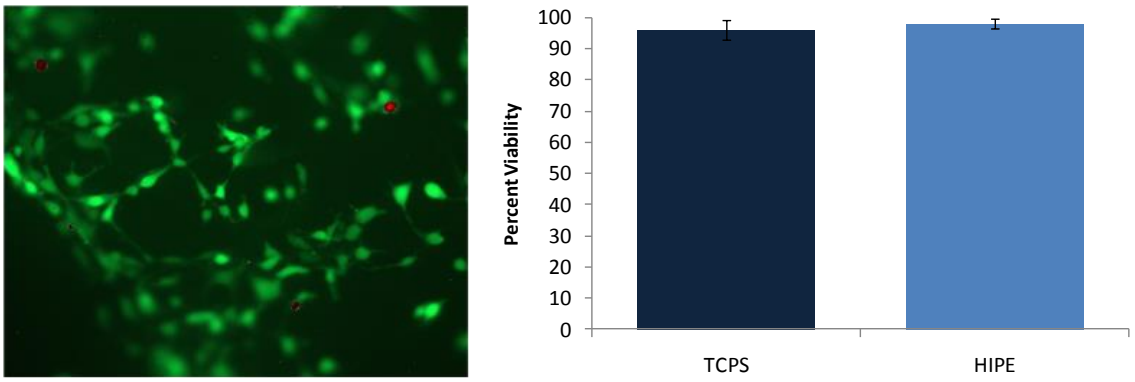

Figure 2.5. 24 hour 3T3 live/dead analysis of 5 wt% PGPR polyHIPEs. (A) Fluorescent image (green = live, red = dead) (B) Comparison of viable cells on tissue culture polystyrene and HIPE. No significant difference was observed between the polystyrene and HIPE demonstrating the potential cytocompatibility of the system.

2.3.4 Effect of PGPR Concentration on Pore Architecture Given that the polyHIPE architecture is dictated by the emulsion geometry prior to cure, modulation of emulsion stability may be used to tune the resulting polyHIPE architecture. This requires a brief review of the thermodynamics involved in both emulsion formation and phase separation. The increase in surface energy of an emulsion compared to the non-emulsified components (ΔW) is a product of both the interfacial energy (σ) and the change in surface area (ΔA) upon emulsification.

$$\Delta W = \sigma \cdot \Delta A \quad (2.2)$$

ΔW is the free energy of the interface and corresponds to the reversible work brought into the system during emulsification. The magnitude of ΔW can be considered a measure of the thermodynamic instability of the emulsion and drives phase separation as a means to decrease ΔA. From this relationship, it is evident that ultimate stability against coalescence processes is only achieved if σ approaches zero. The surfactant's

role during emulsification is to reduce this interfacial tension and form a barrier between the two phases.

Two relationships relevant to polyHIPE architecture can be inferred from this discussion: 1) an increase in interfacial tension (↑ σ) will increase the rate of droplet coalescence due to an increase in ΔW; 2) an increase in interfacial tension (↑ σ) will correspond to larger initial droplet sizes (↓ ΔA) for a given ΔW. It follows that the surfactant which directly impacts interfacial tension can be used to tune pore sizes by changing the initial droplet size and/or the rate of droplet coalescence prior to cure. To this end, Williams et al. studied the effect of surfactant concentration on both pore size and wall thickness between droplets.[67] It was reported that a reduction in surfactant concentration could be used to increase pore size by destabilizing the HIPE. In addition, an increase in surfactant concentration was found to decrease wall thickness and induce pore opening upon polymerization. We hypothesized that HIPE stability could be modulated by changing the surfactant concentration to achieve a range of polyHIPE pore sizes and an open-pore morphology. PGPR concentrations from 5 to 40 wt% were utilized to investigate the effect of surfactant concentration on polyHIPE pore architecture. SEM analysis of polyHIPE monoliths was conducted to quantify pore and interconnect size using the 10.7 pixels/μm ratio at 1000x, **Table 2.3**. Decreasing the concentration of PGPR from 20 to 5 wt% was found to increase average pore diameter in PFDMA polyHIPEs (6 to 29 μm), **Figure 2.6**. A narrowing of pore size distributions with increasing surfactant concentration was also observed, **Figure 2.7**.

Table 2.3. The effect of surfactant concentration on polyHIPE architecture.

Surfactant (wt%)	Porosity (%)	Average Pore Diameter (μm)
5	75.1 ± 0.4	29 ± 19
10	75.1 ± 0.3	21 ± 11
15	75.1 ± 0.1	14 ± 8
20	74.1 ± 0.1	4 ± 2

Gravimetric porosity, N = 3, average ± standard deviation. Average pore measurements from image analysis of scanning electron micrographs, N = 150, average ± standard deviation.

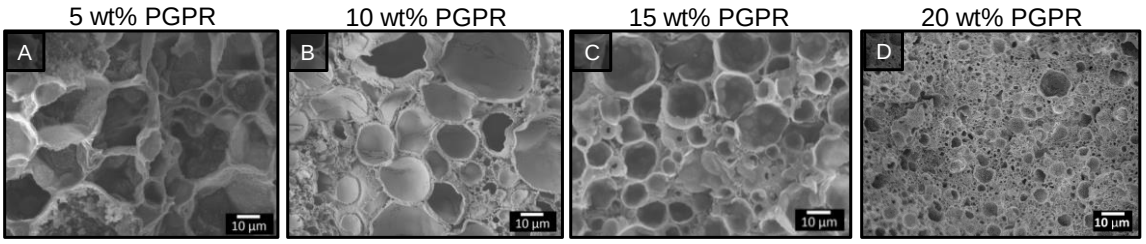

Figure 2.6. Scanning electron micrographs (A,B,C,D) of PFDMA polyHIPEs with increasing surfactant concentrations. It can be seen that pore sizes decrease as PGPR concentration increases from 5-20 wt%.

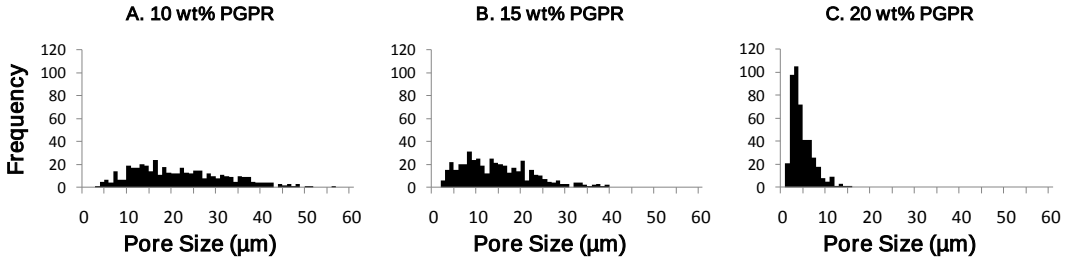

Figure 2.7. Distribution of pore sizes for 75/25 polyHIPEs with varied PGPR concentrations, mixed at 500 rpm. (A) 10 wt%, (B) 15 wt%, and (C) 20 wt%. Pore sizes become more uniform as PGPR content increases.

The decreased pore size observed at higher surfactant concentration was attributed to a decrease in interfacial tension with a corollary decrease in droplet size, as

discussed above. Assuming conservation of organic phase volume, this increase in surface area also decreases the film thickness between droplets;[111] however, this wall thinning was insufficient to lead to pore opening in this system. Based on these preliminary results, it was hypothesized that increased densification in combination with decreasing film thickness would be needed to generate open-pore polyHIPEs. This is the subject of current investigation using alternative fumarate-based macromers. A narrowing of the pore size histograms also indicated that a higher surfactant concentration resulted in a more uniform pore size, **Figure 2.7**. Williams et al. reported that increased pore size homogeneity was observed with increased surfactant due to a reduction in droplet coalescence.[67] However, the droplet coalescence observed in these studies was characterized by a few large pores surrounded by many smaller pores. As illustrated in **Figure 2.7**, there was a continuum of pore sizes observed rather than the more bimodal distribution reported by Williams et al.[67] Ostwald ripening has also been reported to increase the pore size distribution of polyHIPEs. In this process, diffusion of water from smaller droplets to larger droplets causes a more gradual broadening of the pore size distribution.[117] Both of these processes are affected by the nature and concentration of surfactant; however, it is unclear whether droplet coalescence or Ostwald ripening is responsible for the observed difference in pore size distribution. Based on the histograms alone, it appears that Ostwald ripening may be more significant; however, additional studies are needed to make a stronger claim on this front.

2.3.5 Effect of Mixing Speed on Pore Architecture Processing parameters such as mixing speed can also be utilized to tune the pore architecture through manipulation of the emulsion geometry prior to cure. Revisiting the thermodynamic stability of the system yields mechanistic answers for the effect altered mixing speed has on pore size and homogeneity. Varying the mixing speed directly affects the difference in surface energy of the emulsion relative to the non-emulsified components. By adding mechanical energy into the system through mixing, the surface energy of the emulsion is increased yielding a larger change relative to the non-emulsified components (ΔW). This causes an increase in the surface area (ΔA) of the droplets upon emulsification, assuming low interfacial tension due to surfactant (σ). This increase in surface area corresponds with decreased droplet sizes. We hypothesized that pore size and homogeneity can be modulated by altering the free energy of the system resulting in decreased pore diameters and increased homogeneity with an increase in mixing speed.

Mixing speeds of 500, 1000, and 2000 rpm on the FlackTek Speedmixer™ were tested to investigate the effect on pore architecture. Initially, HIPEs with 20 wt% PGPR were utilized resulting in minimal change in pore size with an increase in mixing speed as seen in **Table 2.4**. We hypothesized that destabilizing the emulsion with a lower concentration of PGPR would result in a larger pore size distribution, thereby clearly illustrating the effect of mixing speed. Scanning electron micrographs of both 10 and 20 wt% PGPR compositions at varying mixing speeds are found in **Figure 2.8**. A decrease in pore size was observed with both 10 and 20 wt% PGPR specimens as mixing speed was increased (500 to 2000 rpm). As discussed, the trend was more evident with the 10

wt% PGPR specimens, **Table 2.4**, and further illustrates the effect of surfactant on emulsion stability and pore architecture. The narrowing of the histograms in **Figure 2.9** from 500 to 2000 rpm indicates a more homogeneous pore size distribution which is illustrated in the SEM images. As stated previously, increased surfactant produced an increase in pore homogeneity due to decreased surface energy. Combining both mixing speed and surfactant had a large effect on pore size homogeneity as observed in **Figure 2.9** by increasing the surface area of the emulsion and decreasing the interfacial energy of the droplets, respectively, to reduce droplet size and coalescence.

Table 2.4. The effect of mixing speed on polyHIPE pore structure with a constant volume fraction (75/25) and varied surfactant concentration (10 and 20 wt% PGPR).

Mixing Speed (rpm)	[PGPR]	Average Pore Diameter (μm)
500	10 wt%	21 ± 11
	20 wt%	4 ± 2
1000	10 wt%	8 ± 4
	20 wt%	3 ± 2
2000	10 wt%	4 ± 3
	20 wt%	2 ± 1

Average pore measurements from image analysis of scanning electron micrographs, N = 150, average ± standard deviation.

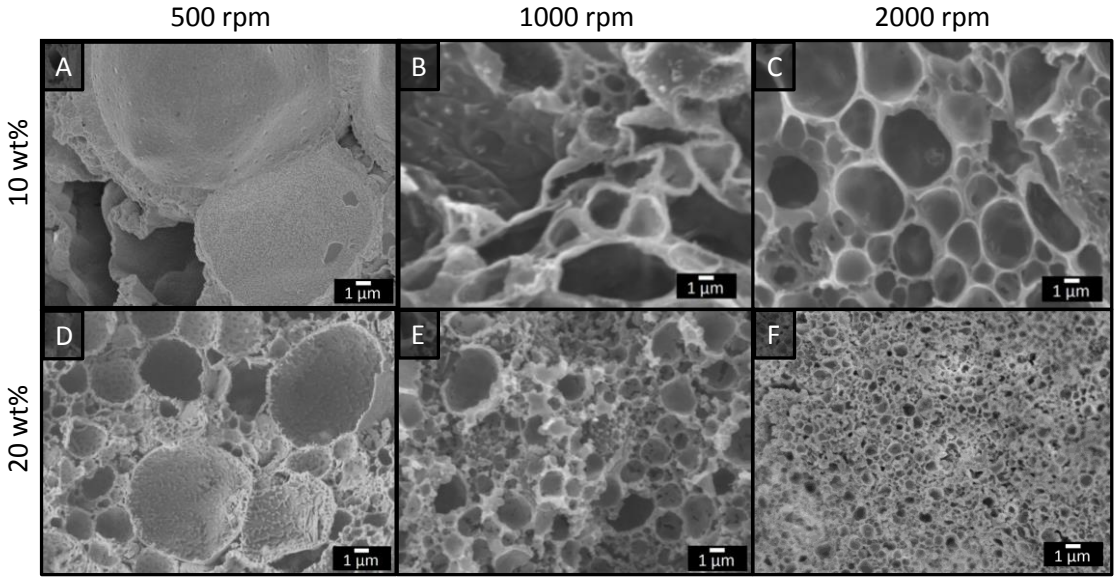

Figure 2.8. Scanning electron micrographs of PFDMA polyHIPEs fabricated at increasing mixing speeds. (A-C) 10 wt% PGPR (A) 500 rpm (B) 1000 rpm (C) 2000 rpm, (D-F) 20 wt% PGPR (D) 500 rpm (E) 1000 rpm (F) 2000 rpm. A decrease in pore size is seen with an increase in mixing speed.

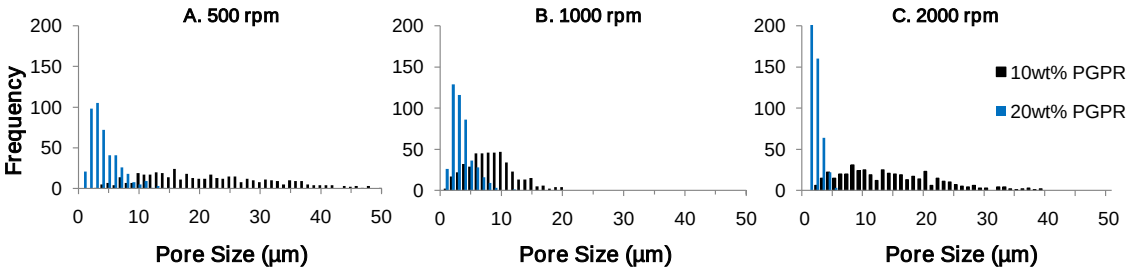

Figure 2.9. Distribution of pore sizes for 75/25 polyHIPEs fabricated with 10 (black) and 20 wt% PGPR (blue) at 500, 1000, and 2000 rpm.

2.4 Conclusions

The application of emulsion templating in the development of tissue engineering scaffolds is a relatively new area of orthopedic research. In this study, polyHIPEs were fabricated without toxic solvents or monomers at cure temperatures appropriate for *in*

situ deployment. These new polyHIPEs have potential application as an injectable, tissue engineered bone graft. Injectable grafts that are also biodegradable and porous offer unique advantages over current alternatives in terms of deployment and tissue integration. In addition, investigation of the effect of surfactant structure on HIPE stability elucidated additional structural features that can be used to rationally select surfactants for new polyHIPE compositions. This transition from a time-intensive trial and error method of selecting surfactants will facilitate additional biodegradable polyHIPE formulations with utility in a wide range of tissue engineering applications.

CHAPTER III

INJECTABLE POLYMIPE SCAFFOLDS FOR SOFT TISSUE REGENERATION[†]

3.1 Introduction

Injury caused by trauma, burns, surgery, or disease often results in soft tissue loss, most commonly skin, muscle, adipose, and cartilage.[139] These tissues have unique properties that drive various functions such as: supporting vasculature, body locomotion, and impact protection.[23, 139] The lack of viable donor tissue to treat these injuries often results in scarring and impaired function. Tissue engineering aims to improve on current options through the use of a porous scaffold combined with stem cells and bioactive factors that are designed to regenerate the damaged tissue. Scaffolds have been fabricated using a variety of polymers to restore the function and regenerate these tissues; however, clinical success is often limited by poor graft properties.[23-26, 75, 140, 141]

Soft tissue scaffolds are often designed to have tunable moduli and strengths comparable to the target tissue.[4, 142-144] A common feature of soft tissue that is often poorly replicated in scaffolds is elasticity and an ability to withstand repeated loading without loss of function.[8, 24, 26, 145] Improved biomaterial scaffolds should be designed to match tissue modulus and strength while also retaining desired elastomeric and fatigue-resistant properties. In addition, these materials need to support cells and growing tissue, typically with an interconnected porous structure and biodegradable chemistry.[44, 146-148]

[†] Reprinted with permission from "Injectable PolyMIPE Scaffolds for Soft Tissue Regeneration," by Robert S. Moglia, Jennifer L. Robinson, Andrea D. Muschenborn, Tyler J. Touchet, Duncan J. Maitland, and Elizabeth Cosgriff-Hernandez, Polymer 2014, 55 (1), 426-434. Copyright (2014) Elsevier.

Of particular design importance is the interconnected porous structure of the scaffold, which facilitates mass transport. This is especially true for newly implanted scaffolds that lack vasculature to support tissue and cells. The size of a tissue engineered construct is constrained by the diffusion limit of nutrients to cells at the center of the construct.[129, 149] Porosity and pore size need to be easily modulated in a tissue engineered scaffold to allow for increased fluid permeability, and thus nutrient flux, in order to enable larger defects to be regenerated.[129]

Tissue engineers have developed numerous fabrication strategies to create 3D scaffolds that meet these various requirements.[12, 14, 16, 17, 44, 109, 146, 147, 150, 151] The fabrication process dictates scaffold architecture and the resultant mechanical properties, degradation rate, and cellular response. These methods often utilize toxic solvents and high temperatures or pressures during fabrication.[56, 65, 108, 109] The scaffolds must then be purified and shaped to fit the defect, commonly with the use of computer generated molds made from clinical imaging techniques.[38, 45, 152] Molds are reliant upon the accuracy of the images, increase cost, and delay patient treatment. Research has shown that *in situ* forming scaffolds can better fill irregularly shaped defects, thus improving contact with surrounding tissue and eliminating the need for costly molding techniques.[87] An elastomeric, biodegradable, and porous scaffold that can be fabricated at body temperature without the use of toxic components could be injected into the defect without the need for extensive imaging or mold casting and can potentially improve tissue regeneration beyond current methods. Hydrogel scaffolds have been studied as injectable scaffolds because their mechanical properties approximate soft

tissues, but they typically have 10-100 nm mesh sizes that limit cellular infiltration and migration to the rate of scaffold degradation.[153] Hydrogels with larger pores have also been fabricated, but are commonly non-biodegradable or non-injectable.[154] Polyurethane foams have recently been formed *in situ* by injecting isocyanates and polyols which react rapidly to conform to the defect.[155] In animal studies, this material successfully regenerated bone tissue without notable toxicity or inflammation in the surrounding tissue despite injecting isocyanates directly into the defect site.[155] Other researchers have conducted animal studies of injectable two-component polyurethane foams and found mild short-term side effects.[156]

Emulsion templating can be used to generate an injectable graft that cures to a porous foam *in situ*. Emulsions with water volumes between 40-74% are termed medium internal phase emulsions (MIPEs), the polymerized form is termed a polyMIPE. Prior to curing, the emulsion has a mayonnaise-like consistency capable of flow through a syringe and space-filling irregularly shaped defects.[157] Historically this technique required the use of toxic solvents to control macromer viscosity or high cure temperatures.[35, 36, 45, 71, 134] Our lab recently fabricated emulsion templated scaffolds without solvent that cure at body temperature and are biodegradable.[157] Successful deployment through a syringe with microscale integration in a bone defect was also demonstrated.[158] The properties of these injectable foams can be tuned by altering pore size, porosity, composition, and macromer/polymer chemistry.

This study details the fabrication and characterization of poly(ester urethane urea) based polyMIPEs as candidates for soft tissue scaffolds. The compositional effects

on polyMIPE pore architecture and mechanical properties were determined to illustrate the range and control of scaffold properties. The porous media properties, permeability and form factor, were also measured in order to better compare pore interconnectivity of several compositions. Finally, human mesenchymal stem cell (hMSC) viability and morphology was studied as an early indicator of whether these scaffolds can support tissue regeneration.

3.2 Materials and Methods

3.2.1 Materials Polyglycerol polyricinoleate (PGPR 4125) was donated by Paalsgard. All other chemicals were purchased from Sigma-Aldrich and used as received.

3.2.2 PCL-Isocyanate Synthesis Isocyanate functionalized prepolymers were synthesized in bulk. Briefly, polycaprolactone (PCL) diol or triol (530, 900 Mn respectively) was heated with 50°C air and added dropwise to a reaction flask charged with hexamethylene diisocyanate (HDI, 2.02 x mol diol, 9.00 x mol triol), **Figure 3.1**. The reaction was heated to 80 °C for 90-120 minutes and reaction progress was monitored with FTIR spectroscopy every 30 minutes until complete. The product was washed with hexane to remove excess HDI and dried under vacuum overnight. The final products were colorless liquids with a viscosity similar to honey. The prepolymer structure was confirmed using ^{1}H NMR (300 MHz, $CdCl_3$): PCL-diisocyanate (PCL-DI) δ 1.33-1.47 (m, 8H), 1.52 (q, 4H), 1.60-1.75 (m, 8H), 2.30-2.40 (m, 4H), 3.18 (s, 2H), 3.33 (q, 2H), 3.70-3.73 (m, 2H), 4.09 (t, 4H), 4.24-4.27 (m, 2H), 4.77 (s, 1H). PCL-

triisocyanate (PCL-TI) δ 0.91(t, 3H), 1.33-1.52 (m, 8H), 1.60-1.75 (m, 8H), 2.31-2.38 (m, 4H), 3.18 (s, 2H), 3.33 (m, 2H), 4.04-4.11 (m, 4H), 4.74 (s, 1H).

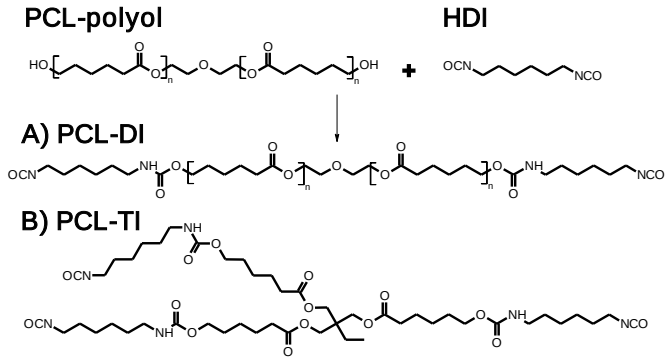

Figure 3.1. Chemical structures of PCL-isocyanate polyurethane prepolymers. PCL-polyols are functionalized with HDI in bulk to synthesize isocyanate terminated macromers. (A) PCL-diisocyanate (PCL-DI) and (B) PCL-triisocyanate (PCL-TI).

3.2.3 MIPE Fabrication PCL-DI and –TI were mixed with the surfactant PGPR in a 3-necked round bottom flask prior to emulsification. This mixture was stirred with a glass stirring rod fitted with a D-shaped PTFE paddle connected to an overhead stirrer motor for 10 minutes. The aqueous solution, comprised of varied amounts of 1,4-diazabicyclo[2.2.2]octane (DABCO) and calcium chloride (1% v/v) in reverse osmosis water, was added at a rate of 1 mL/min using a syringe until it totaled 50% v/v, while constant stirring at 300 rpm was maintained. The emulsion was stirred for 10 additional minutes to ensure emulsion homogeneity. The MIPE was then transferred to a 50 mL polypropylene tube and immersed in a bead bath at 37 °C for 48 h. All specimens were dried *in vacuo* at room temperature for 24 h prior to characterization, **Figure 3.2**.

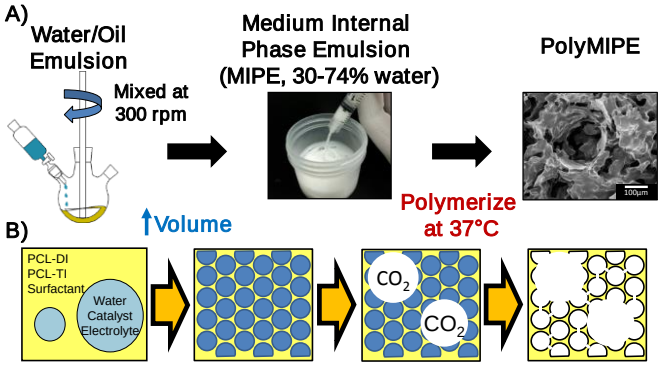

Figure 3.2. PolyMIPE fabrication scheme. **(**A) The isocyanate macromers were mixed with surfactant while water was added to form medium internal phase emulsions. The MIPEs viscosity allows them to be injected through a syringe prior to polymerizing in the body. (B) The isocyanates react with water to produce primary amines and carbon dioxide, increasing porosity beyond the aqueous volume fraction, a limiting factor for typical styrene-based polyMIPEs.

3.2.4 Gravimetric Analysis PolyMIPE porosity was measured gravimetrically. Briefly, dried MIPE samples were cut into cubic sections (9 × 9 × 3 mm) and weighed. Following eq (1), the MIPE porosity can be calculated by comparing MIPE density (ρ_M) with the neat polymer density (ρ_P). Neat polymer density was assumed to equal 1 g/cm^3, a reasonable value for polymers. Reported values are an average of nine sections per polyMIPE composition.

$$(3.1) \qquad Porosity = 1 - \frac{\rho_M}{\rho_P}$$

3.2.5 Characterization of Scaffold Architecture Scanning electron microscopy (SEM) was utilized to characterize polyMIPE pore architecture. Circular specimens were sectioned into quarters, fractured at the center of the quarter, sputter-coated with gold, and imaged using SEM (JEOL NeoScope JCM-5000). Images at 20× were utilized to determine the average void diameter and 50x to measure water template pores, **Figure**

3.3. Three specimens of each composition were generated and then three sections were cut from each monolith. Three horizontal lines were drawn across the image, dissecting it into four equal rectangles. Starting with the topmost mark, measurements were made on the first 10 voids crossed by the lines to minimize user bias. Averages void sizes for each polyMIPE composition are reported (n = 90). Water pores/interconnects were measured similarly except that 30 pores/openings were measured per image, average interconnects per composition are reported (n = 270). A statistical correction was calculated to account for the random fracture plane through spherical voids and pores, $2/\sqrt{3}$.[159] The average diameter values were multiplied by this correction factor resulting in a more accurate description of pore diameter.

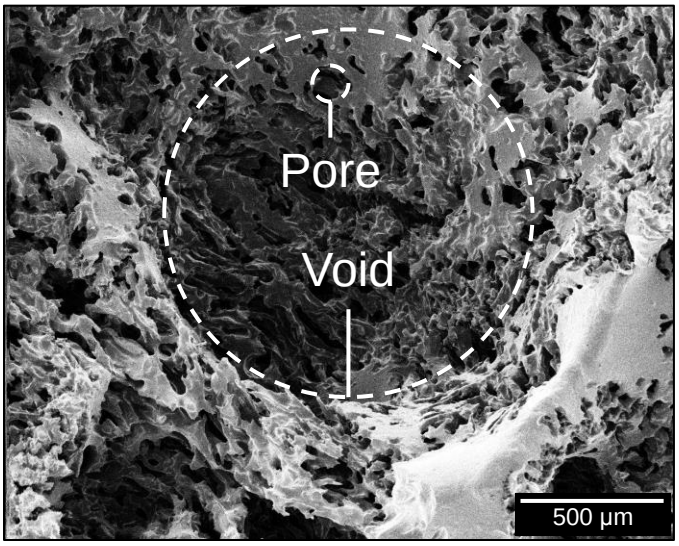

Figure 3.3. SEM comparing voids and pores observed in polyMIPE scaffolds.

3.2.6 Compression Testing The foams were tested in compression with an RSA III (TA, Delaware) dynamic mechanical analyzer, equipped with a 30 N load cell. Four

specimens were taken from each sample. The test specimens were cut into flat rectangular shapes (10 × 10 × 4 mm) and compressed at 50 μm/s. Tangent modulus was calculated at 5% strain and strength at 20%. Reported moduli data were an average of the three sections for each sample tested (n = 12).

3.2.7 Cyclic Loading and Strain Recovery Samples were subjected to three compressive loading–unloading cycles from 0 to 50% strain and back to 0% at 50 μm/s (~1 %/s). The dimensions (diameter and height) of the samples were measured with calipers after each cycle to ensure that the stress–strain curves always started from the new unloaded specimen height. The samples rested for 2-3 minutes between cycles as dimensions were measured and samples re-positioned on the compression platen. New sample height was divided by the previous cycle height to calculate strain recovery.

3.2.8 Permeability Testing Scaffold interconnectivity was characterized by measuring their respective intrinsic/Darcy's permeability using the Forchheimer-Hazen-Dupuit-Darcy equation:

$$-\frac{\partial P}{\partial x} = \frac{\mu}{K} v_0 + \rho C v_0^2 \quad (3.2)$$

where $-\frac{\partial P}{\partial x}$ is the pressure gradient along the sample in the direction of flow (Pa/m), μ is the dynamic viscosity of the fluid (Pa·s), K is the intrinsic permeability of the (scaffold, sample) (m^2), v_0 is the Darcy velocity (flow rate divided by cross-sectional area of the (scaffold, sample)) (m/s), ρ is the density of the fluid (kg/m^3), and C is the form factor of the (scaffold, sample) (m^{-1}). The experimental details for measuring the permeability and form factor of porous polymers have been described elsewhere by

Muschenborn et al.; briefly, MIPEs were polymerized inside 3D printed sample holders (inner diameter = 15.1 mm, outer diameter = 18.9 mm) containing three 4 × 4 mm pressure port openings, 15 mm apart from one another.[160] The sample holders had o-rings to isolate each pressure port. Each sample holder was then inserted into a custom-built measuring chamber, and two pressure transducers (PX429-2.5G5V, Omegadyne Inc) were connected at the upstream and downstream pressure port locations. Water flow at room temperature was enabled via a gear pump (Chemsteel R106, Oberdorfer), a servo motor (750 W M-series, Applied Motion Products), and a motor controller (BLuAC5-Q, Applied Motion Products). The output voltage of the pressure transducers was recorded at 1 Hz through a data acquisition system (USB6251, National Instruments) for 120 seconds. The flow rate was measured by hand using a stop watch and a graduated cylinder. A second-order least squares fit to the data of pressure gradient plotted against Darcy velocity was implemented for nine values to calculate the samples' porous media properties, permeability and form factor.[160] The Reynolds number at each velocity point was calculated as the ratio of the second term to the first term on the right side of Equation 3.2.[161]

3.2.9 Cytocompatibility Initial hMSC viability and morphology studies were conducted on 2:1 PCL-DI:PCL-TI films and 50% PCL-DI : 50% PCL-TI polyMIPEs to assess cytocompatibility. Cell viability was determined using the Live/Dead Viability/Cytotoxicity Kit (Molecular Probes) and morphology accessed by imaging cells stained with CellTracker™ Orange (Molecular Probes). The hMSCs were obtained from the Center for the Preparation and Distribution of Adult Stem Cells at Texas A&M

Health Science Center College of Medicine and cultured *in vitro* with Minimal Essential Medium α (MEM α, Gibco) supplemented with 16.5% heat-inactivated fetal bovine serum (FBS, Atlanta Biologicals), and 1% L-Glutamine (200 mM, Gibco). Cells were cultured to 80% confluency and utilized at Passages 4-5. Samples were prepared for cell seeding as follows: 3 hour 70% ethanol sterilization, ethanol wetting ladder and progressive solvent extraction, and overnight media incubation supplemented with 40% v/v FBS in MEM α. Following overnight incubation in 37 °C, 5% CO_2, medium was removed, specimens were dried in the hood for 15 min, washed 1× with PBS, and preconditioned with growth medium for 15 min. Cells were seeded at 5,000 cells/film and 100,000 cells/foam. Live/Dead staining was conducted at 3, 24, and 72 hours and cell adhesion and morphology on foams was assessed at 3 and 24 hours. For viability analysis, images of each of the four specimens were obtained through Raster patterning (n = 20) for each timepoint using a fluorescence microscope (Nikon Eclipse TE2000-S). Observation of hMSC morphology was completed with one sample imaged with rastor patterning ($n = 5$) at each timepoint.

3.2.10 Statistical Analysis The data are displayed as mean ± standard deviation for each composition. A Student's *t* test was performed to determine any statistically significant differences between compositions. All tests were carried out at a 95% confidence interval ($p < 0.05$).

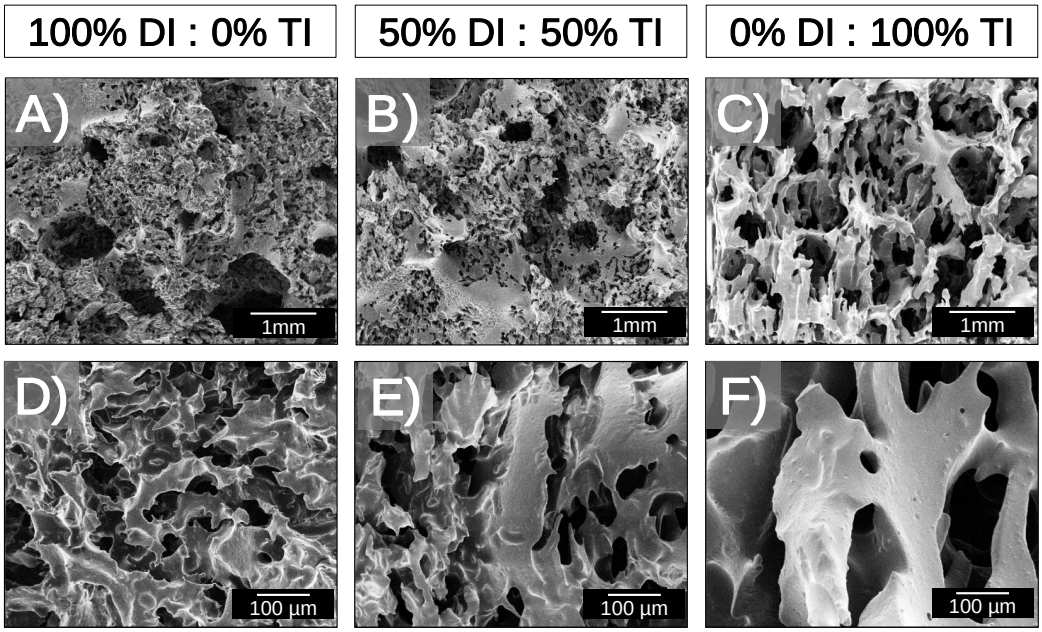

Figure 3.4. Scanning electron micrographs of the polyMIPE scaffolds indicated an open-pore interconnected structure. A bimodal pore distribution was also observed due to the difference in pores formed by (A,B,C) carbon dioxide generation and those resulting from (D,E,F) water templating.

3.3 Results and Discussion

3.3.1 Pore Architecture All of the scaffolds exhibited a bimodal pore structure composed of discrete 1-2 mm voids surrounded by 30-400 µm pores, **Figure 3.4** and **Figure 3.5**. The pore size remained relatively unchanged despite large differences in void diameter between compositions. Increased PCL-TI concentration significantly increased void size once it exceeded 50%, from 1 to 1.3 mm. This phenomena was observed by David and Silverstein in a similar system and hypothesized to be caused by side products of urea formation.[109] Briefly, the isocyanate functional groups react with the encapsulated water to form amine end groups with the liberation of carbon dioxide. These amine end groups react rapidly with remaining isocyanates to form urea linkages

in the resulting polymer network. David and Silverstein determined that the large pores were caused by carbon dioxide and the smaller pores formed by water droplets.[109] They hypothesized that carbon dioxide would separate from both the organic and aqueous phases, merge, and form the observed voids.[109] This is consistent with the present study, except the water-templated pores are not as clearly defined. Instead, the walls of the voids are porous with irregular interconnects between them, **Figure 3.4 D,E,F**. The oblong shapes of these interconnects indicate that the emulsion is relatively unstable and is undergoing droplet coalescence, whereas stable emulsions would result in spherical pores.[56, 109] Additionally, some interconnects appear to be torn open. This is most likely the result of carbon dioxide escaping from the polymerizing emulsion after the pore walls had mostly gelled.

The effect of catalyst concentration on pore structure was also evaluated and the results summarized in **Table 3.1**. Void size decreased from ~ 0.9 to 0.7 mm with increased DABCO concentration. The increased cure rate from higher DABCO amounts was hypothesized to cause rapid polymer wall strengthening that better resisted expansion from carbon dioxide production and forced the gas to find existing exit paths and thus form smaller voids. Foaming in polyurethane foams has long been studied for industrial and commercial uses. Anti-foamers (or pore openers) have been used to prevent or control foam cell production and size.[162-164] The Guelcher group has used calcium stearate pore openers in their injectable bone grafts to form interconnects and tune pore size.[70, 162, 163, 165] Although it was not studied here, a biocompatible pore opener could potentially be used to homogenize void sizes in this injectable system.

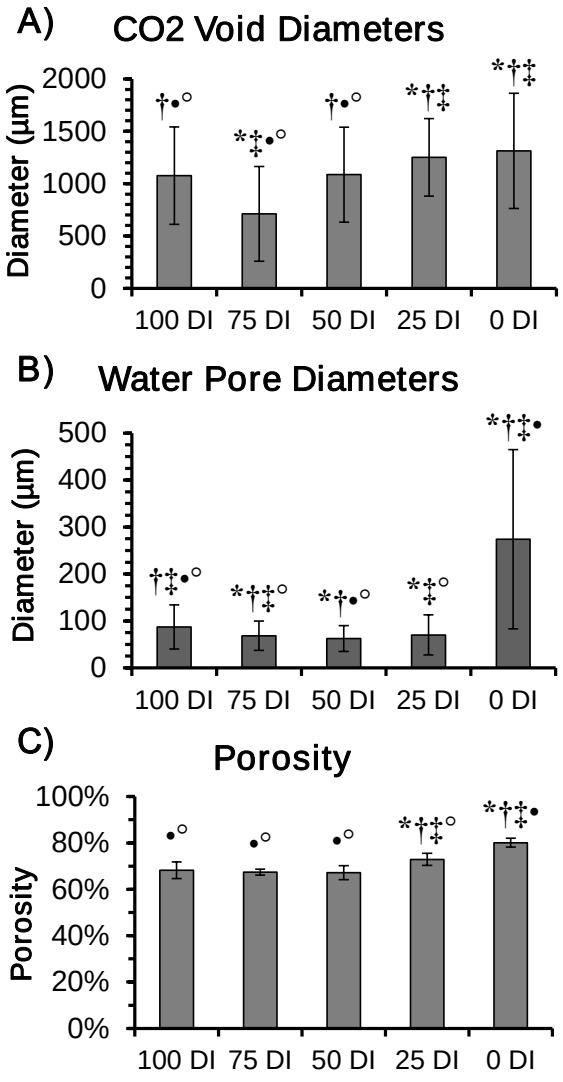

***** : $p < 0.05$ compared to 100% PCL-DI
† : $p < 0.05$ compared to 75% PCL-DI
‡ : $p < 0.05$ compared to 50% PCL-DI
• : $p < 0.05$ compared to 25% PCL-DI
° : $p < 0.05$ compared to 0% PCL-DI

Figure 3.5. (A) Average CO2 void diameters, (B) average pore diameters, and (C) average porosities of polyMIPEs with varied PCL-DI : PCL-TI ratio and constant water volume fraction.

The effect of catalyst concentration on pore structure was also evaluated and the results summarized in **Table 3.1**. Void size decreased from ~ 0.9 to 0.7 mm with

increased DABCO concentration. The increased cure rate from higher DABCO amounts was hypothesized to cause rapid polymer wall strengthening that better resisted expansion from carbon dioxide production and forced the gas to find existing exit paths and thus form smaller voids. Foaming in polyurethane foams has long been studied for industrial and commercial uses. Anti-foamers (or pore openers) have been used to prevent or control foam cell production and size.[162-164] The Guelcher group has used calcium stearate pore openers in their injectable bone grafts to form interconnects and tune pore size.[70, 162, 163, 165] Although it was not studied here, a biocompatible pore opener could potentially be used to homogenize void sizes in this injectable system.

Table 3.1. Effect of catalyst and PCL-TI crosslinker on cure time, pore sizes, and porosity.

DABCO (wt %)	PCL-DI (wt %)	PCL-TI (wt %)	Tack Free Time (hours)	Void Size (μm)	Water Pore Size (μm)	Porosity (%)
0	75	25	5.5	1021 ± 583 °	181 ± 230 †‡•°	70 ± 6 °
0	50	50	5.0	881 ± 454 •°	101 ± 60 *‡•°	70 ± 2 ‡•°
0	25	75	5.5	919 ± 386 •°	131 ± 99 *†•	73 ± 4 †•°
0.1	50	50	4.5	1086 ± 454 ‡°	62 ± 28 *†‡°	67 ± 2 †‡°
1	50	50	4.0	721 ± 264 *†‡•	127 ± 71 *†•	64 ± 2 *†‡•

***** : $p < 0.05$ compared to 75% PCL-DI, 0% DABCO
† : $p < 0.05$ compared to 50% PCL-DI, 0% DABCO
‡ : $p < 0.05$ compared to 25% PCL-DI, 0% DABCO
• : $p < 0.05$ compared to 50% PCL-DI, 0.1% DABCO
° : $p < 0.05$ compared to 50% PCL-DI, 1% DABCO

3.3.2 Scaffold Porosity A benefit of the carbon dioxide blowing process is increased porosity, as evidenced by polyMIPE expansion during polymerization. In traditional emulsion templating, porosity is limited by the template volume fraction, 50%

in this study. However, due to foaming, these polyMIPE porosities ranged from 64-76%, Figure 5C, while higher porosity scaffolds could be fabricated they often exhibited poor mechanical properties. Porosity increased with PCL-TI content due to the increase in total isocyanate groups, and decreased with increased catalyst concentration. For example, a MIPE with 100% PCL-TI would have approximately 1.25x the number of isocyanates of a 100% PCL-DI emulsion. Increasing catalyst concentration, from 0 to 1 wt%, for a 50% PCL-TI polyMIPE decreased porosity from 70 to 64%. This corresponded with a decrease in void size from approximately 881 µm to 721 µm while water pore size did not follow any trend. This decrease in porosity was not attributed to reduced carbon dioxide generation given that the total number of isocyanates was constant which indicates that the carbon dioxide generation was most likely unchanged. The increase in catalyst was hypothesized to increase polymer film strength more rapidly, thus resisting carbon dioxide void expansion and decreasing total porosity. These results indicate that changing isocyanate content or reaction rate with catalyst could be used to modulate scaffold porosity and expansion *in situ* through control of the carbon dioxide blowing mechanism. Researchers have shown that increasing scaffold porosity increases cell viability and growth.[71, 72, 75, 77, 79, 80, 83] Also, the expansion could help the graft "space fill" the defect, improving tissue integration.[35, 38, 45, 70, 157, 163] There is concern over the safety of carbon dioxide blowing *in vivo* resulting from reacting isocyanates into the human body. Recently, researchers have safely injected foaming isocyanate-functionalized prepolymers for a variety of applications and no deleterious side effects were noted in relation to the presence of free-isocyanates or the blowing

process.[155, 156, 162, 165] Similar to pore size, porosity of polyurethane foams has been studied extensively and can be further controlled using methods beyond the scope of this study.[164]

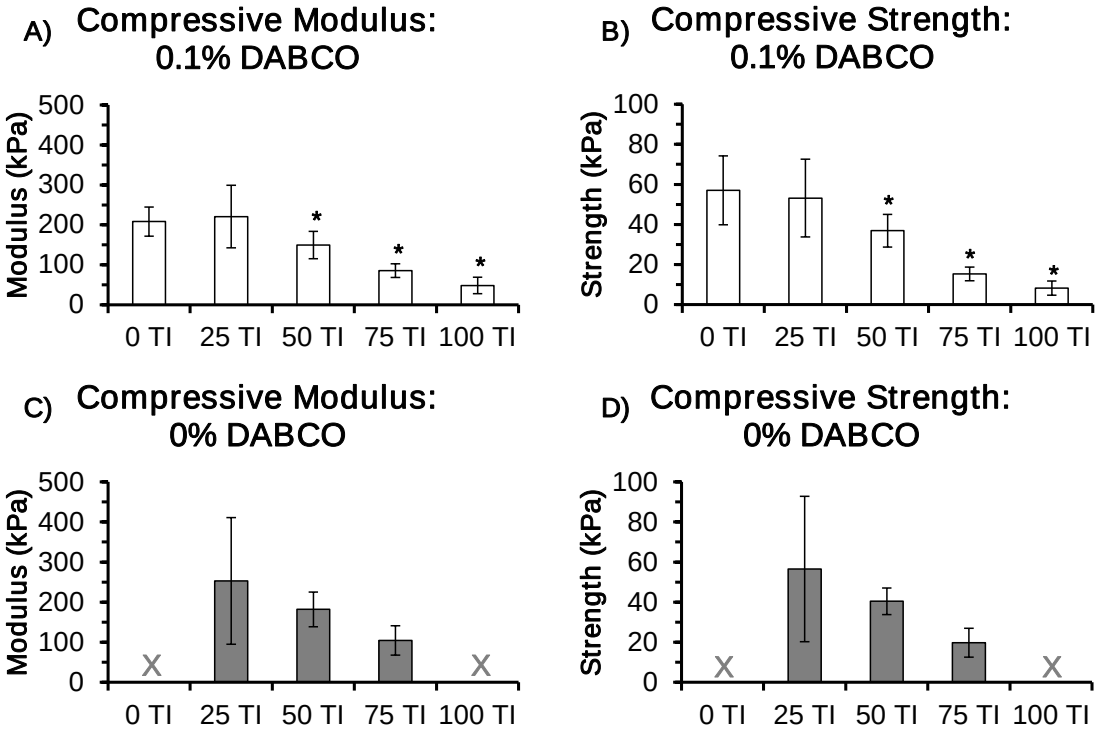

***** : $p < 0.05$ compared to all other compositions
† : $p < 0.05$ compared to 25% PCL-TI, 0.1 wt% DABCO
‡ : $p < 0.05$ compared to 75% PCL-TI, 0.1 wt% DABCO

Figure 3.6. (A) Compressive modulus and (B) strength of polyMIPEs with increasing PCL-TI content (0.1 wt% DABCO). (C) Compressive modulus and (D) strength of polyMIPEs without DABCO.

3.3.3 Mechanical Properties PolyMIPE compressive modulus and strength decreased with decreasing PCL-DI content. The 100 and 75% PCL-DI with 0.1 wt% DABCO were the stiffest and strongest compositions tested, with a modulus and strength

approximately 215 and 55 kPa, respectively (**Figure 3.6**). These values decreased steadily to 48 and 8 kPa as PCL-TI was increased to 100%. The greatest change occurred when 75% TI was reached, afterwards modulus and strength decreased by nearly half of the 50% TI values. Catalyst concentration did not have a significant effect on the properties of the 25, 50, and 75% PCL-TI scaffolds, with the 0 (**Figure 3.6C** and **Figure 3.6D**) and 0.1% (**Figure 3.6A** and **Figure 3.6B**) compositions behaving near identically. However, the uncatalyzed 25% PCL-TI polyMIPEs were less consistent than their catalyzed counterparts, as evidenced by the large standard deviation. Furthermore, the 100% PCL-TI and 100% PCL-DI polyMIPEs were too macroporous to make mechanical specimens, represented by '**X'** in **Figure 3.6**.

The reductions in compressive modulus and strength with increasing PCL-TI content was not anticipated given the increase in crosslink density that is typically observed with higher macromer functionality. The observed trend corresponded with increases in pore size and porosity. However, the difference between the strongest and weakest scaffolds was a five-fold change with only a 13% increase in porosity. Therefore, the change in porosity is unlikely to be solely responsible for the reduction in compressive properties. It was hypothesized that the PCL-TI disrupted secondary chain interactions within the polymer network, specifically changes in crystallinity and hydrogen bonding. The PCL-diol and –triol are semicrystalline with melting temperatures of 7 (37% crystalline) and 21 °C (29% crystalline), respectively, as determined with differential scanning calorimetry. Upon endcapping the macromers with isocyanate groups, PCL-DI becomes more crystalline as evidenced by increased

viscosity and opacity, whereas the PCL-TI displayed a reduction in crystallinity becoming less viscous and transparent. Hydrogen bonding between the newly formed urethane linkage is also more favorable in the linear PCL-DI.[166] The steric hindrance of the branched PCL-TI structure most likely prevents intra-chain hydrogen bonding and impedes inter-chain hydrogen bonding and crystal formation. Additional physical crosslinking occurs after polymerization due to the formation of urea linkages that can undergo bidentate hydrogen bonding.[146] Bidentate bonds form between the two active hydrogens and the nitrogen of the urea linkages and thus result in stronger hydrogen bonding when compared to urethane linkages with only one active site. This hypothesis was supported by FTIR spectral analysis of hydrogen bonding of the urethane and urea carbonyls of the polyMIPE scaffolds. Peaks assigned to the free, hydrogen bonded, and bidentate hydrogen-bonded urea carbonyls (1680, 1654, 1625 cm^{-1} respectively) were used to assess relative levels of hydrogen bonding. PCL-TI rich polyMIPEs displayed a reduction of 1625 cm^{-1} peak indicating a reduced level of hydrogen bonding.

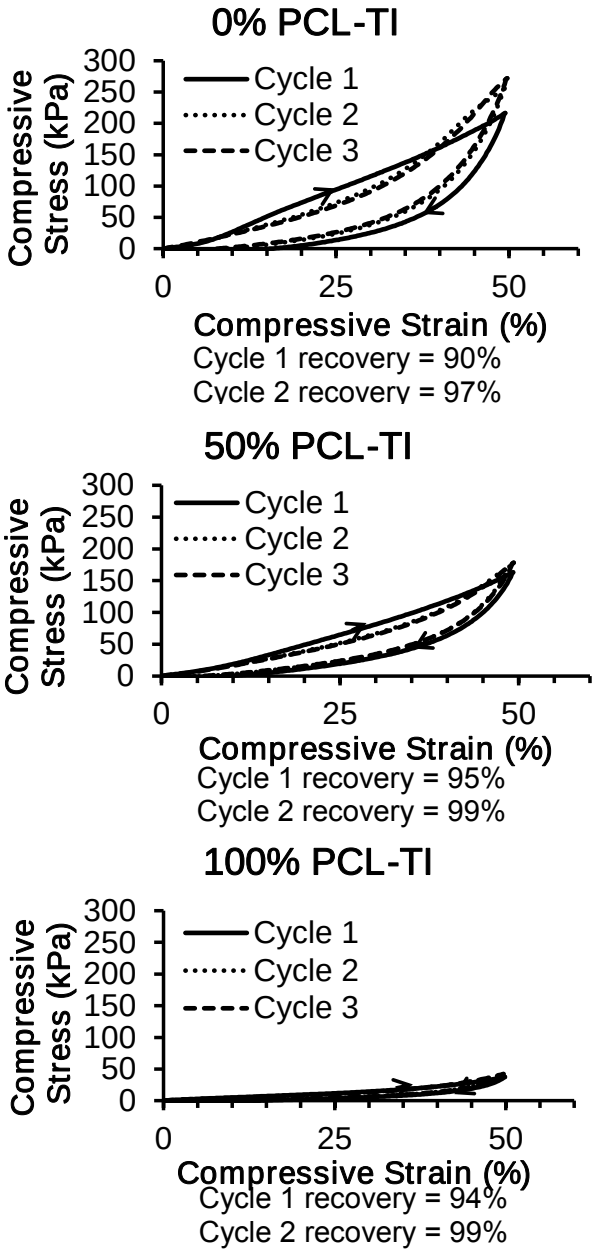

Figure 3.7. Representative loading-unloading curves for (A) 0%, (B) 50%, and (C) 100% PCL-TI polyMIPEs with 0.1 wt% DABCO.

Initial strain recovery increased with PCL-TI content, and approached 100% upon subsequent loading, **Figure 3.7**. These properties allowed the scaffolds to recover

from large strains, as can be seen in the video file included with supplementary information. The 100% PCL-DI samples exhibited the lowest initial recovery of the catalyzed scaffolds, approximately 90%, and the highest recovery was found with the 50% PCL-DI scaffolds, approximately 95%. All initial strain recoveries were equal to or greater than 90% for all scaffolds tested. Subsequent strain recoveries were always higher than the initial values, commonly approaching 100%. Subsequent recovery, like initial recovery, improved with increased PCL-TI content. Likewise, hysteresis between the loading and unloading curves decreased with subsequent loading and PCL-TI content. This behavior is similar to conditioning seen in other polyurethane materials and characteristic of the "Mullin's effect".[167-170]

The observed decrease in hysteresis and increased strain recovery after the first cycle is most likely due to chain reorganization during compression. Strain first breaks physical crosslinks in the network, predominantly hydrogen bonding between urethane and ureas in these foams, prior to loss of chemical crosslinks. In a series of loading cycles, the first conditioning cycles generates a new network with permanent set associated with the loss of these physical bonds. Subsequent cycles do not exceed the strain needed to cause further loss of netpoints and therefore have a high level of strain recovery. Similar phenomena have been observed in polyurethanes under tensile strain.[167, 170-172] This behavior was most pronounced in the PCL-DI rich compositions, which exhibited the lowest initial strain recovery and largest hysteresis, due to the increased hydrogen bonding observed in these chains. PCL-TI also exhibited this behavior to a lesser extent, with almost no hysteresis, due to the increase in covalent

crosslinking and reduced hydrogen bonding of the PCL-TI network. Overall, these properties are similar to many soft tissues in the body and can be tuned to closely match them by changing the ratio of branched crosslinkers to linear chain extenders.[24, 173] Furthermore, these properties mimic those of injectable hydrogels with the advantage of being porous and elastomeric.[23, 24, 141, 152, 174]

3.3.4 Scaffold Permeability Several researchers have attempted to determine the ideal pore size for tissue engineered scaffolds by comparing scaffold properties with *in vivo* and *in vitro* studies. The majority found that porosities between 57 and 75% with 80-500 μm pores regenerated tissue *in vivo*.[71-83] However, results are often contradictory and may be specific to cell type. For example, a more metabolically active cell may need a higher nutrient flux that corresponds with a more permeable scaffold. As such, researchers have been maximizing porosity with the assumption that fluid permeability and nutrient flux will increase beyond the limits of diffusion and allow larger defects to be treated. Pore interconnectivity and fluid permeability are inherently linked and can be quantified in many ways, including Darcy's permeability constant.[91, 128] Permeability is mathematically related to pore size, porosity, and tortuosity. Tortuosity is a unit-less measure of the fluid path length through the porous medium relative to the end-to-end path length, with lower values correlating to an increase in pore interconnectivity.[175] Several researchers have studied permeability in tissue engineered scaffolds to find relationships between pore structures and cell/tissue viability.[129] Darcy's permeability constant can be related to solute diffusion, and thus cell viability for similar scaffold geometries and types.[91, 128, 129]

Permeability and form factor are constitutive geometrical parameters of the porous medium and depend on the energy losses that arise when a fluid flows through it.[176-178] These losses are due to viscous forces and inertial drag that result from the fluid's resistance to motion and friction as it flows over the porous scaffold. Thus, permeability is inversely proportional to the surface area of contact between the solid and the fluid, and form factor is proportional to the projected cross-sectional area of the obstructing solid perpendicular to the direction of the flow. Consequently, a scaffold with highly interconnected pores would have higher permeability and a lower form factor.

In this study, the Reynolds numbers ranged between 0.088 and 1.250, but were mostly below 1, indicating that flow was primarily in the Darcian regime.[177] The Darcian regime is dominated by viscous energy losses, which are inversely proportional to permeability. Permeability increased four-fold with PCL-TI content, and form factor decreased by an order of magnitude, **Figure 3.8**. These changes are most likely due to the void, pore, and porosity differences noted earlier. The 100, 75, and 50% PCL-DI compositions have similar pore sizes and porosities, therefore it follows that their permeabilities are almost equal (~1.60×10^{-10} m^2). Permeability begins to increase with the 25 and 0% PCL-DI polyMIPEs to 3 and 4×10^{-10} m^2 respectively, which had significantly higher average pore diameters and porosities than the lower concentrations. Overall, these results confirm that all of the tested compositions possess interconnected porous networks, despite having emulsion volume fractions of only 50%. The blowing process of the isocyanate reaction with water allows these materials to not only increase

their porosity above volume fraction but is also hypothesized to drive interconnect formation as carbon dioxide tries to escape the scaffold.

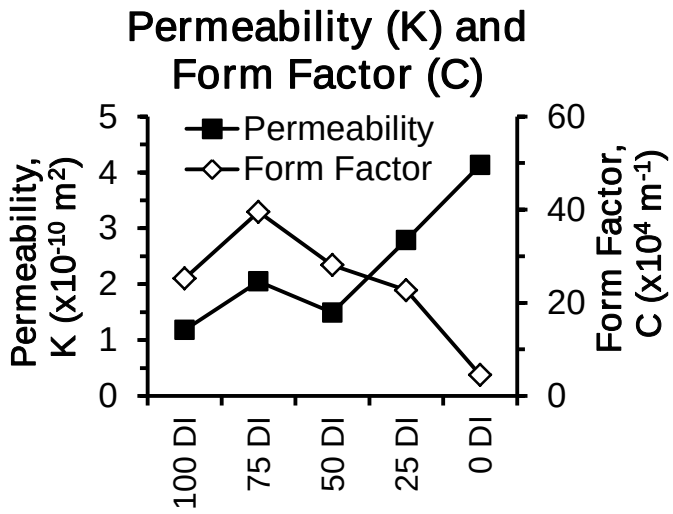

Figure 3.8. Darcy permeability "K" and form factor "C" of polyMIPEs with varied PCL-DI : PCL-TI ratio and constant water volume fraction.

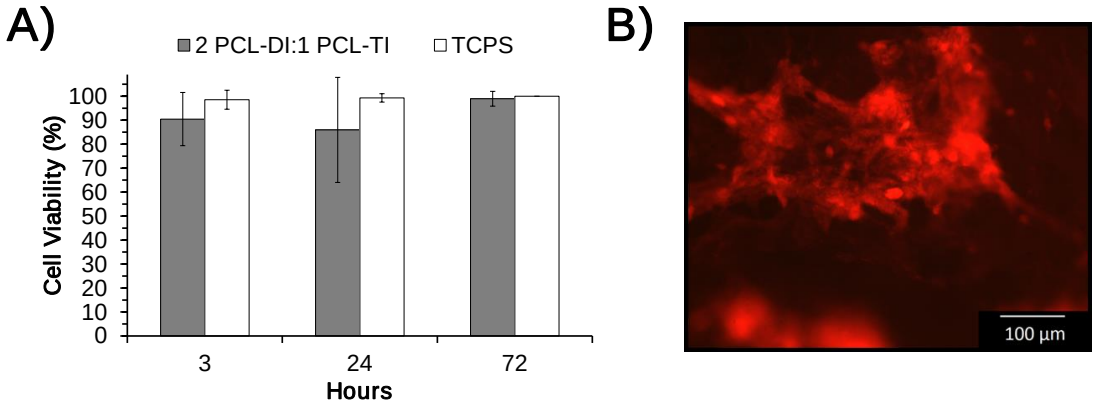

Figure 3.9. (A) Cell viability of neat PUU films and (B) micrograph of hMSCs spread on polyMIPE scaffold.

3.3.5 Cytocompatibility As an initial test of cytocompatibility, percent cell viability was tested on neat polymer films of similar composition to the porous scaffold but without any catalyst or surfactant. These films exhibited greater than 95% viability after 72 hours with no significant difference to the tissue culture polystyrene (TCPS) control at any time point. These results indicate that the polymer chemistry is cytocompatible and support the use of this system for biomedical applications, **Figure 3.9**. Neat films were used to isolate the effect of polymer chemistry on cell viability and due to the complications associated with testing viability on porous specimens. Subsequent analysis of hMSCs seeded on polyMIPE specimens (75% PCL-DI: 25% PCL-TI, 0.1 wt% DABCO) indicated that hMSCs were able to adhere and spread on the foam as characterized by the numerous pseudopodia extending from the bright red cell nuclei. The results indicate that the cells thrived for up to 24 hours on the polyMIPE despite the presence of DABCO (0.1 wt%). Of the handful of catalysts typically used in polyurethane and polyurea syntheses, DABCO is considered the most cytocompatible but still regarded as a health hazard by many.[179] Tanzi et al. found the IC50 of DABCO in solution to be 0.013 and 0.071 wt% for human endothelial cells and Swiss 3T3 fibroblasts after 72 hours, respectively.[179] A key difference between the studies is how the cells were exposed to the catalyst. In Tanzi et al., the cells were cultured in solutions containing DABCO, but in this study DABCO had to leach out of the scaffold before contacting cells.[179] This leaching mechanism could explain the cell spreading at 24 hours when very little DABCO had escaped the polymer, but longer time points need to be investigated before any conclusions on cytocompatibility can be drawn. The isocyanate

chemistry of this system is advantageous in this regard, since the presence of water will result in conversion to amines that react with remaining isocyanates, without catalyst. Utilizing these reactions could allow for certain polyMIPEs to retain their biocompatibility, be injected into patients, and cured *in situ* with similar final properties to their catalyzed counterparts. Previously, isocyanates had been found to be carcinogenic but those harmful isocyanates were very low-molecular weight aromatic monomers. Novel injectable polyurethane foams have been safely deployed in animal studies without serious adverse reactions.[155, 156, 162, 165] The improved biocompatibilitiy was hypothetically linked to the increased molecular weights of the isocyanate prepolymers and are similar to the macromers described here.[70, 155, 162, 165] Therefore, these macromers are not expected to cause adverse reactions *in vivo*. Additionally, the surfactant layer is hypothesized to act as a barrier between the prepolymers and cells, further mitigating potential side effects prior to polymerization. Future studies will examine the effects of catalyst concentration and polyMIPE composition on cell viability and spreading, as well as test the cytocompatibility of unpolymerized PCL-isocyanate macromers.

3.4 Conclusions

Emulsion templating of tissue engineering scaffolds is a relatively new area of research that can be used to generate injectable foams with tunable mechanical properties. In this study, elastomeric polyMIPEs were fabricated at body temperature without toxic solvents and with viscosities appropriate for *in situ* deployment through a

syringe. In addition to the porosity generated from the water droplet phase of the emulsion, a chemical blowing mechanism generated additional porosity through carbon dioxide generation. The interconnected porous structure of the resulting foams yielded high graft permeability that is expected to enable improved mass transport and regeneration *in vivo*. Finally, initial human mesenchymal stem cell (hMSC) cytocompatibility testing supported the use of these candidate scaffolds in regenerative applications. Overall, these new scaffolds have potential application as biodegradable and injectable tissue engineered grafts for soft tissue regeneration and offer unique advantages in deployment and tissue integration over current methods.

CHAPTER IV

INJECTABLE POLYHIPES WITH RAPID *IN SITU* CURING

4.1 Introduction

Emerging fields like tissue engineering are driving the development of novel materials with specialized properties to serve as temporary 3D matrices to regenerate complex tissues.[180] Material chemistry and physical architecture are critical to guiding regeneration. An interconnected porous structure is needed to encourage cell growth, nutrient and metabolic waste transport, and neovascularization.[2] Bone and other structural tissues also require that these porous scaffolds have adequate mechanical properties to withstand physiological loading until tissue function is restored.[180, 181] Great effort has been spent developing materials and fabrication strategies to meet these design criteria; however, matching the constraints of tissue regeneration and sufficient mechanical properties to restore function remains challenging given that many of these properties are inversely related to each other. For example, high porosity enhances mass transport to support cell viability but typically reduces mechanical properties. Polymerized high internal phase emulsions (polyHIPEs) are a more recent scaffold fabrication technique that offers unique advantages in meeting these diverse criteria.[54]

PolyHIPEs have been investigated as tissue engineered scaffolds due to their tunable mechanical properties and pore architectures appropriate for tissue regeneration.[54, 157, 158] A unique advantage of the polyHIPEs developed in our lab is their solvent-free fabrication and low cure temperature that permits their use as an injectable

scaffold that cures to rigid foams in the body. This injectability allows these scaffolds to match irregular defect geometries and thus eliminate gaps and micromotion, which could reduce graft failure and revision surgeries.[158, 180, 181] An injectable graft that cures *in situ* would also reduce cost and time associated with computer-aided design and fabrication methods.[182] Finally, the solvent-free fabrication method permits incorporation of bioactive cues to facilitate cell differentiation and promote new tissue growth.[2, 182]

While these scaffolds offer many advantages over alternative bone grafts, current biodegradable formulations require roughly 2 hours to cure at body temperature.[157, 158] Clinicians prefer fast-curing materials that reduce surgical times, lower the patient's risk of infection, and rapidly stabilize defects.[181] Poly(methyl methacrylate) (PMMA) bone cement cures in just 15 minutes and is the most common injectable system used clinically to stabilize orthopedic implants. Although PMMA bone cements are fast and direct, it does not facilitate tissue regeneration because it is highly exothermic, non-degradable, and non-porous. In contrast, an injectable polyHIPE that cures within 15 minutes would be advantageous because it can stabilize the defect and be loaded with cells prior to injection to provide a temporary matrix that supports tissue regeneration. In addition to a rapid cure times, off-the-shelf grafts are preferred to allow use in both emergency and scheduled procedures.[181] Thus, polyHIPE grafts must remain stable in storage for a minimum of 6 months and then cure rapidly after injection to facilitate clinical translation.

Previous iterations of injectable polyHIPE scaffolds relied on thermal initiation, the rate of which increases exponentially with temperature. A graft that cures *in situ* is

constrained to a physiological cure temperature of 37 °C, well below the typical use temperatures of most thermal initiators. In this study, thermal initiation was replaced with a redox initiator system to decrease the set time of the HIPEs. Previous redox-cured polyHIPEs displayed enhanced cure rates but were not designed for biomedical use and often contained toxic or non-degradable components.[183, 184] Here, a method is described that allows for the fabrication of injectable polyHIPEs from biodegradable macromers that can be stored for months at a time and then rapidly cures *in situ*. This proposed method involves making two separate but near-identical HIPEs: the first with an oxidizing initiator and the second with a reducing agent. Redox-paired initiators allow for the rapid polymerization at low temperatures while the use of a double-barrel syringe keeps the components separate and unpolymerized until the two components are mixed upon injection via a static mixing head. By carefully selecting initiator concentrations, this system has the potential to permit stable storage of the uncured emulsion and rapid curing after injection into the defect. To this end, we investigated the effect of redox initiator concentration on polyHIPE properties for three materials: ethylene glycol dimethacrylate (EGDMA), butanediol dimethacrylate (BDMA), and propylene fumarate dimethacrylate (PFDMA). The effects of redox concentration and ratio on cure time, pore architecture, and compressive modulus and strength were evaluated in relation to use in orthopedic applications. Overall, these studies demonstrate the potential of this new method of fabricating rapid-curing polyHIPEs with long shelf-lives for utility as tissue engineered bone grafts.

4.2 Materials and Methods

4.2.1 Materials Polyglycerol polyricinoleate (PGPR 4125) was donated by Paalsgard. All other chemicals were purchased and used as received from Sigma Aldrich unless otherwise noted.

4.2.2 PFDMA Synthesis PFDMA was synthesized in a two-step process adapted from Timmer et al.[185] First, propylene oxide was added dropwise to a solution of fumaric acid and pyridine in 2-butanone (2.3:1.0:0.033 mol) and refluxed at 75°C for 18 hours. Residual propylene oxide and 2-butatone were removed by distillation and the product redissolved in dichloromethane. Residual acidic byproducts and water were removed with washing, and the product dried under vacuum to yield the diester bis (1,2 hydroxypropyl) fumarate product. The diester was then endcapped with methacrylate groups using methacryloyl chloride in the presence of triethylamine. The molar ratios of the diester, methacryloyl chloride, and triethylamine were 1:2.1:2.1, respectively. Hydroquinone was added to the diester to inhibit crosslinking during synthesis at a molar ratio of 0.008:1. The reaction was maintained below -10˚C to reduce undesirable side reactions and stirred vigorously under a nitrogen blanket. The macromer was neutralized overnight with 2 M potassium carbonate. Residual triethylamine and methacrylic acid were removed with an aluminum oxide column (7 Al_2O_3:1 TEA). The integration ratio of methacrylate protons to fumarate protons in the ^1H NMR spectra was used to confirm > 90% functionalization for all macromers prior to polyHIPE fabrication. (300 MHz, $CdCl_3$) δ 1.33 (dd, 3H, CH3), 1.92 (s, 3H, CH3), 4.20 (m, 2H, -CH2-), 5.30 (m, 1H, -CH-), 5.58 (s, 1H, -C=CH2), 6.10 (s, 1H, -C=CH2), 6.84 (m, 2H, -CH=CH-).

4.2.3 EGDMA and BDMA Inhibitor Removal EGDMA and BDMA purchased from Sigma Aldrich were purified to remove inhibitors prior to use. The macromers were filtered through an aluminum oxide column to remove monomethyl ether hydroquinone. The purified products were stored at 4 °C under a nitrogen blanket until used for HIPE fabrication.

4.2.4 PolyHIPE Fabrication HIPEs were fabricated using a FlackTek Speedmixer DAC 150 FVZ-K according to a protocol adapted from Moglia et al.[157] Briefly, macromer was mixed with 10 wt% PGPR 4125 and a varied amount of benzoyl peroxide (0.5-5.0 wt%) prior to emulsification. A second mixture consisting of macromer, 10 wt% PGPR, and a varied amount of trimethylaniline (TMA, 0.5-5.0 wt%) was also combined prior to emulsification. Once both were thoroughly mixed, an aqueous solution of calcium chloride (1 wt%) was then added to the organic phases (75% v) in 3 additions and mixed at 500 rpm for 2.5 minutes each. HIPEs were placed in double barrel syringe and the two components mixed upon injection using a static mixing head (5 mL syringe with 3 cm straight mixer, Sulzer Mixpac K-System). HIPEs were then placed in a 37°C bath to initiate polymerization (**Figure 4.1)**.

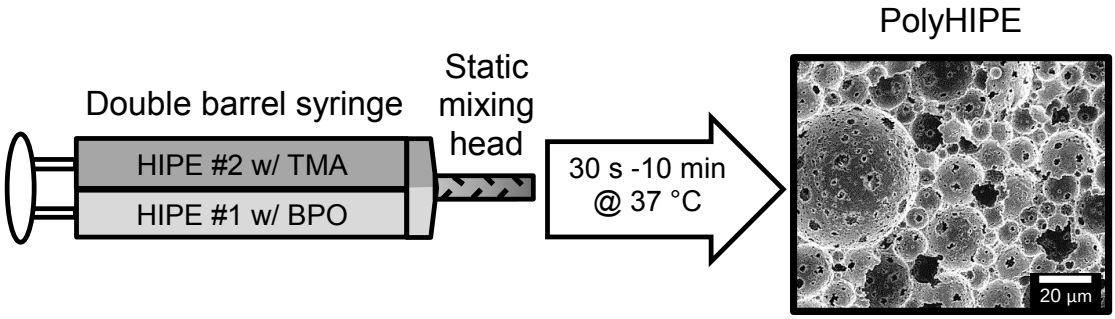

Figure 4.1. Schematic of the double-barrel syringe system.

4.2.5 Rheological Analysis PolyHIPE cure time was characterized using an Anton Paar MCR 301 rheometer based on a process adapted from Foudazi et al.[186] HIPEs were injected through a mixing head to facilitate redox initiation directly onto the 37 °C plate. Storage and loss moduli were measured every 15 s using a parallel-plate configuration with a 1 mm gap and 0.5% strain. Work time is presented as the onset of increasing storage modulus and set time is presented as the tan δ minimum, which corresponds to storage modulus yielding.

4.2.6 Scanning Electron Microscopy PolyHIPEs were dried *in vacuo* for 24 hr to remove water prior to characterization of pore architecture. Average pore and interconnect size of each composition was determined using scanning electron microscopy (SEM, JEOL 6500). Circular specimens from three separate polyHIPE specimens were sectioned into quarters and fractured at the center. Each specimen was coated with gold and imaged in a rastor pattern yielding five images. Pore size measurements were completed on the first ten pores that crossed the median of each 500x magnification micrograph. Average pore sizes for each polyHIPE composition are reported (n=450). A statistical correction was calculated to account for the random fracture plane through spherical voids and pores, $2/\sqrt{3}$.[159] Average diameter values were multiplied by this correction factor resulting in a more accurate pore diameter description.

4.2.7 Mechanical Testing PolyHIPE compressive properties were measured using an Instron 3300 equipped with a 1000-N load cell. ASTM D1621-04a was utilized to determine the compressive modulus and strength of the polyHIPEs.[135] Each polyHIPE

specimen was sectioned into three discs (15mm diameter, 5 mm thick) using an Isomet® saw and compressed at a strain rate of 50 μm/s. The compressive modulus was calculated from the slope of the linear region after correcting for zero strain and the compressive strength was identified as the stress at the yield point or 10% strain, whichever occurred first. Reported moduli and strength data were averages of 9 specimens for each composition tested.

4.2.8 Gel Fraction Gel fraction was measured gravimetrically to evaluate the extent of network formation. After curing for 24 hr, polyHIPE samples were sectioned into 15mm by 1 mm discs. Mass was recorded for each specimen after vacuum drying for 48 hr, incubating in 100X dichloromethane at 20 °C for 48 hr, and vacuum drying again until a constant mass was achieved. The final weight divided by the initial weight was assessed as the gel fraction.

4.2.9 Long Term Storage Uncured PFDMA HIPEs were stored at 4°C for up to six months and sampled each month to determine the impact of storage on polyHIPE architecture and mechanical properties. After a sample was removed, it was thawed for 60 minutes then injected through a syringe and cured for 48 hours prior to characterization, as described above.

4.3 Results and Discussion

4.3.1 Effect of Redox Initiator Concentration on Work and Set Time Prior to curing, all HIPEs flowed like viscous fluids but were rheologically similar to gels (E' > E"), as is expected for HIPEs.[186, 187] Their moduli remained relatively constant before

curing began, indicating that the emulsions were stable without significant phase separation.[186] Work time is defined by ISO1997 as the "period of time, measured from the start of mixing, during which it is possible to manipulate a dental material without an adverse effect on its properties" and set time is accepted as the point at which a polymer network is formed.[186] Previously, we reported a cure time for PFDMA of approximately 2 hours (5 wt% BPO)[157]; whereas, both EGDMA and BDMA require over 10 hours to set with thermal initiation alone. Utilization of the reducing agent TMA in combination with BPO dramatically reduced work and set time for all materials from hours to minutes. This corresponded to an order of magnitude increase in rate over thermal initiation alone.[157] Increasing total redox initiator concentration from 0.5 wt% to 5 wt% also decreased both work and set times for all materials, **Figure 4.2**. For EGDMA, redox initiation with 0.5 wt% decreased work time to 3.5 minutes and set time to 5 minutes. Increasing initiator concentration to 1 wt% further decreased work time to 30 seconds and set time to 1 minute. BDMA displayed a slower set and work times than EGDMA under the same conditions. At 0.5 wt%, BDMA's work time and set time was 5 and 7.5 minutes, respectively, with a further decrease to 1 and 2 minutes at 1.0 wt%. PFDMA had similar work and set times to BDMA with (0.1 wt%: 6 and 7 minutes, 1 wt%: 1 and 1.3 minutes). All of the 5 wt% compositions cured before measurements could be taken with the rheometer (< 30 seconds).

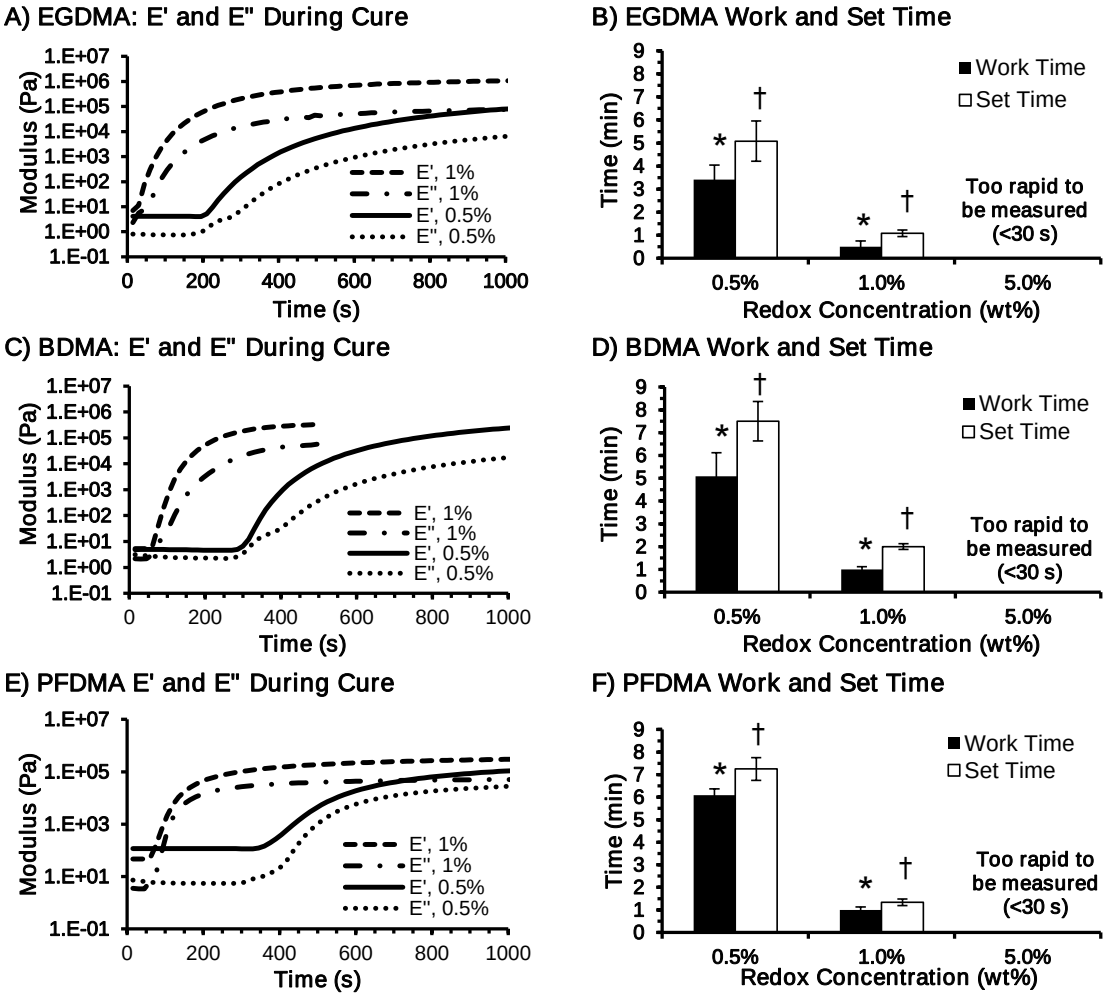

*: P > 0.05 compared to 0.5 and 1.0 wt% work times
†: P > 0.05 compared to 0.5 and 1.0 wt% set times

Figure 4.2. Rheological analysis of redox polyHIPEs during polymerization. Storage and loss moduli during EGDMA (A), BDMA (C), and PFDMA (E) polyHIPE polymerization and work and set times for EGDMA (B), BDMA (D), and PFDMA (F) polyHIPEs at 37 °C with 1.0 TMA:1.0 BPO ratio.

PMMA bone cement is one of the most prevalent injectable biomaterials in orthopedic applications because it transitions from a low viscosity liquid to a rigid solid within 15 minutes.[188-191] The PMMA physical transition allows surgeons to work with either a liquid or puddy to best suite their procedure and is a contributing factor in PMMA's widespread use.[190] The findings from this study demonstrate the utility of the

redox system to increase the cure rate of the polyHIPEs to ranges comparable to PMMA bone cements. We also demonstrated that the cure rate can be further modulated from <30s to 10 minutes by changing the redox initiator concentration. In contrast to PMMA which is non-porous, non-biodegradable, and highly exothermic with peak temperatures reaching 110°C,[192] these polyHIPEs cure to porous and degradable materials with a maximum exotherm of only 42 °C. This low exotherm would be critical if the scaffolds are to be used synergistically with stem cells or growth factors.

4.3.2 Effect of Redox Initiator Concentration on Network Formation

Additional rheological and gel fraction data was analyzed to investigate the impact of redox initiation concentration on the network formation in candidate polyHIPEs. In each material, an induction period was evident prior to an increase in modulus that was dependent on macromer chemistry (EGDMA<BDMA<PFDMA) that was primarily responsible for the difference in cure times, **Figure 4.2**. It was hypothesized that reduced radical diffusion and steric hindrances associated with increased macromer molecular weight resulted in longer induction periods, especially in the low initiator concentration compositions.[193] PFDMA, BDMA, and EGDMA have molecular masses of ~362, 226, and 198 g/mol, respectively. HIPE viscosity trended with macromer molecular weight with PFDMA almost 30 times more than EGDMA. The increased viscosity likely inhibited initiator diffusion and reaction in the PFDMA HIPEs as compared to EGDMA HIPEs.[193, 194] This induction period decreased and the moduli slopes increased as initiator concentration was raised from 0.5 to 1.0 wt%, suggesting increased polymerization rate.[195] This was attributed to increased initiation sites leading to more

chains growing simultaneously and causing chain molecular weight to increase more rapidly.

Table 4.1. The effect of macromer and initiator chemistry on average gel fractions, pore diameters, and interconnect diameters of various polyHIPE formulations.

Material	Redox Initiator (wt%)	Gel Fraction (%)	Pore Diameter (μm)	Interconnect Diameter (μm)
EGDMA	0.5	86.1 ± 2.8	27 ± 12 *	3 ± 2
	1.0	89.1 ± 0.5	20 ± 10	3 ± 1
	5.0	89.0 ± 1.0	19 ± 12	3 ± 1
BDMA	0.5	85.8 ± 0.4	14 ± 6	3 ± 1
	1.0	89.3 ± 0.4	14 ± 6	3 ± 1
	5.0	92.1 ± 0.3	13 ± 7 †	2 ± 1
PFDMA	0.5	77.9 ± 1.7	5 ± 3 ‡	1 ± 1
	1.0	81.0 ± 0.8	6 ± 3	1 ± 1
	5.0	85.6 ± 0.8	6 ± 3	1 ± 1

Material	TMA:BPO (wt%:wt%)	Gel Fraction (%)	Pore Diameter (μm)	Interconnect Diameter (μm)
EGDMA	0.5:1.0	87.8 ± 0.7	19 ± 8	3 ± 1
	1.0:1.0	89.1 ± 0.5	20 ± 10 ●	3 ± 1
	5.0:1.0	86.5 ± 1.9	17 ± 11	2 ± 1

*: P <0.001 compared to EGDMA 1.0 and 5.0 wt% pore sizes
†: P <0.05 compared to BDMA 0.5 and 1.0 wt% pore sizes
‡: P <0.01 compared to PFDMA 1.0 and 5.0 wt% pore sizes
●: P <0.01 compared to 0.5:1.0 and 5.0:1.0 TMA:BPO pore sizes

Gel fraction (**Table 4.1**) was utilized to compare extent of network formation in polyHIPEs after 24 hr of curing and ranged from 78 to 92% for all compositions, **Table 4.1**. As expected, increasing initiator concentration correlated with increased gel fraction. PFDMA gel fraction increased the most from 78 to 86%. BDMA gel fraction also increased significantly with higher initiator concentrations (86 to 92%); whereas,

EGDMA gel fractions only increased from 86 to 89%. Both EGDMA and BDMA had significantly higher gel fractions than the corresponding PFDMA polyHIPEs, likely due to steric hindrance and reduced radical diffusion associated with its higher molecular weight. Additionally, highly crosslinked microgels could form and begin to stearically hinder further crosslinking, increasing network defects and free-ends.[193] Overall, these polyHIPEs showed excellent network formation that was further enhanced at higher initiator concentration.

4.3.3 Effect of Redox Initiator Concentration and Storage on Pore Architecture The impact of the rapid, redox-initiated cure on polyHIPE micro-architecture was examined to ensure retention of desirable pore size and interconnection. EGDMA polyHIPEs possessed the largest pore diameters (**Table 4.1**, **Figure 4.3**), almost double the size of BDMA and quadruple the size of PFDMA pores at each initiator concentration. Traditionally, pore size has been used as a marker of emulsion stability with smaller pore size indicating enhanced stability and reduced droplet coalescence prior to the gel point.[67, 114] In this study, increasing pore size correlated with decreasing HIPE viscosity: PFDMA (11.0 Pa*s), BDMA (0.464 Pa*s) and EGDMA (0.343 Pa*s). This was consistent with the previous literature reports of increased emulsion viscosity impeding droplet coalescence and resulting in smaller pores.[183] Despite differences between materials, scanning electron micrographs revealed that average pore and interconnect diameter were not affected by redox initiator concentration for most materials. The 0.5% EGDMA was the exception with an average pore size of 26 μm, significantly larger than the 1.0 and 5.0% polyHIPEs (20 μm) and

indicative that some amount of coalescence occurred prior to the gel point. The rapid cure of both the 1.0 and 5.0 wt% EGDMA polyHIPEs reduced droplet coalescence and thus no change in pore size was observed.

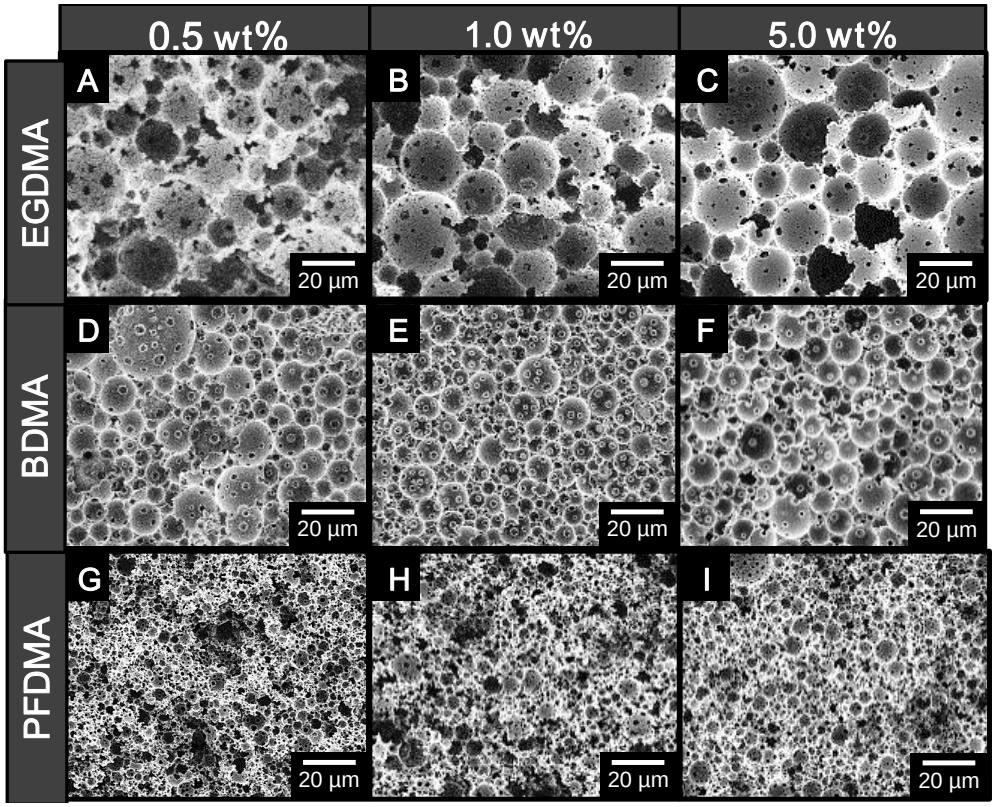

Figure 4.3. Representative SEMs illustrating the effect of initiator concentration on pore architecture of EGDMA (A, B, C), BDMA (D, E, F), and PFDMA (G, H, I) polyHIPEs.

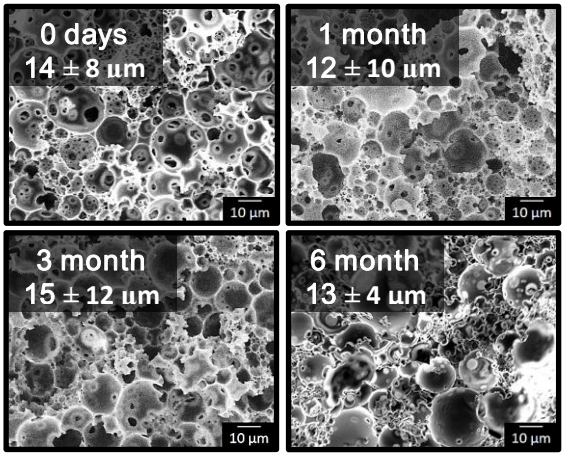

Figure 4.4. Representative SEMs of PFDMA polyHIPEs after storing unpolymerized HIPEs at 4 °C for up to 6 months.

Although there are no clear targets for ideal pore diameters to regenerate tissues, these pore sizes are relatively small compared to the general goal of >100 μm; however, recent studies indicate that <40 μm pores improve regeneration.[78, 85] We have demonstrated previously that emulsion composition and processing can be modified to increase or decrease pore diameter but this was not the focus of this study.[67, 111, 157, 158] BDMA and EGDMA polyHIPEs possessed pore diameters up to 60 μm when cured via thermal initiation (data not shown). We hypothesized that the use of the static mixing head in this study decreased pore size by imparting extra shear forces on the emulsion and further breaking droplets down to smaller diameters. Therefore, use of a large diameter mixing head should minimize the impact on pore diameter for all materials and compositions tested.

A crucial element of the double-barrel system is that the two HIPEs can be stored separately until needed, and the shelf-life can be further extended by storing at reduced

temperatures. PFDMA HIPEs were stored at 4 °C with samples removed and cured to examine any effect of storage on pore size indicating droplet coalescence or phase separation over time. No significant change in pore architecture was observed over a period of 6 months (**Figure 4.4**). This same technique could be used with any emulsion, but is especially useful for these solvent-free polyHIPEs that could encapsulate live cells or other biological therapeutics which could then be cryogenically stored without losing efficacy. Also, this method could facilitate scale-up with a central facility making the emulsion-filled syringes and transported to facilities where needed.

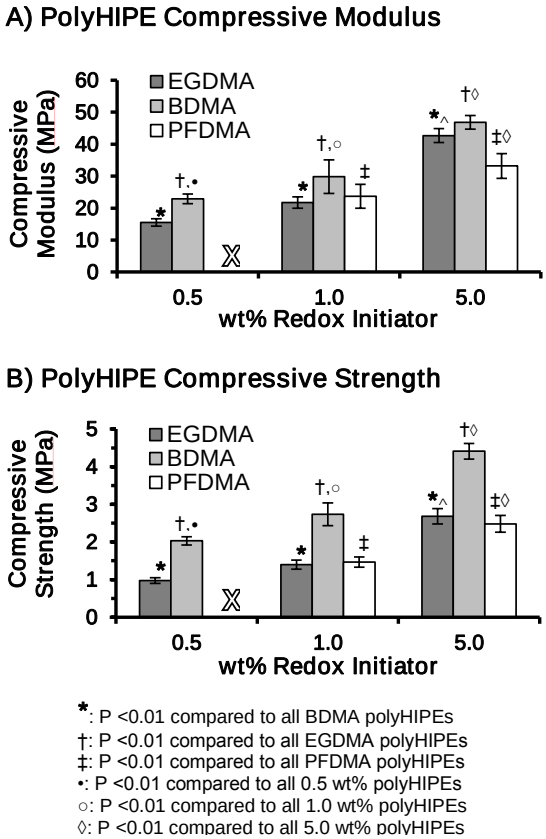

Figure 4.5. The effect of initiator concentration on compressive modulus (A) and strength (B) for each material. One composition had large regions of uncured material and was not tested, denoted with X.

4.3.4 Effect of Redox Initiator Concentration on Compressive Properties

Compressive modulus and strength are clinically important for bone grafts in stabilizing defects. Increased defect stability would reduce the necessity for immobilization and allow for earlier loading which has established benefits in stimulating bone regeneration.[196] Although the polyHIPEs set within several minutes, specimens were sectioned after a 24 hour cure for further characterization. Compressive modulus and strength increased as redox initiator concentration increased for all materials tested, **Figure 4.5**. BDMA was significantly stiffer and stronger than both EGDMA and PFDMA for each concentration tested. These differences in strength were more pronounced than the modulus, with even the weakest BDMA (0.5 wt% initiator) having a higher yield strength than all but the strongest EGDMA and PFDMA polyHIPEs (5.0 wt% initiator). The 0.5 wt% PFDMA samples were not tested in compression because they possessed large regions of uncured HIPE (reflected in their lower gel fraction). We hypothesize that the high viscosity of PFDMA decreased mixing efficiency of the two HIPEs and limited radical diffusion resulting in regions of uncured HIPEs. This was not observed in the 1.0 or 5.0% PFDMA HIPEs due to the higher concentration of initiator which limited the role of radical diffusion throughout the material. A longer static mixing head may eliminate the uncured regions in the 0.5% redox PFDMA. Representative loading curves are presented in **Figure 4.6**. EGDMA polyHIPEs were brittle and reduced to a compacted powder after compressive testing; whereas, both BDMA and PFDMA retained their dimensions. Toughness for all materials appeared to

increase at higher initiator concentrations with 5 wt% redox BDMA and PFDMA specimens showing no signs of brittle fracture.

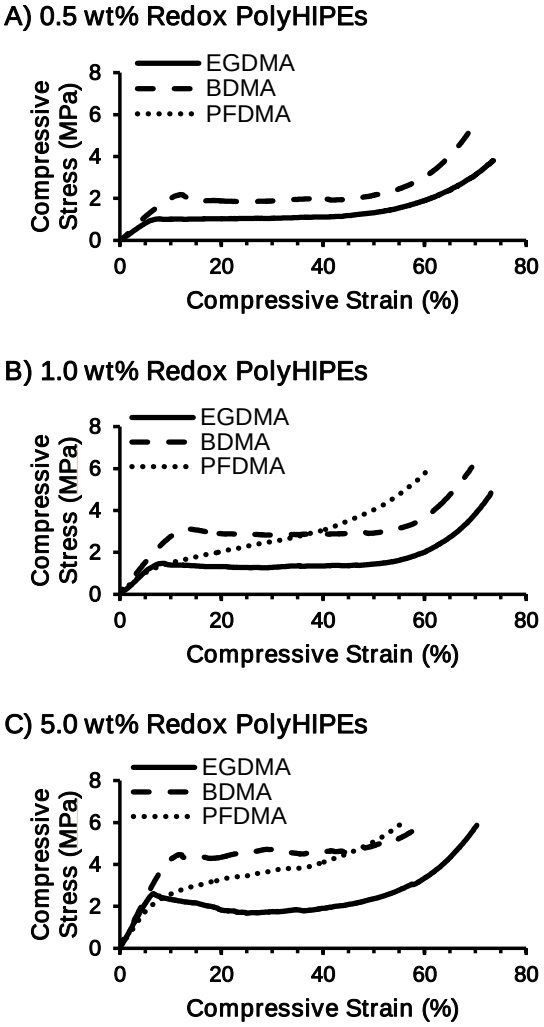

Figure 4.6. Representative compressive loading curves for each material and initiator concentration.

These porous materials approach the compressive properties of cancellous bone when matched by density, indicating the potential to mechanically stabilize the defect and elicit the appropriate mechanical cues to regenerate bone.[2, 34, 197] Furthermore, some

studies have shown that the mechanical properties required to trigger bone formation may be much lower than those of fully matured bone tissue.[189] In addition, the redox initiator system in these studies resulted in a rapid maturation of mechanical properties as compared to thermal initiation alone. Previously, the compressive modulus and strength of PFDMA polyHIPEs thermally cured with 5 wt% BPO increased over a 2 week incubation at 37 °C, **Figure 4.7**. In that time, modulus increased from 8.5 to 43 MPa and strength from 0.4 to 3 MPa. In contrast, the 5 wt% redox PFDMA polyHIPEs achieved similar properties within 24 hr of incubation and remained constant for the 2 weeks tested. As such, the redox system could potentially be used as an immediate fixation device and/or allow patients to begin loading the injury site more quickly which can improve patient outcomes.[196]

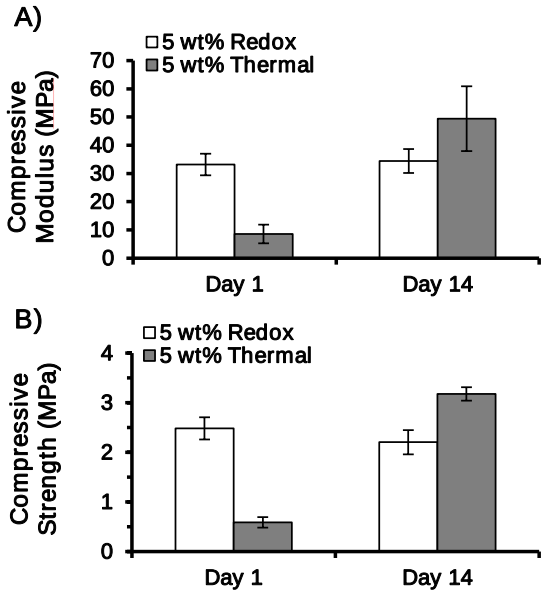

Figure 4.7. The effect of incubation for 1 and 14 days at 37 °C on PFDMA polyHIPE compressive (A) modulus and (B) strength.

4.3.5 Effect of TMA:BPO Ratio on PolyHIPE Properties The ratio of reductant to oxidant was also investigated to decouple the effects of rapid curing rates from increased initiator concentration. As expected, increasing the relative amount of TMA to BPO resulted in decreased work and set times, 90 to 30 seconds and 2.5 to 1 minute, respectively (**Figure 4.8A**). It should be noted that the 5.0 wt% TMA:1.0 wt% BPO HIPE set before testing could begin (< 20 seconds). We hypothesize that increasing the relative amount of TMA increases its availability to react with BPO, resulting in faster radical production and initiation. Other researchers have shown similar results with BPO/TMA systems and identified the formation of the BPO-TMA complex as the rate limiting step in radical production.[198, 199] As such, the faster initiation would allow the HIPEs to form a network more quickly and increase the cure rate. The compressive data collected after 24 hours indicated that redox initiator ratio had little to no effect on compressive modulus and strength (**Figure 4.8B, 4.8C**). There was also minimal effect on pore architecture. Average pore diameter varied slightly as the relative amount of TMA was increased, but no clear trend was observed. The 1.0:1.0 ratio had the largest average pore diameter (20 μm) with 0.5 and 5.0:1.0 slightly smaller at 19 and 17 μm, respectively. Although statistically significant, these differences are small and overall pore architecture is similar between the compositions.

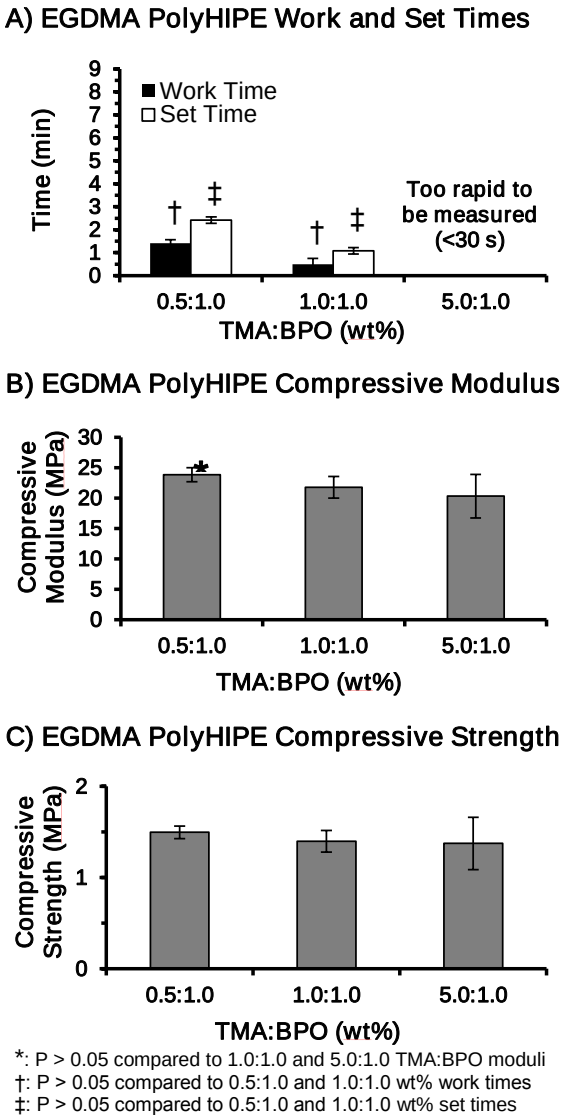

Figure 4.8. The effect of increasing TMA: BPO ratio in EGDMA polyHIPEs on: (A) work and set times, (B) compressive modulus, and (C) compressive strength.

Overall, these results demonstrate that the polyHIPE work and set time can be tuned independently from other polyHIPE properties (compressive modulus and strength, pore and interconnect diameter) with small variations in the reductant:oxidant ratio. For biomedical devices, especially tissue engineered grafts, this provides

researchers a route to preserve graft physical properties and cytocompatibility while optimizing work and set time to meet physician preferences.

4.4 Conclusions

This study demonstrates the benefits of redox-initiated polyHIPEs delivered using double-barrel syringes as tissue engineered bone grafts. Redox initiation reduced work and set times from hours to minutes matching current products like PMMA bone cement. These reduced cure times were also achieved with lower concentrations of total initiator that may enhance material cytocompatibility. Increasing redox initiator concentration increased compressive modulus and strength with minimal impact on pore architecture. Further modulation of the reductant:oxidant ratio decoupled set time from compressive modulus and strength allowing for increased tunability of future scaffold properties. The use of the double-barrel syringe permitted the emulsions to be stored for months at reduced temperatures and then undergo rapid on-demand curing upon injection due to mixing of the two components. Overall, the methodology developed in these studies facilitates clinical translation of this technology by providing new graft materials with improved attributes that maintain similar handling and deployment of traditional PMMA bone cements.

CHAPTER V

POLYHIPE MICROSPHERES FOR CONTROLLED RELEASE OF GROWTH FACTORS

5.1 Introduction

Bone grafting techniques have improved rates of healing and bone regeneration, but some cases require additional aid to induce calcification and neovascularization.[200, 201] Growth factors such as bone morphogenetic protein-2 (BMP-2), are used to enhance bone regeneration in many surgeries but are expensive and can have dangerous side effects.[202, 203] The INFUSE bone graft is one FDA approved product comprised of a collagen sponge imbued with an excess of BMP-2, 1000X the amount naturally found *in vivo*.[204] Despite the large amount of BMP-2, studies have found the INFUSE graft to offer little improvement over other methods with an expected success rate of 57.1% compared to 56.7% without using BMP-2 [205]. This is hypothesized to be a result of poor growth factor retention, up to 50% of BMP-2 released in the first 24 hours[206], discharging expensive and potent growth factor into the body, potentially calcifying adjacent soft-tissue. Further, the amount of BMP-2 required to keep later dosages in the effective range increases treatment costs by over $10,000. A new material with sustained release of lower dosages up to 21 days could maximize regeneration while reducing both cost and health risks.[204]

A variety of different systems have been studied including hydrogels, nanoparticles, and microparticles.[204] Recently, these systems have been investigated as

additives to tissue engineered scaffolds as a means to induce or control bioactivity. Although hydrogels can be used to encapsulate drugs and cells, they typically have weak mechanical properties which limits their use as a component in load bearing devices because they can act as stress concentrators in a graft and result in brittle failure under physiological loading.[207] Typical hydrogel mesh sizes limit the diffusion of large proteins out of the matrix to degradation rates, further limiting the specific molecules used.[208] Emulsification-evaporation methods can be used to produce nano- or microparticles with tunable porosities and sizes. These particles are usually injected but can also be integrated with tissue grafts to allow for site specific delivery [209] and their tunability allows for fine control over the drug release profile. However, these systems require a relatively large amount of solvent, limiting which proteins can be encapsulated or requires them to be loaded post-fabrication, reducing encapsulation efficiency.[210] A tunable and solvent-free system would broaden the number of potential proteins and decrease fabrication costs associated with using organic solvents. Additionally, this type of system could be added to a tissue engineered graft to improve treatment effectiveness and reduce healthcare costs to the patient.

We propose using the polyHIPE system developed in our laboratory to generate microspheres that are solvent-free, high porosity, and tunable.[157, 158] Additionally, these microspheres' pore architecture and material composition would match our injectable scaffolds', theoretically eliminating concerns of stress concentrators and thus retaining favorable mechanical properties. Using known principles, particle and pore size could be adjusted to tune encapsulation efficiency and release profiles. Furthermore, the solvent-

free fabrication allows growth factors to be encapsulated in the initial steps which should hypothetically increase encapsulation efficiency over other techniques. The porous structure would allow large proteins such as BMP-2 to percolate through the polyHIPE microspheres slowly and maintain effective concentrations only at the site of injury, preventing risks associated with excess growth factors.[208]

In this study, porous polyHIPE microspheres were chosen for use as a drug delivery system. This system is fabricated using emulsion templating without solvent to ensure biocompatibility and improve drug encapsulation efficiency. The effect of different fabrication parameters on particle size and pore diameter were investigated. One candidate composition was then selected to demonstrate proof of concept as an rhBMP-2 delivery system.

5.2 Materials and Methods

5.2.1 Materials Polyglycerol polyricinoleate (PGPR 4125) was donated by Paalsgard. All other chemicals were purchased and used as received from Sigma Aldrich unless otherwise noted.

5.2.2 Macromer Filtration Macromer purchased from Sigma Aldrich was purified to remove inhibitor prior to use. Ethyleneglycol dimethacrylate (EGDMA) was filtered through an aluminum oxide column to remove monomethyl ether hydroquinone.

5.2.3 PolyHIPE Fabrication Primary HIPEs were fabricated using a FlackTek Speedmixer DAC 150 FVZ-K according to a protocol adapted from Moglia et al.[157] Briefly, EGDMA was mixed with PGPR (10, 20, or 30 wt% of the macromer) and 2

wt% of the organically soluble photoinitiatior, 2,2-Dimethoxy-2-phenylacetophenone (DMPA), prior to emulsification. Once thoroughly mixed, an aqueous solution containing calcium chloride (1 wt%) was then added to the organic phase (75% v) in 3 additions and mixed at 500 rpm for 2.5 minutes each.

5.2.4 Microsphere Fabrication Microspheres were fabricated via a fluidics double emulsion technique (w/o/w) adapted from Gokmen et al., **Figure 5.1**.[211] The primary HIPE was injected drop wise (KD Scientific-100 Infusion Pump) into an external aqueous phase containing 3 wt% poly(vinyl alcohol) (Harvard PHD 2000 Infusion Pump) and passed through UV excitation (UVP High Performance Transilluminator 365 nm) for a duration of 2.5 minutes to initiate polymerization. Three sets of fabrication parameters were used to obtain distinct particle diameter profiles ranging from 300-800 microns, summarized in **Table 5.1**. Microspheres with 800 micron diameter were made using a 27G blunt needle with a HIPE injection rate of 0.20 mL h^{-1} and the external phase was pumped at 1.2 ml min^{-1} using 1.59 mm ID Tygon tubing. 500 μm microspheres were made by increasing the external flow rate to 5.6 ml min^{-1}. The 300 μm spheres were made with a blunted 30G needle and a HIPE injection rate of 1.0 mL h^{-1}, and the continuous phase was pumped at 6.0 ml min^{-1} using 0.79 mm ID Tygon tubing. Collected microspheres were filtered using vacuum aspiration and dried *in vacuo* for a minimum of 24 hours.

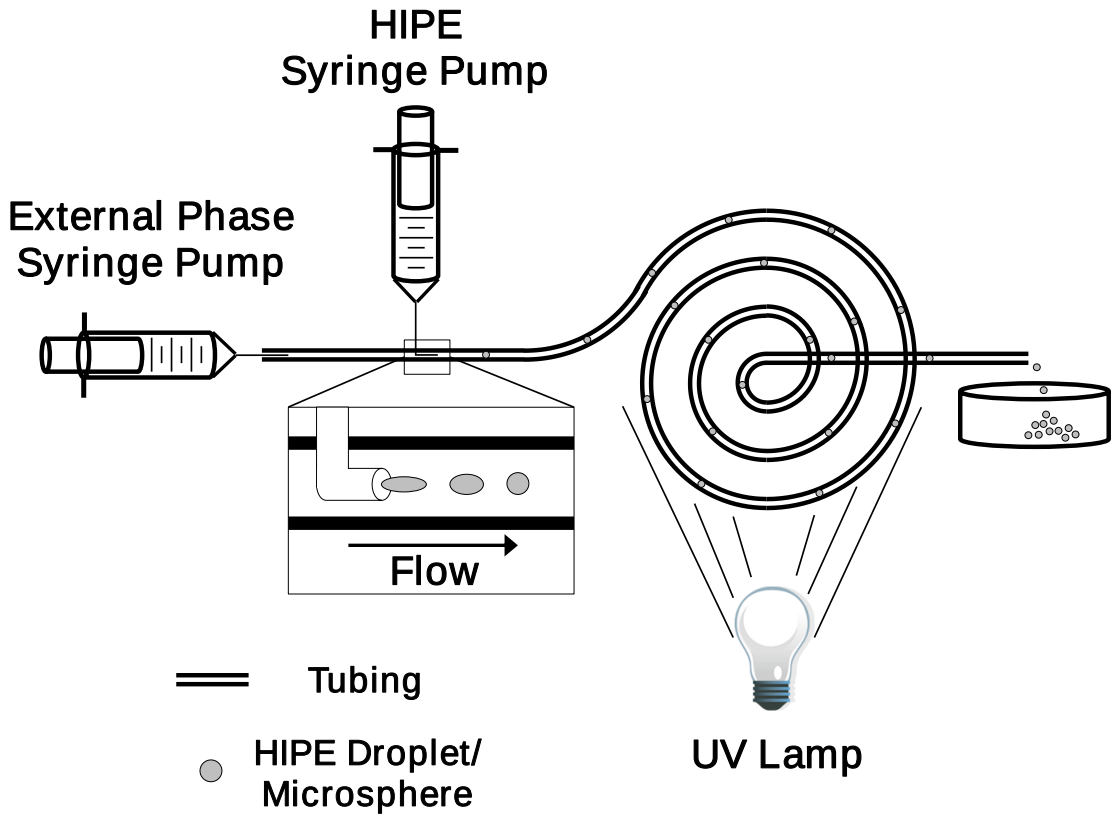

Figure 5.1. Schematic of microsphere fabrication. HIPE is injected through a needle parallel to the flow of 3 wt% PVA solution and polymerized via UV irradiation. Polymerized particles are collected and filtered prior to use.

Table 5.1. Summary of microsphere fabrication parameters.

Tubing Diameter (mm)	HIPE Injection Rate (mL/hr)	Needle Size (gauge)	Aqueous Flow Rate (mL/min)	Particle Diameter (μm)
0.8	1.0	30	6.0	260 ± 30
1.6	1.0	27	5.6	460 ± 40
1.6	0.2	27	1.2	750 ± 40

5.2.5 rhBMP-2 PolyHIPE Microsphere Fabrication Similar to the standard polyHIPE fabrication, an organic phase is made of 500 mg EGDMA, 150 mg PGPR, and

10 mg DMPA. Then, 5000 ng rhBMP-2 (E. coli expressed, R&D systems) is added to 1.5 mL of deionized water to make the aqueous phase. The two phases are mixed in the same procedure as standard HIPEs. These rhBMP-2 HIPEs were made into ~800 μm microspheres following the same procedures outlined above.

5.2.6 Loading Efficiency of rhBMP-2 Microspheres Loading efficiency of rhBMP-2 loaded microspheres was determined by crushing the microspheres and incubating in the presence of 3 ml deionized water with agitation for 15 hours in a 15 ml centrifuge tube. The tube was spun down at 3500 rpm for 5 min to pellet the crushed particles and the aqueous phase removed. The pellet was reagitated with 1 ml deionized water on a vortexer and separated like before. Protein concentration was determined with CBQCA (Sigma Aldrich) and fluorescence measured with a plate reader (Tecan Infinite 200 Pro) using a 7-point calibration curve. From this concentration, the concentration of rhBMP-2 successfully encapsulated in the particles was calculated and compared to the theoretical maximum based on initial HIPE concentration.

5.2.7 SEM Analysis Average particle, pore and interconnect diameter of varying compositions was determined using SEM (JOEL 6500). PolyHIPE microspheres were subjected to vacuum drying to remove water prior to characterization. A minimum of ten particles were coated with gold, imaged, and particle diameter measured. Pore size measurements were completed on five particles using the first ten pores that crossed the median of each 500X magnification micrograph. Average pore sizes for each polyHIPE microsphere composition are reported (n=50).

5.3 Results and Discussion

5.3.1 Microsphere Fabrication Microspheres were made with a fluidics setup inspired by Gokmen et al. because of the resultant monodisperse particle diameters it produced.[211] Reviews by Christopher and Anna, and Gokmen and Du Prez summarize the breadth of work done to understand microfluidic systems that is beyond this study's scope, especially on droplet formation.[212, 213] Using the principles outlined in these reviews, monodisperse particles were fabricated with tunable diameters ranging from 200-800 μm (**Table 5.1**, & **Figure 5.2**) and pore sizes from 10-30 μm (**Figure 5.3**). The tunability of the system is ideal for the laboratory setting, allowing facile adjustment of microparticle properties from minor changes to the process. This solvent-free setup is also a favorable method to pursue at scale because it allows for facile incorporation of cells and other biological agents directly into the microparticles.

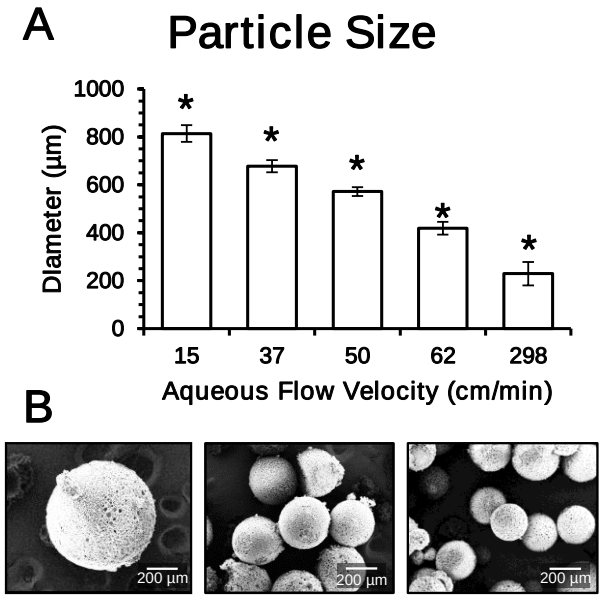

Figure 5.2. (A) The effect of external phase flow rate on average particle size with (B) representative SEM data.

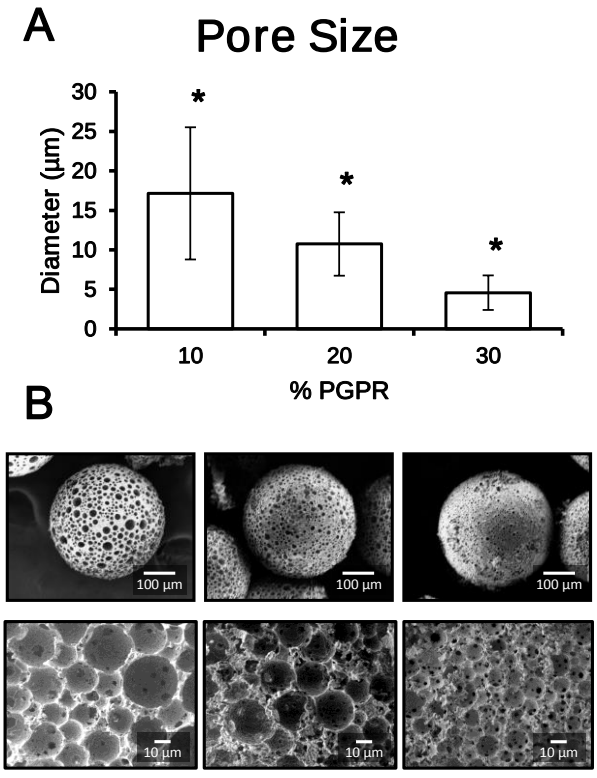

Figure 5.3. (A) The effect of HIPE PGPR concentration on average particle pore size with (B) representative SEM data.

Continuous phase flow velocity and droplet phase viscosity were two of the most important factors contributing to droplet size, shape, and uniformity.[212, 213] These qualities dictate the shear forces at the injection site and cause droplets to "drip" from the needle, typically in spheres. EGDMA was chosen for the HIPEs because of their low viscosity, necessary to form uniform droplets in the aqueous continuous phase. Balance between the continuous and droplet phase flow rates maintained efficient and monodisperse droplet size, as outlined by Cramer et al.[214] Excessive droplet flow rates resulted in "jetting" from the needle tip which forms small and variable droplets. Most of these relationships hold true when the Reynolds number is <<1, indicating laminar flow, and explains why the smaller tubing was used to achieve particle diameters below 500 µm.[212]

The inherent tunability of the initial w/o HIPE allowed for control of microsphere pore architecture independent of particle diameter. An interconnected pore structure was formed by selecting an organically soluble photo initiator and it is theoretically possible to instead form a closed pore microsphere by switching to an aqueous initiator system or decreasing internal water volume.[158] Pore diameter is dependent on surfactant concentration with increased amounts causing decreased interfacial energy between the water and organic phases, thereby allowing surface area between the phases to increase which manifests as smaller internal droplet sizes and thus smaller pores.[67, 111, 157] This phenomenon was observed here with pore size decreasing from 20 to 5 µm as PGPR concentration was increased from 10 to 30 wt%, **Figure 5.3**.

Independent control of both particle diameter and pore structure is ideal for controlling drug release profiles, critical for optimizing future therapies. Tortuosity is a unit-less measure of the fluid path length through the porous medium relative to the end-to-end path length.[175] Tortuosity increases with a decrease in pore size and results in a decreased diffusion gradient between the microsphere center and edge, decreasing drug release rate.[129] The same principle allows path length (i.e. release rate) to be controlled by changing particle diameter, with larger particles releasing slower than similar small particles.[215]

Burst release occurs when a relatively large portion of drug releases immediately after deployment. Considering the price of effective drugs and growth factors, this type of release phenomenon is widely considered a waste of resources therapeutically and economically[216] Smaller particles have higher aspect ratios and are more prone to burst release kinetics because their increased surface area allows for relatively more drug/protein to quickly diffuse away from the particle surface.[216, 217] Finally, slow drying of particles can cause the encapsulated drug to concentrate near the particle surface and increase burst release, but freeze-drying has been shown to completely prevent this effect.[218] All of these factors must be considered in future protein release studies.

Finally, the pore structures obtained are identical to monolithic forms of EGDMA polyHIPEs, potentially yielding a continuous polymeric structure with no stress concentrators that can result from additives. An initial study of polyHIPE compressive modulus and strength after adding 1 wt% microparticles showed no statistical difference from the control scaffold (**Figure 5.4**). Although future studies with

increased amounts of microspheres need to be conducted, this supports the hypothesis that their common pore structure will mitigate any negative effects on mechanical properties. These studies should also account for different particle and pore size to fully understand their effects.

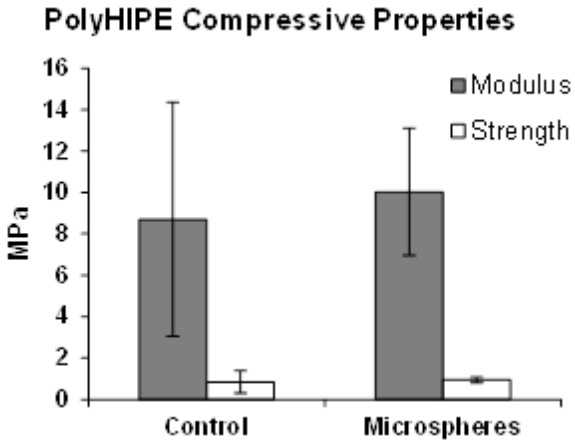

Figure 5.4. Effect of microsphere incorporation on scaffold compressive modulus and strength.

5.3.2 rhBMP-2 Encapsulation in PolyHIPE Microspheres These particles' effectiveness as a therapy relies on their ability to encapsulate and protect drugs and growth factors. To this end, rhBMP-2 was dissolved into the aqueous phase of the HIPE and encapsulated into microspheres with a diameter of ~800 μm and average pore size of 14 μm. CBQCA determined an encapsulation efficiency of 73 ± 3% compared to theory. Many microparticles are fabricated using the emulsion-solvent evaporation method which can have encapsulation efficiencies as low as 15% during crosslinking and purification.[210] Subject to specific methods used, retained proteins can be inactivated via mixing with organic solvents and extreme heat.[219, 220] The method utilized here

crosslinks within minutes at room temperature and eliminates the need for purification because it is solvent-free, theoretically increasing encapsulation efficiency and protecting the rhBMP-2. Encapsulation efficiency could be improved by further decreasing pore size, fabricating particles with a closed shell, or increasing the concentration of the external aqueous phase. These methods would work by decreasing the rate of diffusion by lengthening the path length, decreasing coefficient of diffusion, or decreasing the concentration gradient.[217, 221]

5.4 Conclusions

This study describes a method of producing tunable microspheres with theoretically high encapsulation efficiency and bioactivity retention that can be utilized to deliver site specific therapy in bone fusion or regeneration. The solvent-free nature of this method allowed for safe and efficient microsphere fabrication and protein retention, reducing fabrication costs and the amount of growth factor needed. Independent control of particle and pore geometry was demonstrated using the principles of emulsion templating and microfluidics, which should facilitate gradual release of rhBMP-2 over several weeks and increase treatment effectiveness while simultaneously reducing the risk of side effects.

These microspheres can be utilized in combination with tissue engineered scaffolds to promote regeneration of complex tissues by loading with various drugs or cells, without negatively impacting scaffold mechanical properties. Control of microsphere pore architecture can be matched to the scaffold and minimize the impact

on composite mechanical properties, a critical feature for load-bearing applications. The interconnected porous structure of these microspheres is more favorable for therapeutic release of large proteins like IgG which are too large to diffuse readily through hydrogels.

Studies are underway to evaluate protein bioactivity retention and release profiles over time as a function of particle and pore geometry. Microsphere osteoinductivity will be compared to a short "burst" of protein using hMSCs and ALP production. These microparticles are promising drug-delivery vehicles to enhance bioactivity of bone grafts without sacrificing mechanical properties. Their high loading efficiency and tunable release rates can potentially reduce the amount of drug needed to regenerate damaged bone, eliminate side effects, and decrease health care costs.

CHAPTER VI

CONCLUSIONS

6.1 Summary

In this body of work, a variety of emulsion templated materials were developed for use as injectable scaffolds to further tissue engineering therapies. Current treatment options rely on donor tissue or poorly matched synthetic materials that later require revision treatments. Injectable systems are advantageous in tissue repair because of their ability to space-fill irregular defects resulting from injury, deformity, or tumor resection without the need for expensive fabrication to shape or custom-build devices. We have demonstrated that these unique porous scaffolds can space-fill irregular tissue defects, rapidly polymerize at body temperature, and possess appropriate and tunable mechanical properties. Emulsion compositions were designed to eliminate the toxic solvents commonly used to fabricate biodegradable polyHIPEs without sacrificing high porosity and mechanical properties. First, surfactant chemical structure was studied to elucidate new structure-property relationships affecting emulsion formation and resultant pore structures. A variety of methacrylate and isocyanate polymers were utilized to facilitate rapid scaffold polymerization at body temperature and maintain cytocompatibility. Varying polymer composition resulted in tunable scaffold mechanical properties similar to bone and soft tissues. Use of redox initiation dramatically reduced cure times from hours to minutes and improved compressive properties without compromising pore

architecture. These studies demonstrated the ability of emulsion templated scaffolds to improve upon current scaffold materials used to treat injuries.

The principles learned in developing these scaffolds were also used to create porous polyHIPE microspheres which could potentially increase graft bioactivity. Growth factors like rhBMP-2 are commonly used to improve bone regeneration *in vivo*, but the excessive dosages have caused their cost and safety to be questioned by many researchers. An improved drug delivery system could decrease the required amount and thereby reduce treatment cost and side effects. These microspheres possessed the same porous structure and material properties as the scaffolds but could be easily loaded with drugs and growth factors to promote and guide tissue regeneration. Microspheres loaded with a small amount of rhBMP-2 exhibited a high encapsulation efficiency of 73%. In future studies, these particles can be incorporated into the scaffolds to guide cell differentiation and tissue regeneration directly at the site of injury.

In summary, we have developed a library of injectable porous materials that can be used to improve tissue regeneration. Furthermore, the emulsion chemistry structure-property relationships explored here can be used in designing future polyHIPEs for tissue engineering or other applications.

6.2 Significance of Work

Chapter II described the fabrication and development of the first solvent-free and biodegradable polyHIPE. PFDMA's highly reactive methacrylate end-groups and a low molecular weight resulted in a low-viscosity emulsion that cured at body temperature,

and ultimately opened up the possibility of incorporating living cells or proteins inside the emulsions. Prior to this, the majority of polyHIPEs used styrene/divinylbenzene systems which were not degradable, and any biodegradable polymers required solvents to reduce their viscosity and allow emulsification which did not allow for an injectable system or cell encapsulation. Additionally, the effect of hydrogen bonding sites in surfactant chemical structures on emulsion stability was discussed for the first time. Surfactant selection has previously been accomplished by utilizing the HLB method to narrow down choices, and then trial-and-error to find the best one. With thousands of possible surfactants to choose from, this process was time consuming and wasteful. The new selection criteria is based on molecular hydrophobicity predictions and key surfactant structure features provided a rational selection methodology for new biodegradable formulations. Indeed, we have used this method to select new macromer chemistries with a 100% success rate.

The PUU scaffolds produced in Chapter III were the first injectable polyMIPEs to have elastomeric properties. In contrast to the first generation PFDMA polyHIPEs that were rigid and brittle, these materials were pliable and exhibited elastic recovery close to 100% after large strains. This demonstrated that injectable scaffolds could be applied to treat both hard and soft tissues. Another advantage of the PUU system was the increased porosity caused by carbon dioxide blowing during polymerization, enhancing the emulsion's space-filling properties, and resulting in large interconnected pores which can theoretically increase nutrient flux over non-porous soft-tissue scaffolds.

The double-barrel syringe storage and delivery system developed in Chapter IV solved two future obstacles to clinical translation. The first generation polyHIPEs developed in Chapter II required up to 2 hours to cure and had to be made shortly before use. Surgeons would not be able to "close-up" a patient until the scaffold had hardened and leaving incisions open for 2 hours would likely be put patients at an unacceptably high risk for infection. Additionally, surgeons would have been required to make the emulsions prior to the procedure which could take up to 30 minutes and user-specific handling could affect the final scaffold properties. This study determined that pre-cured emulsions could be stored for up to 6 months at 4 °C prior to use without any significant effect on pore structure, allowing HIPEs to be made uniformly at a central plant and then shipped to clinics in pre-packaged syringes. The first generation polyHIPEs also relied on thermal initiation to polymerize, and increasing cure temperature would decrease set time but put the patient at risk of acute tissue necrosis. The use of redox pair initiators dramatically decreased cure time from hours to minutes for PFDMA, EGDMA, and BDMA polyHIPEs without increasing the scaffold's curing exotherm. The double-barrel syringe system permitted HIPEs to be safely stored until needed and cure rapidly on-demand comparable to current materials such as PMMA bone cement. Furthermore, this system could be applied to large scale with two emulsion streams mixing just prior to mold filling, and used in fabricating any porous media with temperature sensitive components.

Finally, chapter V demonstrated another use of the emulsion templated polyHIPEs to improve the bioactivity of the load-bearing scaffolds. Here, HIPE droplets

were made via a double emulsion process adapted from microfluidics fabrication techniques. Typically this process and all others to develop drug eluting microspheres require solvents and thus purification before use. Our system is solvent-free, which eliminates the need for purification and thus reduces manufacturing costs. Additionally, drugs and growth factors can be added to the aqueous phase of the initial emulsion instead of being added later. Both of these advantages result in higher theoretical loading efficiencies and bioactivity retention over traditional drug-loaded microsphere fabrication techniques.

In summary, these studies have resulted in a solvent-free method to fabricate a variety of porous materials that can be used to advance tissue engineering. Beyond tissue engineering, these studies have also investigated the relationships between surfactant chemical structures and polymer chemistry on emulsion formation and resultant material properties, specifically in solvent-free systems which had not been studied before.

6.3 Challenges and Future Directions

These studies lay the foundation for a successful and effective tissue engineered scaffold, but much work still needs to done and questions answered. Several methods to tune pore size have been presented, most notably through controlling surfactant concentration and mixing speeds. However, the changes remained on the order of tens of microns and it would be ideal to increase that range to 100 μm or greater. A class of surfactant termed “defoamers” has been used extensively in the production of PU foams to facilitate cell collapse in polymer-air foams. Typically a defoamer would

counterbalance another surfactant in order to stabilize pores up to a certain size but cause the collapse of larger ones. Previously, calcium stearate was investigated to increase thermally initiated PFDMA polyHIPEs but it often caused complete collapse before the emulsion could polymerize. Attempting to add the defoamer closer to the gel point was slightly more successful but resulted in a heterogeneous pore structure. With the introduction of redox initiation and its shorter cure times, calcium stearate should be reevaluated as a possible means to increase pore size. A small amount of calcium stearate suspended in water could be added while the redox HIPEs are mixed, promoting droplet coalescence until the gel point is reached and pore structure set. These tests should be run with either EGDMA or BDMA because their decreased viscosity and larger pore sizes would magnify any observable changes. Alternatively, incorporating small amphiphilic molecules such as PEG 600 has been shown to increase droplet coalescence, and thus pore and interconnect size. The amphiphile is hypothesized to increase water droplet size (and thus pore diameter) in a similar manner as Ostwald ripening. The amphiphile is thought to increase water molecule transport through the uncured polymer film separating suspended droplets, increasing average droplet size by causing some to expand and others to shrink. Either of these approaches may yield an increased pore and interconnect size, but any new components would have to be evaluated for cytocompatibility as well their effect on mechanical properties.

In addition to increasing pore and interconnect sizes, there is the need to decouple the two features. Until now, emulsion destabilization has been the pursued method of increasing either but always affects both. Therefore, increasing pores will

usually increase interconnect size. This is an acceptable trade-off for the near future, but there may come a time where it would be ideal to keep one property constant while modifying the other. Interconnects form as a result of polymer film shrinkage during polymerization, and typically the thinnest film occurs where two droplets are tangent to each other. Very large interconnects have been achieved in classic styrene/divinylbenzene polyHIPEs because these systems also incorporated solvent. During polymerization, the solvent would become increasingly insoluble in the polymer and aggregate to the cell walls between droplets. Upon drying, the solvent would be removed leaving large interconnects between pores. This exact mechanism is not possible in the solvent-free systems described here but it could potentially be mimicked using a semi-miscible or rapidly degrading monomer. A minute amount of low molecular weight polyanhydride without reactive endgroups could be mixed with a reactive macromer such as EGDMA. Upon initiation, EGDMA would begin to crosslink and potentially separate from the anhydride monomers which could form a film between droplets. Anhydride bonds degrade rapidly in the presence of water; our lab has observed degradation beginning within minutes of exposure. This could mimic the effect seen in solvent containing styrene systems and potentially provide a way to independently tune interconnect and pore size.

The porous microspheres are a promising method to impart bioactivity into the polyHIPE scaffolds. Although this first formulation successfully incorporated rhBMP-2, higher encapsulation efficiencies are desired. The rhBMP-2 is hypothesized to be lost during microsphere fabrication due to diffusion between the relatively high

concentration of rhBMP-2 in the microsphere and the dilute external aqueous phase. Fabrication of closed pore microspheres would stop this diffusion and theoretically increase encapsulation efficiency. Upon degradation, the pore walls would open or become more permeable to rhBMP-2 and release would begin. Decreasing internal water volume and making polyMIPEs is one method to decrease pore interconnectivity and requires no new formulations. Alternatively, use of an aqueous phase initiator has been shown to promote close pore formation in polyHIPEs.

With a closed pore microsphere system, degradation would have to be quick and tunable to control growth factor release. Unfortunately, EGDMA's high crosslink density makes it a slow degrading polymer. Recently, thiol-ene crosslinking chemistries have been explored for future polyHIPE formulations and show increased degradation rates proportional to thiol content. These thiol-ene emulsions could be used to make closed pore microspheres with controllable degradation, hypothetically increasing encapsulation efficiency and release kinetics.

Finally, these scaffolds have been designed and tested in the lab and their *in vitro* properties are being studied concurrently, but they must be tested *in vivo* to truly advance the knowledge of graft performance. The load-bearing nature of these scaffolds should require a study on changes in mechanical properties during any *in vivo* studies, specifically testing changes in modulus, strength, and fatigue. While simple hydrolytic degradation has been evaluated via mass loss under accelerated conditions, it should also result in decreased compressive modulus and strength. The damaged tissue is hypothesized to regenerate which may alleviate any loss in modulus and strength.

Therefore, it may be telling to implant pre-formed, cylindrical specimens into rat ulnar defects. These defects remain relatively unloaded, mitigating any fatigue or creep/stress-relaxation that could affect the implants. Then at set times, explanting scaffolds and subjecting them to 3-point bending tests to calculate changes in modulus, strength, or fatigue strength compared to day 0 properties. These results could be compared with accompanying radiographs or CT scans to measure bone growth and related to restoration of function.

Although there are many studies remaining before these devices can be used in the clinic, this system offers potential for an off-the-shelf treatment to improve tissue regeneration over current methods. The studies proposed would further improve the knowledge of polyHIPE interconnect formation and *in vivo* scaffold performance.

REFERENCES

1. Wang, X.; Shen, X.; Li, X.; Mauli Agrawal, C., Age-related changes in the collagen network and toughness of bone. *Bone* **2002,** 31, (1), 1-7.

2. Karageorgiou, V.; Kaplan, D., Porosity of 3D biomaterial scaffolds and osteogenesis. *Biomaterials* **2005,** 26, 5474-5491.

3. Chen, G.; Ushida, T.; Tateishi, T., Development of biodegradable porous scaffolds for tissue engineering. *Materials Science and Engineering: C* **2001,** 17, (1-2), 63-69.

4. Yang, S.; Leong, K. F.; Du, Z.; Chua, C. K., The design of scaffolds for use in tissue engineering. Part I: Traditional factors. *Tissue Engineering* **2001,** 7, (6), 679-89.

5. Alila Medical Media, Bone structure. www.shutterstock.com.

6. Biewener, A. A., Musculoskeletal design in relation to body size. *Journal of Biomechanics* **1991,** 24, Supplement 1, (0), 19-29.

7. Zioupos, P.; Currey, J. D., Changes in the stiffness, strength, and toughness of human cortical bone with age. *Bone* **1998,** 22, (1), 57-66.

8. Taylor, D., Fatigue of bone and bones: An analysis based on stressed volume. *Journal of Orthopaedic Research* **1998,** 16, (2), 163-169.

9. Freyman, T. M.; Yannas, I. V.; Gibson, L. J., Cellular materials as porous scaffolds for tissue engineering. *Progress in Materials Science* **2001,** 46, (3-4), 273-282.

10. Bhatia, S. N.; Chen, C. S., Tissue engineering at the micro-scale. *Biomedical Microdevices* **1999,** 2, (2), 131-144.

11. Busby, W.; Cameron, N. R.; Jahoda, C. A. B., Tissue engineering matrixes by emulsion templating. *Polymer International* **2002,** 51, 871-881.

12. Harris, L. D.; Kim, B.-S.; Mooney, D. J., Open pore biodegradable matrices formed with gas foaming. *Journal of Biomedical Materials Research* **1998,** 42, (3), 396-402.

13. Kim, T. K.; Yoon, J. J.; Lee, D. S.; Park, T. G., Gas foamed open porous biodegradable polymeric microspheres. *Biomaterials* **2006,** 27, 152-159.

14. Pham, Q. P.; Sharma, U.; Mikos, A. G., Electrospinning of polymeric nanofibers for tissue engineering applications: a review. *Tissue Engineering* **2006,** 12, (5), 1197-1211.

15. Rose, F. R. A. J.; Oreffo, R. O. C., Bone tissue engineering: hope vs hype. *Biochemical and Biophysical Research Communications* **2002,** 292, (1), 1-7.

16. Hacker, M.; Ringhofer, M.; Appel, B.; Neubauer, M.; Vogel, T.; Young, S.; Mikos, A. G.; Blunk, T.; Gopferich, A.; Schulz, M. B., Solid lipid templating of macroporous tissue engineering scaffolds. *Biomaterials* **2007,** 28, (24), 3497-3507.

17. Mistry, A. S.; Cheng, S. H.; Yeh, T.; Christenson, E.; Jansen, J. A.; Mikos, A. G., Fabrication and *in vitro* degradation of porous fumarate-based polymer/alumoxane nanocomposite scaffolds for bone tissue engineering. *Journal of Biomedical Materials Research, Part A* **2009,** 89A, (1), 68-79.

18. Gailani, G.; Benalla, M.; Mahamud, R.; Cowin, S. C.; Cardoso, L., Experimental determination of the permeability in the lacunar-canalicular porosity of bone. *Journal of Biomechanical Engineering* **2009,** 131, (10), 101007-7.

19. Ruckenstein, E., The concentrated emulsion approach to toughened polymer composites: a review. *Polymer Composites* **1997,** 18, (3), 320-331.

20. Konttinen, Y. T.; Zhao, D.; Beklen, A.; Ma, G.; Takagi, M.; Kivela-Rajamaki, M.; Ashammakhi, N.; Santavirta, S., The microenvironment around total hip replacement prostheses. *Clinical Orthopaedics and Related Research* **2005**, 28-38.

21. Artico, M.; Ferrante, L.; Pastore, F. S.; Ramundo, E. O.; Cantarelli, D.; Scopelliti, D.; Lannetti, G., Bone autografting of the calvaria and craniofacial skeleton: historical background, surgical results in a series of 15 patients, and review of the literature. *Surgical Neurology* **2003,** 60, 71-79.

22. Chen, J.; Horan, R. L.; Bramono, D.; Moreau, J. E.; Wang, Y.; Geuss, L. R.; Collette, A. L.; Volloch, V.; Altman, G. H., Monitoring mesenchymal stromal cell developmental stage to apply on-time mechanical stimulation for ligament tissue engineering. *Tissue Engineering* **2006,** 12, (11), 3085-3095.

23. Hemmrich, K.; von Heimburg, D.; Rendchen, R.; Di Bartolo, C.; Milella, E.; Pallua, N., Implantation of preadipocyte-loaded hyaluronic acid-based scaffolds into nude mice to evaluate potential for soft tissue engineering. *Biomaterials* **2005,** 26, (34), 7025-7037.

24. Amsden, B., Curable, biodegradable elastomers: emerging biomaterials for drug delivery and tissue engineering. *Soft Matter* **2007,** 3, 1335-1348.

25. Chandrashekar, N.; Mansouri, H.; Slauterbeck, J.; Hashemi, J., Sex-based differences in the tensile properties of the human anterior cruciate ligament. *Journal of Biomechanics* **2006,** 39, (16), 2943-2950.

26. Akizuki, S.; Mow, V. C.; Müller, F.; Pita, J. C.; Howell, D. S.; Manicourt, D. H., Tensile properties of human knee joint cartilage: I. Influence of ionic conditions, weight bearing, and fibrillation on the tensile modulus. *Journal of Orthopaedic Research* **1986,** 4, (4), 379-392.

27. Samartzis, D.; Shen, F. H.; Matthews, D. K.; Yoon, S. T.; Goldberg, E. J.; An, H. S., Comparison of allograft to autograft in multilevelanterior cervical discectomy and fusion with rigid plate fixation. *The Spine Journal* 3, (6), 451-459.

28. Chau, A.; Mobbs, R., Bone graft substitutes in anterior cervical discectomy and fusion. *European Spine Journal* **2009,** 18, (4), 449-464.

29. Liu, X.; Ma, P. X., Polymeric scaffolds for bone tissue engineering. *Annals of Biomedical Engineering* **2004,** 32, (3), 477-486.

30. Mikos, A. G.; Temenoff, J. S., Formation of highly porous biodegradable scaffolds for tissue engineering. *Electronic Journal of Biotechnology* **2000,** 3, (2), 114-119.

31. Costantino, P. D.; Hiltzik, D.; Govindaraj, S.; Moche, J., Bone healing and bone substitutes. *Facial Plastic Surgery* **2002,** 18, 13-26.

32. Seal, B. L.; Otero, T. C.; Panitch, A., Polymeric biomaterials for tissue and organ regeneration. *Materials Science and Engineering* **2001,** R34, 147-230.

33. Mercuri, L. G.; Giobbie-Hurder, A., Long-term outcomes after total alloplastic temporomandibular joint reconstruction following exposure to failed materials. *Journal of Oral and Maxillofacial Surgery* **2004,** 62, 1088-1096.

34. Svaldi-Muggli, D.; Burkoth, A. K.; Anseth, K. S., Crosslinked polyanhydrides for use in orthopaedic applications: degradation behavior and mechanics. *Journal of Biomedical Materials Research* **1999,** 46, 271-278.

35. Peter, S. J.; Kim, P.; Yasko, A. W.; Yaszemski, M. J.; Mikos, A. G., Crosslinking characteristics of an injectable poly(propylene fumarate)/β-tricalcium phosphate paste and mechanical properties of the crosslinked composite for use as a biodegradable bone cement. *Journal of Biomedical Materials Research* **1999,** 44, 314-321.

36. Peter, S. J.; Lu, L.; Kim, D. J.; Mikos, A. G., Marrow stromal osteoblast function on a poly(propylene fumarate)/β-tricalcium phosphate biodegradable orthopaedic composite. *Biomaterials* **2000,** 21, 1207-1213.

37. Peter, S. J.; Nolley, J. A.; Widmer, M. S.; Merwin, J. E.; Yaszemski, M. J.; Yasko, A. W.; Engel, P. S.; Mikos, A. G., *In vitro* degradation of a poly(propylene fumarate)/β-tricalcium phosphate composite orthopaedic scaffold. *Tissue Engineering* **1995,** 1, 41-52.

38. Burdick, J. A.; Anseth, K. S., Photoencapsulation of osteoblasts in injectable RGD-modified PEG hydrogels for bone tissue engineering. *Biomaterials* **2002,** 23, 4315-4323.

39. Fromstein, J. D.; Woodhouse, K. A., Elastomeric biodegradable polyurethane blends for soft tissue applications. *Journal Of Biomaterials Science. Polymer Edition* **2002,** 13, (4), 391-406.

40. Fisher, J. P.; Holland, T. A.; Dean, D.; Engel, P. S.; Mikos, A. G., Synthesis and properties of photocross-linked poly(propylene fumarate) scaffolds. *Journal Of Biomaterials Science. Polymer Edition* **2001,** 12, (6), 673-687.

41. Timmer, M. D.; Horch, A. R.; Ambrose, C. G.; Mikos, A. G., Effect of physiological temperature on the mechanical properties and network structure of biodegradable poly(propylene fumarate)-based networks. *Journal Biomaterial Science Polymer Edition* **2003,** 14, (4), 369-382.

42. Ergun, A.; Yu, X.; Valdevit, A.; Ritter, A.; Kalyon, D. M., *In vitro* analysis and mechanical properties of twin screw extruded single-layered and coextruded multilayered poly(caprolactone) scaffolds seeded with human fetal osteoblasts for bone tissue engineering. *Journal of Biomedical Materials Research Part A* **2011,** 99A, (3), 354-366.

43. Gogolewski, S.; Gorna, K.; Turner, A. S., Regeneration of bicortical defects in the iliac crest of estrogen-deficient sheep, using new biodegradable polyurethane bone graft substitutes. *Journal of Biomedical Materials Research* **2006,** 77A, (4), 802–810.

44. Guan, J.; Fujimoto, K. L.; Sacks, M. S.; Wagner, W. R., Preparation and characterization of highly porous, biodegradable polyurethane scaffolds for soft tissue applications. *Biomaterials* **2005,** 26, (18), 3961-3971.

45. Jabbari, E.; Wang, S.; Lu, L.; Gruetzmacher, J. A.; Ameenuddin, S.; Hefferan, T. E.; Currier, B. L.; Windebank, A. J.; Yaszemski, M. J., Synthesis, material properties, and biocompatibility of a novel self-cross-linkable poly(caprolactone fumarate) as an injectable tissue engineering scaffold. *Biomacromolecules* **2005,** 6, (5), 2503-2511.

46. Pêgo, A. P.; Poot, A. A.; Grijpma, D. W.; Feijen, J., Biodegradable elastomeric scaffolds for soft tissue engineering. *Journal of Controlled Release* **2003,** 87, (1-3), 69-79.

47. Schmedlen, R.; Masters, K.; West, J., Photocrosslinkable polyvinyl alcohol hydrogels that can be modified with cell adhesion peptides for use in tissue engineering. *Biomaterials* **2002,** 23, 4325-4332.

48. Tai, H.; Sergienko, A.; Silverstein, M. S., High internal phase emulsion foams: copolymers and interpenetrating polymer networks. *Polymer Engineering and Science* **2001,** 41, (9), 1540-1552.

49. Christenson, E.; Anseth, K.; van den Beucken, J.; Chan, C.; Ercan, B.; Jansen, J.; Laurencin, C.; Li, W.; Murugan, R.; Nair, L.; Ramakrishna, S.; Tuan, R.; Webster, T.; Mikos, A., Nanobiomaterial applications in orthopedics. *Journal of Orthopaedic Research* **2007,** 25, (1), 11-22.

50. Langer, R.; Vacanti, J. P., Tissue engineering. *Science* **1993,** 260, (5110), 920-926.

51. Kenley, R.; Yim, K.; Abrams, J.; Ron, E.; Turek, T.; Marden, L.; Hollinger, J., Biotechnology and bone graft substitutes. *Pharmaceutical Research* **1993,** 10, (10), 1393-1401.

52. Sikavitsas, V. I.; Temenoff, J. S.; Mikos, A. G., Biomaterials and bone mechanotransduction. *Biomaterials* **2001,** 22, (19), 2581-2593.

53. Cameron, N. R.; Sherrington, D. C.; Albiston, L.; Gregory, D. P., Study of the formation of the open-cellular morphology of poly(styrene/divinylbenzene) polyHIPE materials by cryo-SEM. *Colloid and Polymer Science* **1996,** 274, 592-595.

54. Akay, G.; Birch, M. A.; Bokhari, M. A., Microcellular polyHIPE polymer supports osteoblast growth and bone formation *in vitro*. *Biomaterials* **2004,** 25, 3991-4000.

55. Hayman, M. W.; Smith, K. H.; Cameron, N. R.; Przyborskia, S. A., Growth of human stem cell-derived neurons on solid three-dimensional polymers. *Journal of Biochemical and Biophysical Methods* **2005,** 62, 231-240.

56. Busby, W.; Cameron, N. R.; Jahoda, C. A. B., Emulsion-derived foams (polyHIPEs) containing poly(ε-caprolactone) as matrixes for tissue engineering. *Biomacromolecules* **2001,** 2, (1), 154-164.

57. Barbetta, A.; Dentini, M.; Zannoni, E. M.; De Stefano, M. E., Tailoring the Porosity and Morphology of Gelatin-Methacrylate PolyHIPE Scaffolds for Tissue Engineering Applications. *Langmuir* **2005,** 21, (26), 12333-12341.

58. Barbetta, A.; Dentini, M.; De Vecchis, M. S.; Filippini, P.; Formisano, G.; Caiazza, S., Scaffolds based on biopolymeric foams. *Advanced Functional Materials* **2005,** 15, (1), 118-124.

59. Cameron, N. R.; Barbetta, A.; Cooper, S. J., High internal phase emulsions (HIPEs) containing divinylbenzene and 4-vinylbenzyl chloride and the morphology of the resulting PolyHIPE materials. *Chemical Communications* **2000**, 221–222.

60. Bokhari, M. A.; Birch, M. A.; Akay, G., Polyhipe polymer: a novel scaffold for *in vitro* bone tissue engineering. *Experimental Medical Biology: Tissue Engineering, Stem Cells, and Gene Therapies* **2003,** 534, 247-254.

61. Hayman, M. W.; Smith, K. H.; Cameron, N. R.; Przyborski, S. A., Enhanced neurite outgrowth by human neurons grown on solid three-dimensional scaffolds. *Biochemical and Biophysical Research Communications* **2004,** 314, (2), 483-488.

62. Cameron, N. R.; Sherrington, D. C.; Ando, I.; Kuroso, H., Chemical modification of monolithic poly(styrene/divinylbenzene) polyHIPE materials. *Journal of Material Chemistry* **1996,** 6, 719-726.

63. Williams, J. M.; Wrobleski, D. A., Spatial distribution of the phases in water-in-oil emulsions. Open and closed microcellular foams from cross-linked polystryene. *Langmuir* **1988,** 4, (3), 656-662.

64. Cameron, N. R.; Sherrington, D. C., Synthesis and characterisation of poly(aryl ether sulfone) polyHIPE materials. *Macromolecules* **1997,** 30, 5860-5869.

65. Lumelsky, Y.; Silverstein, M., Biodegradable porous polymers through emulsion templating. *Macromolecules* **2009,** 42, 1627-1633.

66. Youssef, C.; Backov, R.; Treguer, M.; Birot, M.; Deleuze, H., Preparation of amazingly hard polyHIPE material from a direct emulsion. *Materials Research Society Symposium* **2010,** 1269, 1-6.

67. Williams, J. M.; Gray, A. J.; Wilkerson, M. H., Emulsion stability and rigid foams from styrene or divinylbenzene water-in-oil emulsions. *Langmuir* **1990,** 6, 437-444.

68. Yaszemski, M. J.; Payne, R. G.; Hayes, W. C.; Langer, R.; Mikos, A. G., Evolution of bone transplantation: molecular, cellular and tissue strategies to engineer human bone. *Biomaterials* **1996,** 17, (2), 175-185.

69. Bennett, S.; Connolly, K.; Lee, D. R.; Jiang, Y.; Buck, D.; Hollinger, J. O.; Gruskin, E. A., Initial biocompatibility studies of a novel degradable polymeric bone substitute that hardens *in situ*. *Bone* **1996,** 19, (1, Supplement 1), S101-S107.

70. Hafeman, A. E.; Li, B.; Yoshii, T.; Zienkiewicz, K.; Davidson, J. M.; Guelcher, S. A., Injectable biodegradable polyurethane scaffolds with release of platelet-derived growth factor for tissue repair and regeneration. *Pharmaceutical Research* **2008,** 25, (10), 2387-2399.

71. Lewandrowski, K. U.; Gresser, J. D.; Bondre, S.; Silva, A. E.; Wise, D. L.; Trantolo, D. J., Developing porosity of poly(propylene glycol-co-fumaric acid) bone graft substitutes and the effect on osteointegration: a preliminary histology study in rats. *Journal Of Biomaterials Science. Polymer Edition* **2000,** 11, (8), 879-889.

72. Takahashi, Y.; Tabata, Y., Effect of the fiber diameter and porosity of non-woven PET fabrics on the osteogenic differentiation of mesenchymal stem cells. *Journal of Biomaterials Science-Polymer Edition* **2004,** 15, (1), 41-57.

73. Kuboki, Y.; Jin, Q.; Kikuchi, M.; Mamood, J.; Takita, H., Geometry of Artificial ECM: Sizes of Pores Controlling Phenotype Expression in BMP-Induced Osteogenesis and Chondrogenesis. *Connective Tissue Research* **2002,** 43, (2-3), 529-534.

74. Jin, Q. M.; Takita, H.; Kohgo, T.; Atsumi, K.; Itoh, H.; Kuboki, Y., Effects of geometry of hydroxyapatite as a cell substratum in BMP-induced ectopic bone formation. *Journal of Biomedical Materials Research* **2000,** 52, (4), 841-851.

75. Liu, L.-S.; Thompson, A. Y.; Heidaran, M. A.; Poser, J. W.; Spiro, R. C., An osteoconductive collagen/hyaluronate matrix for bone regeneration. *Biomaterials* **1999,** 20, (12), 1097-1108.

76. Tsuruga, E.; Takita, H.; Itoh, H.; Wakisaka, Y.; Kuboki, Y., Pore Size of Porous Hydroxyapatite as the Cell-Substratum Controls BMP-Induced Osteogenesis. *Journal of Biochemistry* **1997,** 121, (2), 317-324.

77. Kuboki, Y.; Jin, Q.; Takita, H., Geometry of carriers controlling phenotypic expression in BMP-induced osteogenesis and chondrogenesis. *The Journal Of Bone And Joint Surgery. American Volume* **2001,** 83-A Suppl 1, (Pt 2), S105-S115.

78. Hulbert, S. F.; Young, F. A.; Mathews, R. S.; Klawitter, J. J.; Talbert, C. D.; Stelling, F. H., Potential of ceramic materials as permanently implantable skeletal prostheses. *Journal of Biomedical Materials Research* **1970,** 4, 433-456.

79. Fisher, J. P.; Vehof, J. W. M.; Dean, D.; van der Waerden, J. P. C. M.; Holland, T. A.; Mikos, A. G.; Jansen, J. A., Soft and hard tissue response to photocrosslinked poly(propylene fumarate) scaffolds in a rabbit model. *Journal of Biomedical Materials Research* **2002,** 59, (3), 547-556.

80. Kujala, S.; Ryhänen, J.; Danilov, A.; Tuukkanen, J., Effect of porosity on the osteointegration and bone ingrowth of a weight-bearing nickel–titanium bone graft substitute. *Biomaterials* **2003,** 24, (25), 4691-4697.

81. Kruyt, M. C.; de Bruijn, J. D.; Wilson, C. E.; Oner, F. C.; van Blitterswijk, C. A.; Verbout, A. J.; Dhert, W. J. A., Viable osteogenic cells are obligatory for tissue-engineered ectopic bone formation in goats. *Tissue Engineering* **2003,** 9, (2), 327-336.

82. Itoh, M.; Shimazu, A.; Hirata, I.; Yoshida, Y.; Shintani, H.; Okazaki, M., Characterization of CO3Ap-collagen sponges using X-ray high-resolution microtomography. *Biomaterials* **2004,** 25, (13), 2577-2583.

83. Chu, T. M. G.; Orton, D. G.; Hollister, S. J.; Feinberg, S. E.; Halloran, J. W., Mechanical and *in vivo* performance of hydroxyapatite implants with controlled architectures. *Biomaterials* **2002,** 23, (5), 1283-1293.

84. Klawitter, J. J.; Hulbert, S. F., Application of porous ceramics for the attachment of load bearing internal orthopedic applications. *Journal of Biomedical Materials Research* **1971,** 5, (6), 161-229.

85. Madden, L. R.; Mortisen, D. J.; Sussman, E. M.; Dupras, S. K.; Fugate, J. A.; Cuy, J. L.; Hauch, K. D.; Laflamme, M. A.; Murry, C. E.; Ratner, B. D., Proangiogenic scaffolds as functional templates for cardiac tissue engineering. *Proceedings of the National Academy of Sciences* **2010,** 107, (34), 15211-15216.

86. Roy, T. D.; Simon, J. L.; Ricci, J. L.; Rekow, E. D.; Thompson, V. P.; Parsons, J. R., Performance of degradable composite bone repair products made via three-dimensional fabrication techniques. *Journal of Biomedical Materials Research Part A* **2003,** 66A, (2), 283-291.

87. Schultz, R. J.; Johnston, A. D.; Krishnamurthy, S., Thermal effects of polymerization of methyl-methacrylate on small tubular bones. *International Orthopaedics* **1987,** 11, (3), 277-282.

88. Stankus, J. J.; Guan, J.; Wagner, W. R., Fabrication of biodegradable elastomeric scaffolds with sub-micron morphologies. *Journal of Biomedical Materials Research Part A* **2004,** 70A, (4), 603-614.

89. Day, R. M.; Boccaccini, A. R.; Maquet, V.; Shurey, S.; Forbes, A.; Gabe, S. M.; Jérôme, R., *In vivo* characterisation of a novel bioresorbable poly(lactide-co-glycolide) tubular foam scaffold for tissue engineering applications. *Journal of Materials Science: Materials in Medicine* **2004,** 15, (6), 729-734.

90. Barralet, J. E.; Grover, L.; Gaunt, T.; Wright, A. J.; Gibson, I. R., Preparation of macroporous calcium phosphate cement tissue engineering scaffold. *Biomaterials* **2002,** 23, (15), 3063-3072.

91. Marshall, A. J.; Ratner, B. D., Quantitative characterization of sphere-templated porous biomaterials. *AIChE Journal* **2005,** 51, (4), 1221-1232.

92. Lin-Gibson, S.; Cooper, J. A.; Landis, F. A.; Cicerone, M. T., Systematic investigation of porogen size and content on scaffold morphometric parameters and properties. *Biomacromolecules* **2007,** 8, (5), 1511-1518.

93. Barbetta, A.; Massimi, M.; Conti Devirgiliis, L.; Dentini, M., Enzymatic cross-linking vs radical polymerization in the preparation of gelatin polyHIPEs and their performances as scaffolds in the culture of hepatocytes. *Biomacromolecules* **2006,** 7, (11), 3059-3068.

94. Bokhari, M. A.; Akay, G.; Zhang, S.; Birch, M. A., The enhancement of osteoblast growth and differentiation *in vitro* on a peptide hydrogel—polyHIPE polymer hybrid material. *Biomaterials* **2005,** 26, 5198-5208.

95. Gunn, J.; Turner, S.; Mann, B., Adhesive and mechanical properties of hydrogels influence neurite extension. *Journal of Biomedical Materials Research* **2004,** 72A, (1), 91-97.

96. Hahn, M. S.; Taite, L. J.; Moon, J. J.; Rowland, M. C.; Ruffino, K. A.; West, J. L., Photolithographic patterning of polyethylene glycol hydrogels. *Biomaterials* **2006,** 27, (12), 2519-2524.

97. Kretlow, J. D.; Mikos, A. G., From material to tissue: Biomaterial development, scaffold fabrication, and tissue engineering. *AIChE Journal* **2008,** 54, (12), 3048-3067.

98. Park, S.; Lee, S.; Kim, W., Fabrication of hydrogel scaffolds using rapid prototyping for soft tissue engineering. *Macromolecular Research* **2011,** 19, (7), 694-698.

99. Hearon, K.; Singhal, P.; Horn, J.; Small, W.; Olsovsky, C.; Maitland, K. C.; Wilson, T. S.; Maitland, D. J., Porous shape-memory polymers. *Polymer Reviews* **2013,** 53, (1), 41-75.

100. Neuss, S.; Blomenkamp, I.; Stainforth, R.; Boltersdorf, D.; Jansen, M.; Butz, N.; Perez-Bouza, A.; Knüchel, R., The use of a shape-memory poly(ε-caprolactone)dimethacrylate network as a tissue engineering scaffold. *Biomaterials* **2009,** 30, (9), 1697-1705.

101. Thornton, A. J.; Alsberg, E.; Albertelli, M.; Mooney, D. J., Shape-defining scaffolds for minimally invasive tissue engineering. *Transplantation* **2004,** 77, (12), 1798-1803.

102. Zhang, D.; Petersen, K. M.; Grunlan, M. A., Inorganic–organic shape memory polymer (SMP) foams with highly tunable properties. *ACS Applied Materials & Interfaces* **2012,** 5, (1), 186-191.

103. De Nardo, L.; Bertoldi, S.; Tanzi, M. C.; Haugen, H. J.; Farè, S., Shape memory polymer cellular solid design for medical applications. *Smart Materials and Structures* **2011,** 20, (3), 035004.

104. Barby, D.; Haq, Z., European Patent 0,060,138 (to Unilever). **1982**.

105. Christenson, E. M.; Hiltner, A.; Anderson, J. M., Biodegradation mechanism of polyurethane elastomers. *Corrossion Engineering Science and Technology* **2007,** 42, (4), 312-323.

106. Umez-Eronini, N. O.; Collins, A.; Neal, D. E., Optimisation of bladder stromal culture on polyHIPE *European Cells and Materials* **2002,** 4, (2), 77-78.

107. Tai, H.; Sergienko, A.; Silverstein, M., Organic-inorganic networks in foams from high internal phase emulsion polymerizations. *Polymer* **2001,** 42, 4473-4482.

108. Lepine, O., Preparation of macrocellular PU–PS interpenetrating networks. *Polymer* **2005,** 46, 9653–9663.

109. David, D.; Silverstein, M., Porous polyurethanes synthesized within high internal phase emulsions (HIPEs). *Journal of Polymer Science: Part A: Polymer Chemistry* **2009,** 47, 9.

110. Bokhari, M.; Carnachan, R. J.; A., P. S.; Cameron, N. R., Emulsion-templated porous polymers as scaffolds for three dimensional cell culture: effect of synthesis parameters on scaffold formation and homogeneity. *Journal of Materials Chemistry* **2007,** 17, 4088–4094.

111. Williams, J. M., High internal phase water-in-oil emulsions: influence of surfactants and cosurfactants on emulsion stability and foam quality. *Langmuir* **1991,** 7, 1370-1377.

112. Menner, A.; Bismarck, A., New evidence for the mechanism of the pore formation in polymerising high internal phase emulsions or why polyHIPEs have an interconnected pore network structure. *Macromolecular Symposia* **2006**, (242), 19-24.

113. Mercier, A.; Deleuzea, H.; Mondain-Monval, O., Preparation and functionalization of (vinyl)polystyrene polyHIPEs. Short routes to binding functional groups through a dimethylene spacer. *Reactive & Functional Polymers* **2000,** 46, 67–79.

114. Christenson, E. M.; Soofi, W.; Holm, J. L.; Cameron, N. R.; Mikos, A. G., Biodegradable fumarate-based polyHIPEs as tissue engineering scaffolds. *Biomacromolecules* **2007,** 8, 3806-3814.

115. Lumelsky, Y.; Lalush-Michael, I.; Levenberg, S.; Silverstein, M., A degradable, porous, emulsion-templated polyacrylate. *Journal of Polymer Science Part A: Polymer Chemistry* **2009,** 47, (24), 7043-7053.

116. Lumelsky, Y.; Zoldan, J.; Levenberg, S.; Silverstein, M. S., Porous polycaprolactone-polystyrene semi-interpenetrating polymer networks synthesized within high internal phase emulsions. *Macromolecules* **2008,** 41, 1469-1474.

117. Carnachan, R. J.; Bokhari, M.; Przyborski, S. A.; Cameron, N. R., Tailoring the morphology of emulsion-templated porous polymers. *Soft Matter* **2006,** 2, 608-616.

118. Hainey, P.; Huxham, I. M.; Rowatt, B.; Sherrington, D. C., Synthesis and ultrastructural studies of styrene-divinylbenzene polyHIPE polymers. *Macromolecules* **1991,** 24, (1), 117-121.

119. Porter, B. D.; Oldham, J. B.; He, S. L.; Zobitz, M. E.; Payne, R. G.; An, K. N.; Currier, B. L.; Mikos, A. G.; Yaszemski, M. J., Mechanical properties of a biodegradable bone regeneration scaffold. *Journal of Biomechanical Engineering* **2000,** 122, (3), 286-288.

120. Wolfe, M. S.; Dean, D.; Chen, J. E.; Fisher, J. P.; Han, S.; Rimnac, C. M.; Mikos, A. G., *In vitro* degradation and fracture toughness of multilayered porous poly(propylene fumarate)/β-tricalcium phosphate scaffolds. *Journal of Biomedical Materials Research* **2002,** 61, (1), 159-164.

121. Burdick, J. A.; Padera, R. F.; Huang, J. V.; Anseth, K. S., An investigation of the cytotoxicity and histocompatibility of *in situ* forming lactic acid based orthopedic biomaterials. *Journal of Biomedical Materials Research* **2002,** 63, (5), 484-491.

122. Burdick, J. A.; Frankel, D.; Dernell, W. S.; Anseth, K. S., An initial investigation of photocurable three-dimensional lactic acid based scaffolds in a critical-sized cranial defect. *Biomaterials* **2003,** 24, (9), 1613-1620.

123. Lin, A. S. P.; Barrows, T. H.; Cartmell, S. H.; Guldberg, R. E., Microarchitectural and mechanical characterization of oriented porous polymer scaffolds. *Biomaterials* **2003,** 24, (3), 481-489.

124. Borden, M.; El-Amin, S. F.; Attawia, M.; Laurencin, C. T., Structural and human cellular assessment of a novel microsphere-based tissue engineered scaffold for bone repair. *Biomaterials* **2003,** 24, (4), 597-609.

125. Ruckenstein, E.; Li, H., Rubber toughened styrene/methyl methacrylate/butyl methacrylate composites by the concentrated emulsion pathway. *Journal of Applied Polymer Science* **1994,** 54, (5), 561-568.

126. Ruckenstein, E.; Li, H., Toughened polystyrene composites by the concentrated emulsion pathway. *Journal of Applied Polymer Science* **1994,** 52, (13), 1949-1958.

127. Silverstein, M. S.; Tai, H.; Sergienko, A.; Lumelsky, Y.; Pavlovsky, S., PolyHIPE: IPNs, hybrids, nanoscale porosity, silica monoliths and ICP-based sensors. *Polymer* **2005,** 46, 6682–6694.

128. Despois, J.-F.; Mortensen, A., Permeability of open-pore microcellular materials. *Acta Materialia* **2005,** 53, (5), 1381-1388.

129. Botchwey, E. A.; Dupree, M. A.; Pollack, S. R.; Levine, E. M.; Laurencin, C. T., Tissue engineered bone: Measurement of nutrient transport in three-dimensional matrices. *Journal of Biomedical Materials Research Part A* **2003,** 67A, (1), 357-367.

130. Malachanne, E.; Dureisseix, D.; Cañadas, P.; Jourdan, F., Experimental and numerical identification of cortical bone permeability. *Journal of Biomechanics* **2008,** 41, (3), 721-725.

131. Baroud, G.; Falk, R.; Crookshank, M.; Sponagel, S.; Steffen, T., Experimental and theoretical investigation of directional permeability of human vertebral cancellous bone for cement infiltration. *Journal of Biomechanics* **2004,** 37, (2), 189-196.

132. Menner, A.; Powell, R.; Bismarck, A., A new route to carbon black filled polyHIPEs. *Soft Matter* **2006,** 2, 337–342.

133. Wu, R.; Menner, A.; Bismarck, A., Tough interconnected polymerized medium and high internal phase emulsions reinforced by silica particles. *Journal of Polymer Science Part A: Polymer Chemistry* **2010,** 48, 1979-1989.

134. Mistry, A.; Pham, Q.; Schouten, C.; Yeh, T.; Christensen, E.; Mikos, A.; Jansen, J., *In vivo* bone biocompatibility and degradation of porous fumarate-based polymer/alumoxane nanocomposites for bone tissue engineering. *Journal of Biomedical Materials Research Part A* **2010,** 92A, (2), 451-462.

135. ASTM, C. D. o. P., Standard test method for compressive properties of rigid cellular plastics (D 1621-04a). **2004**, (D 1621-04a).

136. Molinspiration, Interactive logP calculator. www.molinspiration.com.

137. Cameron, N. R.; Barbetta, A., The influence of porogen type on the porosity, surface area and morphology of poly(divinylbenzene) polyHIPE foams. *Journal of Materials Chemistry* **2000,** 10, 2466-2471.

138. Cohen, N.; Silverstein, M., Synthesis of emulsion-templated porous polyacrylonitrile and its pyrolysis to porous carbon monoliths. *Polymer* **2011,** 52, 282-287.

139. Patrick, C. W., Tissue engineering strategies for adipose tissue repair. *The Anatomical Record* **2001,** 263, (4), 361-366.

140. Dhandayuthapani, B.; Yoshida, Y.; Maekawa, T.; Kumar, D. S., Polymeric scaffolds in tissue engineering application: a review. *International Journal of Polymer Science* **2011,** 2011.

141. Hodde, J., Naturally occuring scaffolds for soft tissue repair and regeneration. *Tissue Engineering* **2002,** 8, (2), 295-308.

142. Butler, D. L.; Goldstein, S. A.; Guilak, F., Functional tissue engineering: the role of biomechanics. *Journal of Biomechanical Engineering* **2000,** 122, (6), 570-575.

143. Kim, B.-S.; Mooney, D. J., Scaffolds for engineering smooth muscle under cyclic mechanical strain conditions. *Journal of Biomechanical Engineering* **2000,** 122, (3), 210-215.

144. Kim, B.-S.; Nikolovski, J.; Bonadio, J.; Mooney, D. J., Cyclic mechanical strain regulates the development of engineered smooth muscle tissue. *Nature Biotechnology* **1999,** 17, (10), 979-983.

145. Andrew A, B., Musculoskeletal design in relation to body size. *Journal of Biomechanics* **1991,** 24, Supplement 1, (0), 19-29.

146. Spaans, C. J.; de Groot, J. H.; Dekens, F. G.; Pennings, A. J., High molecular weight polyurethanes and a polyurethane urea based on 1,4-butanediisocyanate. *Polymer Bulletin* **1998,** 41, (2), 131-138.

147. Guan, J.; Sacks, M. S.; Beckman, E. J.; Wagner, W. R., Biodegradable poly(ether ester urethane)urea elastomers based on poly(ether ester) triblock copolymers and putrescine: synthesis, characterization and cytocompatibility. *Biomaterials* **2004,** 25, (1), 85-96.

148. Lee, S.-H.; Kim, B.-S.; Kim, S. H.; Choi, S. W.; Jeong, S. I.; Kwon, I. K.; Kang, S. W.; Nikolovski, J.; Mooney, D. J.; Han, Y.-K.; Kim, Y. H., Elastic biodegradable

poly(glycolide-co-caprolactone) scaffold for tissue engineering. *Journal of Biomedical Materials Research, Part A* **2003,** 66A, (1), 29-37.

149. Rouwkema, J.; Rivron, N. C.; van Blitterswijk, C. A., Vascularization in tissue engineering. *Trends in Biotechnology* **2008,** 26, (8), 434-441.

150. Benhardt, H.; Sears, N.; Touchet, T.; Cosgriff-Hernandez, E., Synthesis of collagenase-sensitive polyureas for ligament tissue engineering. *Macromolecular Bioscience* **2011,** 11, (8), 1020-1030.

151. Courtney, T.; Sacks, M. S.; Stankus, J.; Guan, J.; Wagner, W. R., Design and analysis of tissue engineering scaffolds that mimic soft tissue mechanical anisotropy. *Biomaterials* **2006,** 27, (19), 3631-3638.

152. Landers, R.; Pfister, A.; Hübner, U.; John, H.; Schmelzeisen, R.; Mülhaupt, R., Fabrication of soft tissue engineering scaffolds by means of rapid prototyping techniques. *Journal of Materials Science* **2002,** 37, (15), 3107-3116.

153. Landers, R.; Hübner, U.; Schmelzeisen, R.; Mülhaupt, R., Rapid prototyping of scaffolds derived from thermoreversible hydrogels and tailored for applications in tissue engineering. *Biomaterials* **2002,** 23, (23), 4437-4447.

154. Chen, J.; Park, H.; Park, K., Synthesis of superporous hydrogels: Hydrogels with fast swelling and superabsorbent properties. *Journal of Biomedical Materials Research* **1999,** 44, (1), 53-62.

155. Dumas, J. E.; Prieto, E. M.; Zienkiewicz, K. J.; Guda, T.; Wenke, J. C.; Bible, J. E.; Holt, G. E.; Guelcher, S., Balancing the rates of new bone formation and polymer degradation enhances healing of weight-bearing allograft/polyurethane composites in rabbit femoral defects. *Tissue Engineering: Part A* **2013**.

156. Duggan, M.; Rago, A.; Sharma, U.; Zugates, G.; Freyman, T.; Busold, R.; Caulkins, J.; Pham, Q.; Chang, Y.; Mejaddam, A.; Beagle, J.; Velmahos, G.; deMoya, M.; Zukerberg, L.; Ng, T. F.; King, L. D. R., Self-expanding polyurethane polymer improves survival in a model of noncompressible massive abdominal hemorrhage. *Journal of Trauma- Injury, Infection, and Critical Care* **2013,** 74, (6), 1462-1467.

157. Moglia, R. S.; Holm, J. L.; Sears, N. A.; Wilson, C. J.; Harrison, D. M.; Cosgriff-Hernandez, E., Injectable polyHIPEs as high-porosity bone grafts. *Biomacromolecules* **2011,** 12, (10), 3621-3628.

158. Robinson, J. L.; Moglia, R. S.; Stuebben, M. C.; McEnery, M. A. P.; Cosgriff-Hernandez, E., Achieving interconnected pore architecture in injectable polyHIPEs for bone tissue engineering. *Tissue Engineering: Part A* **2014,** 20, (5-6), 1103-1112.

159. Barbetta, A.; Cameron, N. R., Morphology and surface area of emulsion-derived (PolyHIPE) solid foams prepared with oil-phase soluble porogenic solvents: Span 80 as surfactant. *Macromolecules* **2004,** 37, 3188-3201.

160. Muschenborn, A.; Ortega, J.; Szafron, J.; Szafron, D.; Maitland, D., Porous media properties of reticulated shape memory polymer foams and mock embolic coils for aneurysm treatment. *Biomedical Engineering OnLine* **2013,** 12, (1), 1-13.

161. Geertsma, J., Estimating the coefficient of inertial resistance in fluid flow through porous media. *SPE Journal* **1974,** 14, (5), 445-450.

162. Hafeman, A. E.; Davidson, J. M.; Guelcher, S. A., Effects of polyol, isocyanate, and additives on poly(ester urethane)urea scaffolds: material and *in vivo* histological properties. *PMSE Preprints* **2007,** 97, 546.

163. Hafeman, A. E.; Zienkiewicz, K. J.; Carney, E.; Litzner, B.; Stratton, C.; Wenke, J. C.; Guelcher, S. A., Local delivery of tobramycin from injectable biodegradable polyurethane scaffolds. *Journal of Biomaterials Science, Polymer Edition* **2010,** 21, (1), 95-112.

164. Garrett, P. R., *Defoaming: Theory and Industrial Applications*. Marcel Dekker, Inc.: New York, 1993.

165. Dumas, J. E.; Davis, T.; Holt, G. E.; Yoshii, T.; Perrien, D. S.; Nyman, J. S.; Boyce, T.; Guelcher, S. A., Synthesis, characterization, and remodeling of weight-bearing allograft bone/polyurethane composites in the rabbit. *Acta Biomaterialia* **2010,** 6, (7), 2394-2406.

166. Etter, M. C., Hydrogen bonds as design elements in organic chemistry. *Journal of Physical Chemistry* **1991,** 95, (12), 4601-4610.

167. Christenson, E. M.; Anderson, J. M.; Hiltner, A.; Baer, E., Relationship between nanoscale deformation processes and elastic behavior of polyurethane elastomers. *Polymer* **2005,** 46, (25), 11744-11754.

168. Gogolewski, S., Selected topics in biomedical polyurethanes. A review. *Colloid and Polymer Science* **1989,** 267, (9), 757-785.

169. Mullins, L.; Tobin, N., Theoretical model for the elastic behavior of filler-reinforced vulcanized rubbers. *Rubber Chemistry and Technology* **1957,** 30, (2), 555-571.

170. Qi, H. J.; Boyce, M. C., Stress–strain behavior of thermoplastic polyurethanes. *Mechanics of Materials* **2005,** 37, (8), 817-839.

171. Yeh, F.; Hsiao, B. S.; Sauer, B. B.; Michel, S.; Siesler, H. W., *In-situ* studies of structure development during deformation of a segmented poly(urethane−urea) elastomer. *Macromolecules* **2003,** 36, (6), 1940-1954.

172. Hammond, P. T.; Nallicheri, R. A.; Rubner, M. F., An examination of the strain-induced orientation of hard segment domains in 4,4′-methylenebis(phenyl isocyanate)-based polyurethane-diacetylene segmented copolymers. *Materials Science and Engineering: A* **1990,** 126, (1–2), 281-287.

173. Saraf, H.; Ramesh, K. T.; Lennon, A. M.; Merkle, A. C.; Roberts, J. C., Mechanical properties of soft human tissues under dynamic loading. *Journal of Biomechanics* **2007,** 40, (9), 1960-1967.

174. Gao, J.; Crapo, P. M.; Wang, Y., Macroporous elastomeric scaffolds with extensive micropores for soft tissue engineering. *Tissue Engineering* **2006,** 12, (4), 917-25.

175. Bear, J., *Dynamics of fluids in porous media*. Reprint ed.; American Elsevier Publishing Co.: New York, 2013.

176. Lage, J., The fundamental theory of flow through permeable media from Darcy to turbulence. *Transport phenomena in porous media* **1998,** 2.

177. Dybbs, A.; Edwards, R. V., A new look at porous media fluid mechanics — Darcy to turbulent. In *Fundamentals of Transport Phenomena in Porous Media*, Bear, J.; Corapcioglu, M. Y., Eds. Springer Netherlands: 1984; Vol. 82, pp 199-256.

178. Scheidegger, A. E., *The physics of flow through porous media*. University of Toronto Press: Toronto; Buffalo [N.Y.], 1974.

179. Tanzi, M. C.; Verderio, P.; Lampugnani, M. G.; Resnati, M.; Dejana, E.; Sturani, E., Cytotoxicity of some catalysts commonly used in the synthesis of copolymers for biomedical use. *Journal of Materials Science: Materials in Medicine* **1994,** 5, (6-7), 393-396.

180. Middleton, J. C.; Tipton, A. J., Synthetic biodegradable polymers as orthopedic devices. *Biomaterials* **2000,** 21, (23), 2335-2346.

181. Peter, S. J.; Miller, M. J.; Yasko, A. W.; Yaszemski, M. J.; Mikos, A. G., Polymer concepts in tissue engineering. *Journal of Biomedical Materials Research* **1998,** 43, (4), 422-427.

182. Hou, Q.; De Bank, P. A.; Shakesheff, K. M., Injectable scaffolds for tissue regeneration. *Journal of Materials Chemistry* **2004,** 14, 1915-1923.

183. Butler, R.; Hopkinson, I.; Cooper, A. I., Synthesis of porous emulsion-templated polymers using high internal phase CO_2-in-water emulsions. *Journal of the American Chemical Society* **2003,** 125, (47), 14473-14481.

184. Wu, R.; Menner, A.; Bismarck, A., Macroporous polymers made from medium internal phase emulsion templates: Effect of emulsion formulation on the pore structure of polyMIPEs. *Polymer* **2013**, 54, (21), 5511-5517.

185. He, S.; Timmer, M. D.; Yaszemski, M. J.; Yasko, A. W.; Engel, P. S.; Mikos, A. G., Synthesis of biodegradable poly(propylene fumarate) networks with poly(propylene fumarate)±diacrylate macromers as crosslinking agents and characterization of their degradation products. *Polymer* **2001,** 42, 1251-1260.

186. Foudazi, R.; Gokun, P.; Feke, D. L.; Rowan, S. J.; Manas-Zloczower, I., Chemorheology of poly(high internal phase emulsions). *Macromolecules* **2013**.

187. Mason, T. G.; Lacasse, M.-D.; Grest, G. S.; Levine, D.; Bibette, J.; Weitz, D. A., Osmotic pressure and viscoelastic shear moduli of concentrated emulsions. *Physical Review E* **1997,** 56, (3), 3150-3166.

188. Stryker, HydroSet injectable HA bone substitute. www.stryker.com.

189. Temenoff, J. S.; Mikos, A. G., Injectable biodegradable materials for orthopedic tissue engineering. *Biomaterials* **2000,** 21, 2405-2412.

190. Farrar, D. F.; Rose, J., Rheological properties of PMMA bone cements during curing. *Biomaterials* **2001,** 22, (22), 3005-3013.

191. Parallax Medical, Bone cement. www.parallaxmed.com

192. McMahon, S.; Hawdon, G.; Bare, J.; Sim, Y.; Bertollo, N.; Walsh, W. R., Thermal necrosis and PMMA – A cause for concern? *Journal of Bone & Joint Surgery, British Volume* **2012,** 94-B, (SUPP XXIII), 64.

193. Chiu, Y. Y.; Lee, L. J., Microgel formation in the free radical crosslinking polymerization of ethylene glycol dimethacrylate (EGDMA). I. Experimental. *Journal of Polymer Science Part A: Polymer Chemistry* **1995,** 33, (2), 257-267.

194. Goodner, M. D.; Bowman, C. N., Modeling primary radical termination and its effects on autoacceleration in photopolymerization kinetics. *Macromolecules* **1999,** 32, (20), 6552-6559.

195. Van Assche, G.; Verdonck, E.; Van Mele, B., Interrelations between mechanism, kinetics, and rheology in an isothermal cross-linking chain-growth copolymerisation. *Polymer* **2001,** 42, (7), 2959-2968.

196. Munin, M. C.; Rudy, T. E.; Glynn, N. W.; Crossett, L. S.; Rubash, H. E., Early inpatient rehabilitation after elective hip and knee arthroplasty. *JAMA* **1998,** 279, (11), 847-852.

197. Coombes, A. G. A.; Meikle, M. C., Resorbable synthetic polymers as replacements for bone graft. *Clinical Materials* **1994,** 17, (1), 35-67.

198. Sideridou, I. D.; Achilias, D. S.; Karava, O., Reactivity of benzoyl peroxide/amine system as an initiator for the free radical polymerization of dental and orthopaedic dimethacrylate monomers: effect of the amine and monomer chemical structure. *Macromolecules* **2006,** 39, (6), 2072-2080.

199. Pryor, W. A.; Hendrickson Jr, W. H., The mechanism of radical production from the reaction of N,N-dimethylaniline with benzoyl peroxide. *Tetrahedron Letters* **1983,** 24, (14), 1459-1462.

200. Carlisle, E.; Fischgrund, J. S., Bone morphogenetic proteins for spinal fusion. *The Spine Journal* **2005,** 5, (6, Supplement), S240-S249.

201. Giannoudis, P. V.; Tzioupis, C., Clinical applications of BMP-7 - The UK perspective. *Injury-International Journal of the Care of the Injured* **2005,** 36, 47-50.

202. Paramore, C. G.; Lauryssen, C.; Rauzzino, M.; Wadlington, V. R.; Palmer, C.; Brix, A.; Cartner, S. C.; Hadley, M., The safety of OP-1 for lumbar fusion with decompression - a canine study. *Neurosurgery* **1999,** 44, (5), 1151-1155.

203. Walker, D. H.; Wright, N. M., Bone morphogenetic proteins and spinal fusion. *Neurosurgical Focus* **2002,** 13, (6), 1-13.

204. Bessa, P. C.; Casal, M.; Reis, R. L., Bone morphogenetic proteins in tissue engineering: the road from laboratory to clinic, part II (BMP delivery). *Journal of Tissue Engineering and Regenerative Medicine* **2008,** 2, (2-3), 81-96.

205. Fauber, J. Spinal fusion device: a bone of contention for FDA. http://www.medpagetoday.com/Surgery/Orthopedics/21908

206. Geiger, M.; Li, R. H.; Friess, W., Collagen sponges for bone regeneration with rhBMP-2. *Advanced Drug Delivery Reviews* **2003,** 55, (12), 1613-1629.

207. Chung, H. J.; Park, T. G., Surface engineered and drug releasing pre-fabricated scaffolds for tissue engineering. *Advanced Drug Delivery Reviews* **2007,** 59, (4–5), 249-262.

208. Brazel, C. S.; Peppas, N. A., Mechanisms of solute and drug transport in relaxing, swellable, hydrophilic glassy polymers. *Polymer* **1999,** 40, (12), 3383-3398.

209. Mainardes, R. M.; Silva, L. P., Drug delivery systems: past, present, and future. *Current Drug Targets* **2004,** 5, (5), 449-455.

210. Basmanav, B. F.; Kose, G. T.; Hasirci, V., Sequential growth factor delivery from complexed microspheres for bone tissue engineering. *Biomaterials* **2008,** 29, (31), 4195-4204.

211. Gokmen, M. T.; Van Camp, W.; Colver, P. J.; Bon, S. A. F.; Du Prez, F. E., Fabrication of porous "clickable" polymer beads and rods through generation of high internal phase emulsion (HIPE) droplets in a simple microfluidic device. *Macromolecules* **2009,** 42, (23), 9289-9294.

212. Christopher, G.; Anna, S., Microfluidic methods for generating continuous droplet streams. *Journal of Physics D: Applied Physics* **2007,** 40, (19), R319.

213. Gokmen, M. T.; Du Prez, F. E., Porous polymer particles—A comprehensive guide to synthesis, characterization, functionalization and applications. *Progress in Polymer Science* **2012,** 37, (3), 365-405.

214. Cramer, C.; Fischer, P.; Windhab, E. J., Drop formation in a co-flowing ambient fluid. *Chemical Engineering Science* **2004,** 59, (15), 3045-3058.

215. Klose, D.; Siepmann, F.; Elkharraz, K.; Krenzlin, S.; Siepmann, J., How porosity and size affect the drug release mechanisms from PLGA-based microparticles. *International Journal of Pharmaceutics* **2006,** 314, (2), 198-206.

216. Yeo, Y.; Park, K., Control of encapsulation efficiency and initial burst in polymeric microparticle systems. *Archives of Pharmacal Research* **2004,** 27, (1), 1-12.

217. Jiang, G.; Thanoo, B. C.; DeLuca, P. P., Effect of osmotic pressure in the solvent extraction phase on BSA release profile from PLGA microspheres. *Pharmaceutical Development and Technology* **2002,** 7, (4), 391-399.

218. Huang, X.; Brazel, C. S., On the importance and mechanisms of burst release in matrix-controlled drug delivery systems. *Journal of Controlled Release* **2001,** 73, (2–3), 121-136.

219. Timasheff, S. N., Protein-solvent interactions and protein conformation. *Accounts of Chemical Research* **1970,** 3, (2), 62-68.

220. Yano, K.; Hoshino, M.; Ohta, Y.; Manaka, T.; Naka, Y.; Imai, Y.; Sebald, W.; Takaoka, K., Osteoinductive capacity and heat stability of recombinant human bone morphogenetic protein-2 produced by Escherichia coli and dimerized by biochemical processing. *Journal of Bone and Mineral Metabolism* **2009,** 27, (3), 355-363.

221. Yang, Y.-Y.; Chung, T.-S.; Ping Ng, N., Morphology, drug distribution, and *in vitro* release profiles of biodegradable polymeric microspheres containing protein fabricated by double-emulsion solvent extraction/evaporation method. *Biomaterials* **2001,** 22, (3), 231-241.

222. Moglia, R. S.; Robinson, J. L.; Muschenborn, A. D.; Touchet, T. J.; Maitland, D. J.; Cosgriff-Hernandez, E., Injectable polyMIPE scaffolds for soft tissue regeneration. *Polymer* **2014,** 55, (1), 426-434.

APPENDIX I

INTERPENETRATING POLYMER NETWORK POLYHIPES

A.1 Introduction

Due to their porous structure and composition of acrylic polymer, polyHIPEs typically behave as weak brittle materials. This limits their usefulness in a variety of fields, specifically tissue engineering as brittle fracture would cause catastrophic graft failure and reinjury. The polyHIPEs discussed previously in Chapters 2 and 3 demonstrate that mechanical response can be tuned by material composition, from weak elastomeric foams to rigid structures approaching cancellous bone. Obtaining a tough injectable polyHIPE, having both strength and some elasticity, would be advantageous over current materials.

Composites materials are hybrids of two or more different components which act synergistically to produce unique properties distinct from either component alone. Interpenetrating polymer networks (IPNs) are one type of composite material used to combine the properties of two or more disparate polymer networks in order to improve either: chemical, electrical, or mechanical properties. IPNs and semi-IPN polyHIPEs are typically fabricated one network at a time in a two-step reaction but this cannot be done *in situ*, and thus cannot be injectable.[125, 126]

We propose to use the more recent one-pot approach which has been used to toughen polyHIPEs by combining brittle and flexible polymers and polymerized via separate routes.[1, 48, 127] Here, a brittle EGDMA network will be combined with the

elastomeric PUUs studied in Chapter III. These networks will be crosslinked into two distinct but physically entangled networks simultaneously because the methacrylated monomers undergo radical chain growth while PUs are crosslink via step growth polymerization of isocyanates. Tuning the IPN component ratios should allow for the creation a library of toughened scaffolds with a wide range of various compressive moduli and strength that can match a variety of bodily tissues.

In this study, two different PUU prepolymers were combined with EGDMA alone and together to form IPN polyHIPE scaffolds. The concentration of linear PCL-DI and branched PCL-TI was varied and their effects on resultant pore structures, gel fractions, and compressive properties evaluated. Finally, EGDMA content was kept constant and the ratio of PCL-DI:PCL-TI varied to investigate effects of PUU crosslink density on overall scaffold performance.

A.2 Materials and Methods

A.2.1 Materials Polyglycerol polyricinoleate (PGPR 4125) was donated by Paalsgard. All other chemicals were purchased and used as received from Sigma Aldrich unless otherwise noted.

A.2.2 EGDMA Filtration EGDMA purchased from Sigma Aldrich was purified to remove inhibitor prior to use. The macromer was filtered through an aluminum oxide column to remove monomethyl ether hydroquinone. The purified product was stored at 4 °C under a nitrogen blanket until used for HIPE fabrication.

A.2.3 PCL-Isocyanate Synthesis Isocyanate functionalized prepolymers were synthesized in bulk following the same procedure used in Moglia et al.[222] Briefly, polycaprolactone (PCL) diol or triol (530, 900 Mn respectively) was heated with 50°C air and added dropwise to a reaction flask charged with hexamethylene diisocyanate (HDI, 2.02 x mol diol, 9.00 x mol triol). The reaction was heated to 80 °C for 90-120 minutes and reaction progress was monitored with FTIR spectroscopy every 30 minutes until complete. The product was washed with hexane to remove excess HDI and dried under vacuum overnight. The final products were colorless liquids with a viscosity similar to honey. The prepolymer structure was confirmed using ^{1}H NMR (300 MHz, $CdCl_3$): PCL-diisocyanate (PCL-DI) δ 1.33-1.47 (m, 8H), 1.52 (q, 4H), 1.60-1.75 (m, 8H), 2.30-2.40 (m, 4H), 3.18 (s, 2H), 3.33 (q, 2H), 3.70-3.73 (m, 2H), 4.09 (t, 4H), 4.24-4.27 (m, 2H), 4.77 (s, 1H). PCL-triisocyanate (PCL-TI) δ 0.91(t, 3H), 1.33-1.52 (m, 8H), 1.60-1.75 (m, 8H), 2.31-2.38 (m, 4H), 3.18 (s, 2H), 3.33 (m, 2H), 4.04-4.11 (m, 4H), 4.74 (s, 1H).

A.2.4 PolyHIPE Fabrication HIPEs were fabricated using a FlackTek Speedmixer DAC 150 FVZ-K according to a protocol adapted from Moglia et al.[157] Briefly, EGDMA was combined with varied amounts of PCL-DI (10, 20, and 30 wt%), PCL-TI (10, 20, and 30 wt%), or a blend of both (5 wt% DI:15 wt% TI, 10 wt% DI:10 wt% TI, 15 wt% DI:5 wt% TI). This solution was mixed with 10 wt% PGPR 4125 and a 1 wt% benzoyl peroxide (BPO) prior to emulsification. A second mixture consisting of an identical macromer solution, 10 wt% PGPR, and 1 wt% trimethylaniline (TMA) was also combined prior to emulsification. An aqueous solution of calcium chloride (1 wt%)

was then added to the organic phases (75% v) in 3 additions and mixed at 500 rpm for 2.5 minutes each. HIPEs were placed in double barrel syringe and the two emulsions mixed upon injection using a static mixing head (5 mL syringe with 3 cm straight mixer, Sulzer Mixpac K-System). HIPEs were then placed in a 37°C bath for 48 hr to allow for complete polymerization.

A.2.5 SEM Analysis PolyHIPEs were dried *in vacuo* for 24 hr to remove water prior to characterization. Average pore and interconnect size of varying compositions was determined using scanning electron microscopy (SEM, Phenom Pro). Circular specimens from each polyHIPE composition were sectioned into quarters, fractured at the center, and imaged in a rastor pattern yielding five images. Pore size measurements were completed on the first ten pores that crossed the median of each 2000x magnification micrograph. Average pore sizes for each polyHIPE composition are reported (n=150). A statistical correction was calculated to account for the random fracture plane through spherical voids and pores, $2/\sqrt{3}$.[159] Average diameter values were multiplied by this correction factor resulting in a more accurate pore diameter.

A.2.6 Mechanical Testing PolyHIPE compressive properties were investigated as a function of composition using an Instron 3300, equipped with a 1000-N load cell. ASTM D1621-04a was utilized to determine the compressive modulus and strength of the polyHIPEs.[135] Each polyHIPE specimen was sectioned into three discs (15mm diameter, 5 mm thick) using an Isomet® saw and compressed to 50% strain at 50 μm/s. The compressive modulus was calculated from the slope of the linear region after correcting for zero strain and the compressive strength was identified as the stress at the

yield point or 10% strain, whichever occurred first. Reported moduli and strength data were averages of 3 specimens for each composition tested.

A.2.7 Gel Fraction Gel fraction was measured gravimetrically to evaluate the extent of network formation. After curing for 48 hr, polyHIPE samples were sectioned into 15mm by 1 mm discs. Each specimen was vacuum dried for 48 hr, incubated 48 hr in 100X dichloromethane at 37 °C, and vacuum dried again until a constant mass was achieved. The final weight divided by the initial weight was assessed as the gel fraction. Fourier transform infrared spectroscopy (FTIR) was used to assess the composition of gel fraction extracts.

A.2.8 Statistical Analysis The data are displayed as mean ± standard deviation for each composition. A Student's *t* test was performed to determine any statistically significant differences between compositions. All tests were carried out at a 95% confidence interval ($p < 0.05$).

A.3 Results and Discussion

A.3.1 Pore Structure-Varied PCL *Content* Increasing PCL content in the EGDMA polyHIPEs decreased average pore sizes, as shown in **Figure A.1** and **Table A.1**. PCL-TI had the greatest effect with the 10, 20, and 30 wt% scaffolds exhibiting 17, 13, and 7 μm pores respectively. PCL-DI caused a similar but less drastic decrease in pore size with the 10, 20, and 30 wt% scaffolds possessing 15, 12, and 11 μm pores.

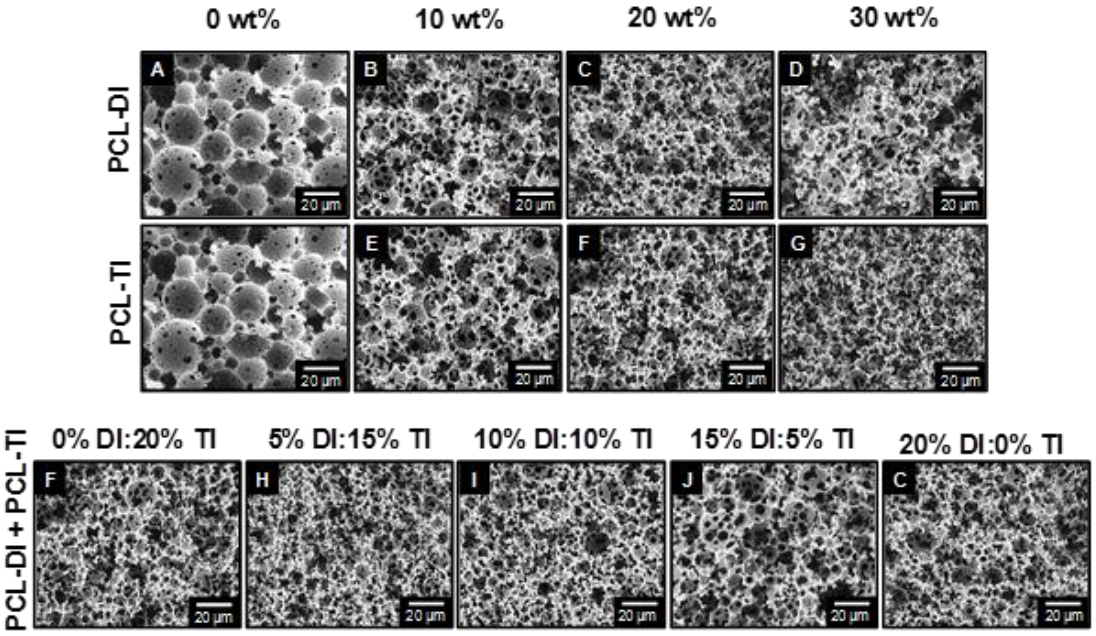

Figure A.1. Representative SEM images of IPN polyHIPE composition on pore structure. (A) 100% EGDMA control, (B & E) 10 wt% PCL 90 wt% EGDMA, (C & F) 20 wt% PCL 80 wt% EGDMA, (D & G) 30 wt% PCL 70 wt% EGDMA. Images H-J demonstrate the effort of varied PCL-DI:PCL-TI with a constant 80 wt% EGDMA: (H) 5 wt%:15 wt%, (I) 10 wt%:10 wt%, (J) 15 wt%:5 wt%.

Interconnect size decreased slightly with increasing PCL content, but both 10 wt% compositions had larger interconnects than the EGDMA control. All of the IPN interconnects were approximately $1/4^{th}$ their corresponding pore size, larger than the EGDMA control's $1/7^{th}$ ratio. This can be interpreted as an increase in pore interconnectedness and is visible in **Figure A-1**. The increased interconnectivity may be a result of CO_2 blowing from the isocyanates reacting with water to form urea bonds.[109, 222] Previously, this reaction caused an increase in pore size for PUU polyMIPEs.[222] Here, the redox polymerization of the EGDMA macromer likely set the emulsion geometry within minutes, faster than CO_2 was formed. We hypothesize that the CO_2 pressure

increased in the water-filled pores, until an escape path was formed via interconnected pores to the scaffold surface. During this pressure build-up, the polymerized regions of cell walls would easily resist deformation, focusing the pressure to less-cured regions between adjacent pores. This focusing may have exerted enough force on polymer wall/film to expand the interconnect size.

Table A.1. Effect of IPN polyHIPE composition on average pore and interconnect size.

Material	% PCL (wt%)	Average Pore (μm)	Average Interconnect (μm)
EGDMA Control	0	20 ± 10 *	3 ± 1
PCL-DI	10	15 ± 5 †‡	4 ± 2
	20	12 ± 4 †	3 ± 1
	30	11 ± 5 †●	3 ± 2
PCL-TI	10	17 ± 6 ○‡	4 ± 2
	20	13 ± 4 ○	3 ± 1
	30	7 ± 5 ○●	2 ± 1
DI:TI	5:15	9 ± 4 □	3 ± 1
	10:10	10 ± 4 □	3 ± 1
	15:5	15 ± 5 ◊□	4 ± 2

*: P <0.001 compared to all other pore sizes
†: P <0.01 compared to all PCL-DI/EGDMA IPN pore sizes
‡: P <0.001 compared to 10% PCL-DI/EGDMA and 10% PCL-TI/EGDMA IPN pore sizes
●: P <0.001 compared to 30% PCL-DI/EGDMA and 30% PCL-TI/EGDMA IPN pore sizes
○: P <0.001 compared to all PCL-TI/EGDMA IPN pore sizes
◊: P <0.001 compared to 5% PCL-DI:15% PCL-TI/EGDMA & 10% PCL-DI:10% PCL-TI/EGDMA IPN pore sizes
□: P <0.001 compared to 20% PCL-DI/EGDMA and 20% PCL-TI/EGDMA IPN pore sizes

There is no simple explanation for the decrease in pore size with increasing PCL content, and further testing would be required to pinpoint the responsible mechanism. The first possibility is that increasing PCL content caused increases to organic phase viscosity, and this phenomenon was observed qualitatively during polyHIPE fabrication.

Increased organic phase viscosity would inhibit droplet coalescence prior to cure and result in smaller average pore sizes. Alternatively, increasing PCL content also raises the macromer phase hydrophobicity, evaluated here via LogP. Previously, increasing hydrophobicity has been linked to increased pore sizes caused by emulsion destabilization.[56, 111, 157, 222] However, there is likely an optimum hydrophobicity associated with each macromer-surfactant system. The closer to the optimum value, the more stable the emulsion will be resulting in smaller water droplets and thus pores diameters. Further studies carefully controlling both macromer viscosity and hydrophobicity are required, in addition to testing with varied surfactants to truly explain these results.

Finally, the amount of PCL-DI relative to PCL-TI was varied and increasing this ratio resulted in an increase in average pore diameter and interconnect size, matching the sizes for the 10 wt% PCL-DI/90 wt% EGDMA polyHIPE. This result further supports the theory of an optimum hydrophobicity because it follows the same trend seen when increasing PCL concentration. PCL-TI is more hydrophobic than PCL-DI and thus would raise the overall macromer hydrophobicity more dramatically than PCL-DI alone, driving it towards optimum values and creating smaller pores.

A.3.2 Gel Fraction Gel fraction was measured to evaluate PUU network formation, and the results are summarized in **Figure A.2**. The EGDMA control had a gel fraction of 90%, an acceptable value considering the surfactant is expected to elute out and would account for 10% of scaffold weight. All PCL-TI compositions showed similar high gel fractions around 90%, statistically similar to the control EGDMA material.

Conversely, the PCL-DI at 10 wt% had a gel fraction of 90% but decreased to 82 and 79% for the 20 and 30 wt% PCL-DI formulations. FTIR analysis of the extraction solutions confirms the presence of PCL-DI for each the 10, 20, and 30 wt% samples, signifying that those materials are likely semi-IPNs with linear PUU chains physically entangled within the EGDMA network. This is expected due to the inability of PCL-DI to form covalent crosslinks and to instead grow linearly in molecular weight. Furthermore, FTIR of the PCL-TI specimens revealed only the presence of unfunctionalized PCL-triol, characterized the lack of urethane or urea associated peaks, and no traces of PCL urethane-ureas. Considering the functionalization of the PCL-TI was ~85%, some unfunctionalized species are expected but rare as it is more likely that molecules would functionalize at least 1 or 2 of the available alcohol groups. This implies that the PCL-TI forms full IPNs even at 10 wt% concentrations.

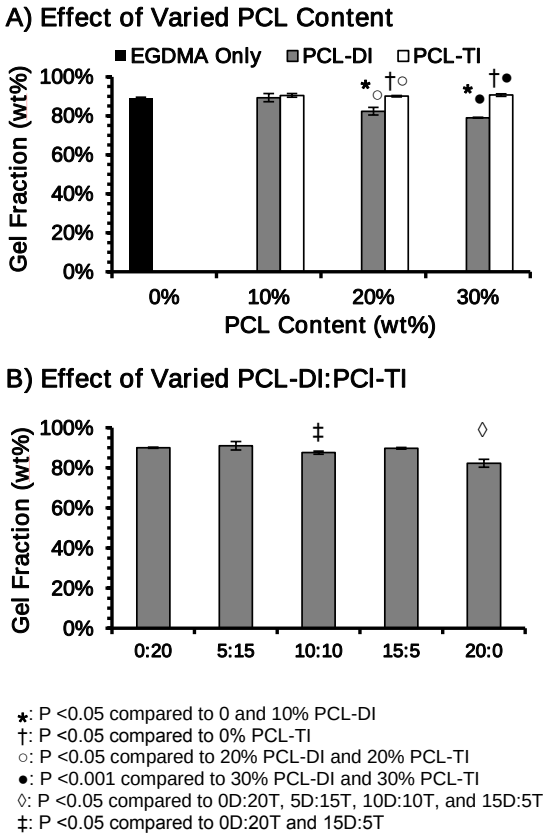

Figure A.2. Effect of IPN polyHIPE composition on gel fraction.

Varying the ratio of PCL-DI:PCL-TI had little effect on gel fraction, except for the 20% DI:0% TI (discussed above) which showed significantly lower gel fraction than the others. This is the only composition of the set without any ability to form covalent crosslinks and thus was expected to form only a semi-IPN. This data shows that even as little as 5% PCL-TI crosslinker and 15% PCL-DI is enough to form a fully crosslinked PUU network.

While this data can be used to infer whether full or semi-IPNs have been created, more extensive work would need to be done. For example, if a linear polymer's molecular weight increased enough it would be difficult to remove from a crosslinked

polymer network. Although it would not truly be an IPN, it could behave like one due to the number of chain entanglements. Alternatively, Lumelsky et al. reported that excess PCL began to phase separate from the acrylate network to form phase separated regions of their material with vastly different properties.[116] If the individual components have sufficiently different Tg's, DSC or DMA can be used to measure phase mixing.[116]

A.3.3 Mechanical Response PolyHIPE modulus and strength decreased as PCL content was increased, **Figure A.3**. The control EGDMA polyHIPE possessed a modulus of ~20 MPa and strength ~1.4 MPa. The modulus for PCL-DI IPNs decreased to 15 MPa for 10 wt% and ~6 MPa for the 30 wt% compositions respectively. Similarly, strength decreased to 0.8 and 0.5 for the 10 and 30 wt% PCL-DI IPNs. PCL-TI containing polyHIPEs exhibited lower average moduli than their PCL-DI equivalent, but similar strengths at 10 and 20 wt% concentrations.

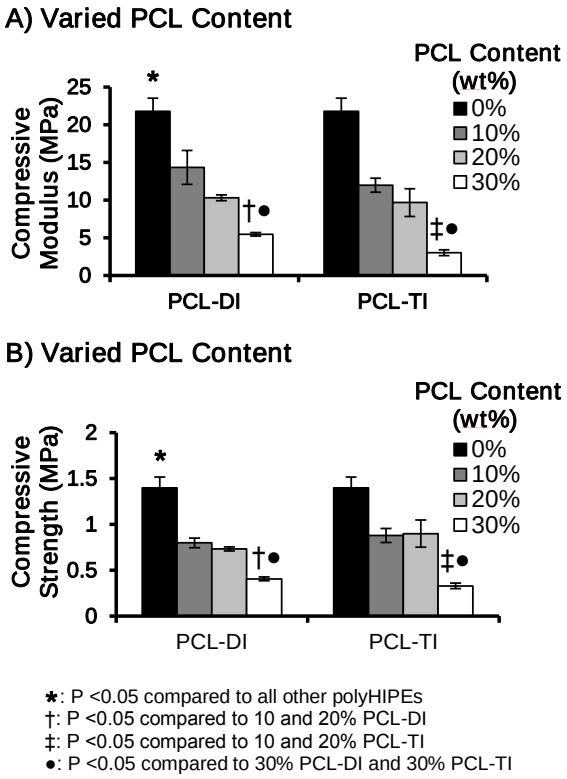

Figure A.3. Effect of PCL-DI and –TI content on IPN polyHIPE compressive (A) modulus and (B) strength.

Varying the ratio of PCL-DI:PCL-TI had very little effect on compressive properties with the exception of the 20% DI:0% TI which was significantly lower than the rest, **Figure A.4**. Unlike the others, the 20% DI:0% TI polyHIPE was the only semi-IPN in the set with no ability to form a covalently crosslinked PUU network. Without the second network to help resist strain, overall crosslink density decreased and therefore behaved as expected.

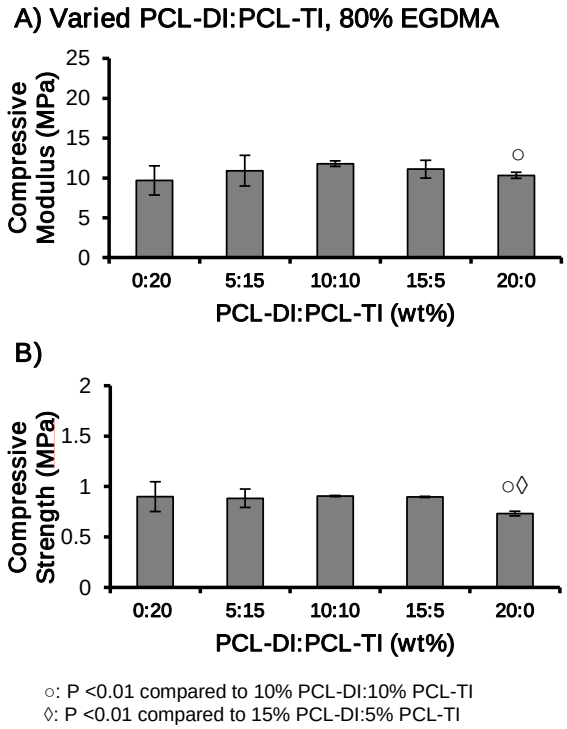

Figure A.4. Effect of PCL-DI:PCL-TI ratio on IPN polyHIPE compressive (A) modulus and (B) strength, with 80 wt% EGDMA.

In the PUU polyMIPEs from Chapter III, PCL-DI scaffolds exhibited an increased modulus and strength due to hydrogen bonding forming physical crosslinks between chains which increased effective crosslink density and thus mechanical properties. In this redox system, the EGDMA network forms much faster than the PUU and possibly prevents the chain reorganization necessary to create secondary bonds, yielding a weaker and more pliable material.

Increasing PCL content was expected to decrease compressive modulus because overall crosslink density is decreasing, especially for the PCL-DI only IPNs. Volume that had been taken up by highly crosslinked EGDMA was replaced by the pliable and elastomeric PUUs. **Figure A.5** shows representative compression curves for each

material, and both the PCL-DI and –TI materials show a broadening and disappearing of the yield point with increasing PCL content. These materials behave less like the brittle EGDMA polyHIPEs and start to resemble the response associated with the pure PUU polyMIPEs.[222] While the decrease in strength is apparent in these plots, the 20% PCL-TI remains an anomaly and exhibits higher strengths than the EGDMA control at strains greater than 20%. This behavior indicates an increase in mechanical toughness, or resistance to brittle fracture. While toughness could not be measured directly in compression, all of the IPN polyHIPEs were noticeably less brittle during handling, and fractured into larger and fewer pieces with increasing PCL content.

IPNs are typically stronger than semi-IPNs because of increased crosslink density leading to more entanglements between the two networks. There is usually some compromise between individual network properties, but Lepine et al. and Lumelsky et al. saw the greatest improvement in mechanical properties after crosslinking the two materials into the same graft-co-polymer network.[108, 116] Therefore, future studies should investigate changing endgroups between the two macromers to facilitate formation of a single graft-co-polymer network with both rigid and elastomeric components.

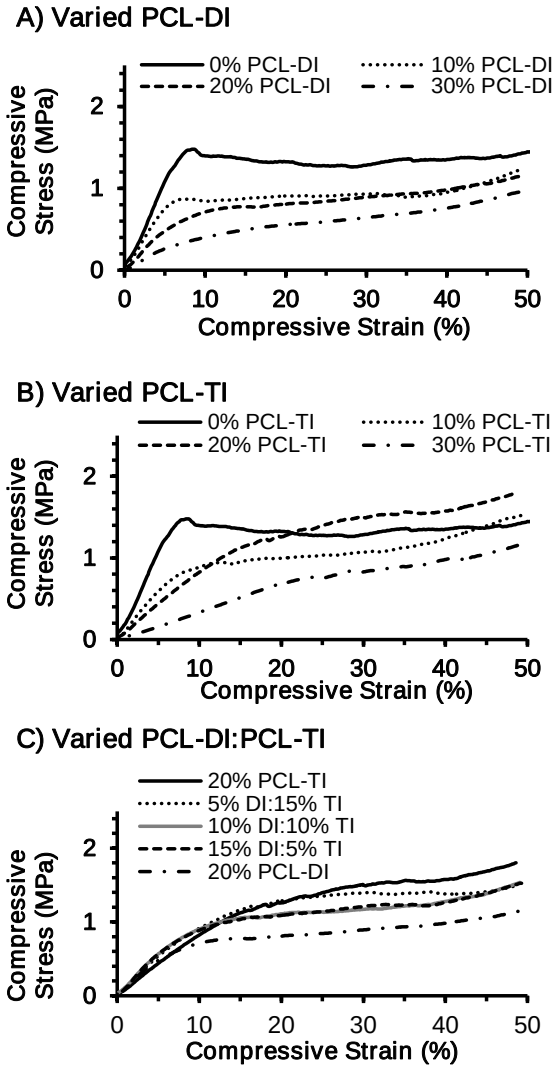

Figure A.5. Representative compression curves for (A) PCL-DI/EGDMA, (B) PCL-TI/EGDMA, and (C) DI:TI/EGDMA IPN polyHIPEs.

A.4 Conclusions

In conclusion, this data shows that combining the PUU prepolymers and rigid EGDMA is a viable method to achieve mechanical properties in between the two types of scaffolds. Here, a range of material modulus, strength, and elasticity were be created by varying polymer concentration, without sacrificing injectability. Previously, IPN

fabrication required a two-step process, making the first network and then swelling it in a solvent/component B mixture to make the IPN. This method requires no solvent to make the IPN and is a one-step process, reducing fabrication costs and time.

However, these IPNs did not increase the fracture toughness of the brittle EGDMA polyHIPEs, and the only composition which did sacrificed too much in terms of modulus and strength. Therefore, alternative options to increase toughness should be considered.